ISBN 0-315-54834-7

Use of Time Domain Reflectometry for the Detection and Measurement of Cerebral Edema

by

Hung Pin Kao

A thesis
presented to the University of Manitoba
in partial fulfillment of the
requirements of the degree of
Master of Science
in
Electrical Engineering

Winnipeg, Manitoba

USE OF TIME DOMAIN REFLECTOMETRY FOR THE DETECTION AND MEASUREMENT OF CEREBRAL EDEMA

BY

HUNG PIN KAO

A thesis submitted to the Faculty of Graduate Studies of the University of Manitoba in partial fulfillment of the requirements of the degree of

MASTER OF SCIENCE

I hereby declare that I am the sole author of this thesis.

I authorize the University of Manitoba to lend this thesis to other institutions or individuals for the purpose of scholarly research.

Hung Pin Kao

I further authorize the University of Manitoba to reproduce this thesis by photocopying or other means, in total or in part, at the request of other institutions or individuals for the purpose of scholarly research.

Hung Pin Kao

The University of Manitoba requires the signatures of all persons using or photocopying this thesis. Please sign below, and give the address and date.

Abstract

The purpose of this thesis was to develop a method of continuously measuring cerebral edema. The technique investigated measured the complex dielectric constant, consisting of the real dielectric constant and loss factor, of a small volume of biological tissue using time domain reflectometry at frequencies between 100 and 1000 MHz. The sample is placed at the end of an open-ended coaxial transmission line. The terminating impedance presented by the tissue may be calculated from the Fourier transforms of the incident wave from a time domain reflectometer and the reflected wave from the sample. For 0.141" cable, which was used in this study, estimated accuracies of less than 5 % were observed for sample thicknesses greater than 3 mm. Strong correlations were observed between dielectric properties of in-vitro canine white matter and its water content during osmotic edema. Real dielectric constant increased while loss factor decreased with increasing water content at each frequency. From preliminary measurements of a vasogenic edema progression in a cat it was observed that the real dielectric constant and loss factor of cerebral tissue both increased with water content.

It was concluded from these results that the tissue real dielectric constant is primarily affected by its water content while tissue loss factor is primarily affected by the loss factor of the accumulated edematous fluid over 100 - 1000 MHz. The technique may enable the detection of all types of edema using the real dielectric constant of the tissue. Since the tissue loss factor reflects the concentration of proteins and ions, the type of edema might also be determined from the measurements. Future use of this technique in-vivo require that the changes in dielectric properties with water content in-vivo be established, as these may be different from in-vitro changes.

Acknowledgements

The author is indebted to his family and especially his parents, Kwan Chi and Yi Ching Kao for their support and encouragement throughout this study. Sincere thanks are given to Dr. Edward Shwedyk and Dr. Erico R. Cardoso for their excellent guidance and assistance.

The author gratefully acknowledges the Power Systems Group for the use of the 7854 Tektronix Oscilloscope and GURU package, Drs. N. L. Stephens, Richard Prewitt and Deepak Bose of the Faculty of Medicine for providing tissue samples used in this study and Ms. Yanita d'Audiffret for her assistance in the preparation of experiments. The contribution of Professor E. Bridges is recognized for many helpful suggestions and discussions in the course of this work.

This financial support of the Natural Sciences and Engineering Research Council of Canada is gratefully acknowledged.

Table of Contents

List of Illustrations

Figures

Tables

Chapter I

Introduction

1.1 Cerebral Edema

Cerebral edema is defined as increase in cerebral volume due to increase in its water content. It is a potentially life threatening condition commonly associated with several diseases of the brain. The increase in tissue volume is often large enough to cause increased intracranial pressure or severe displacement of the brain. Cerebral edema may also cause dysfunction or failure of respiration and circulation.

There are four main types of cerebral edema: vasogenic, cytotoxic, interstitial and osmotic edemas. The characteristics of each condition is outlined below. It should be noted, however, that more than one type may occur in a patient.

1.1.1 Vasogenic Cerebral Edema

Vasogenic edema is the most common form of cerebral edema. It results from the extravasation of water from within blood vessels into the cerebral tissue surrounding an area of damaged cerebral vessel wall. In this type of edema, most of the water accumulates in the white matter of the brain (Figure 1) [16]. Vessel wall damage, or blood brain barrier breakdown, with subsequent edema formation may result from the presence of brain tumors, contusions or hemorrhages. The blood brain barrier depends upon the special morphological features of the endothelial cells of brain capillaries. These cells form a

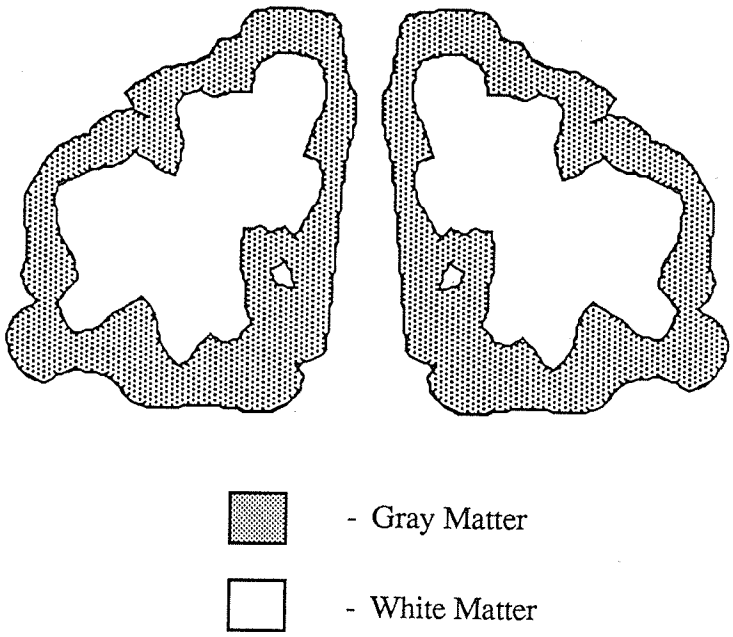

Figure 1: Cerebral Gray and White Matter

semipermeable barrier between the blood and the extracellular space (ECS) of the cerebral tissue. Depending on the chemical and physical characteristics of the compound, transport through the barrier is limited. In general, the ease with which a substance can cross the barrier is directly related to its lipid solubility and inversely related to its molecular size. Only water, carbon dioxide and oxygen can pass through the barrier relatively unrestricted [14]. With injury, the permeability of the barrier is increased, allowing some compounds previously blocked to enter the brain (Figure 2). The content of the accumulated edematous fluid is close in composition to blood plasma, the non-cellular constituent of blood. The cerebral extra-cellular space (ECS), that is, the volume occupied between the cerebral cells, is increased by the edema fluid, thus increasing tissue volume. The spread of edema fluid occurs by pressure and concentration gradients through the cerebral white matter. This results in a "balloon-like" edematous zone, where the accumulation of edema decreases radially from the damaged site [52].

1.1.2 Cytotoxic Cerebral Edema

Cytotoxic edema is produced by swelling of cerebral cells, with an accompanying decrease in ECS volume (Figure 3). It is caused by hypoxia, the cutoff of oxygen to the cells, which in turn, causes a drop in cellular adenosine tri-phosphate (ATP) production. Because of the resulting failure of the ATP dependent sodium pump within the cell membranes, intracellular sodium accumulates rapidly. Water collects in the cells to maintain osmotic equilibrium. Thus, this type of edema only occurs in the white or gray matter areas where ATP production has stopped. Cytotoxic edema is observed after cardiac arrest or asphyxia [16].

1.1.3 Interstitial Cerebral Edema

Interstitial edema is caused by the accumulation of cerebral spinal fluid (CSF) in the periventricular (surrounding the cerebral ventricles) white matter. Most often,

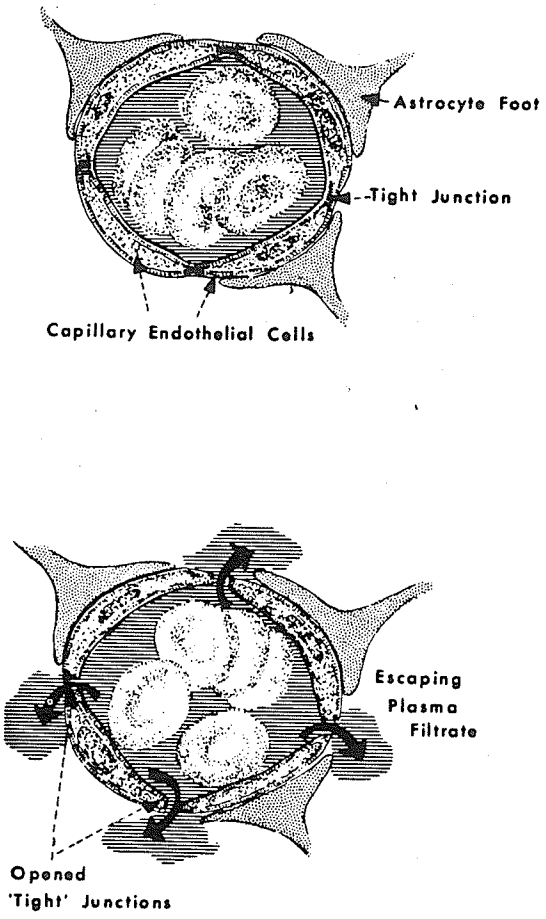

Figure 2: Changes in the permeability of the capillary endothelial cells of the brain capillaries during vasogenic edema

Source: Reference [16]

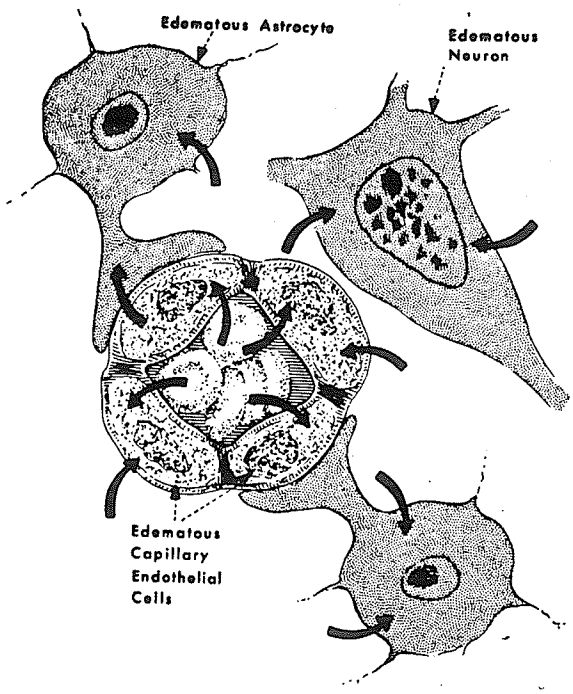

Figure 3: Swelling of endothelial, neuronal and glial cells during cytotoxic edema

Source: Reference [16]

accumulation results from the obstruction of CSF flow from the ventricular system. CSF then collects in the ventricles, resulting in retrograde movement of CSF across the ventricular walls (Figure 4). This form of edema occurs with hydrocephalus, a condition caused by the blockage of normal CSF flow, resulting in abnormal increase of CSF volume in the skull. Unlike other forms of edema, the volume of the periventricular white matter is reduced, rather than increased, because its myelin lipids are dissolved as hydrostatic pressure increases. Brain volume, however, may be increased due to the volume of additional CSF [16].

1.1.4 Osmotic Cerebral Edema

Osmotic edema develops when blood plasma osmolarity falls quickly. To maintain osmotic equilibrium, water flows into the cells of both gray and white matter [51]. This form of edema arises during water intoxication. It can be induced by the administration of distilled water into the blood stream, which reduces plasma osmolarity. In-vitro osmotic edema may be produced by immersion of an excised piece of brain tissue in distilled water.

1.2 Water Content Measurement

Presently, there are three methods commonly used to determine the water content of cerebral white matter, thus allowing the diagnosis of cerebral edema: computerized tomography, wet-dry weight and the gravimetric method. None of these methods can monitor water content continuously.

1.2.1 Computer Axial Tomography

Computer axial tomography, or CAT scanning, is a method of imaging the structure of the brain. The amount of X-ray absorption by the tissue is calculated when a narrow beam of X-rays is passed through a section of the brain at different angles. Detectors receive the beam on the opposite side of the head (Figure 5). Reconstruction of the

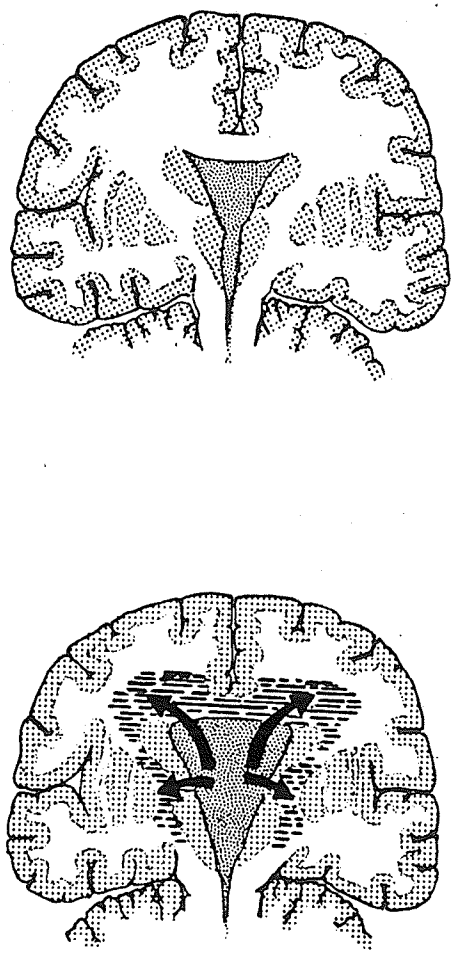

Figure 4: Movement of CSF from the ventricle to the adjacent cerebral white matter during interstitial edema

Source: Reference [16]

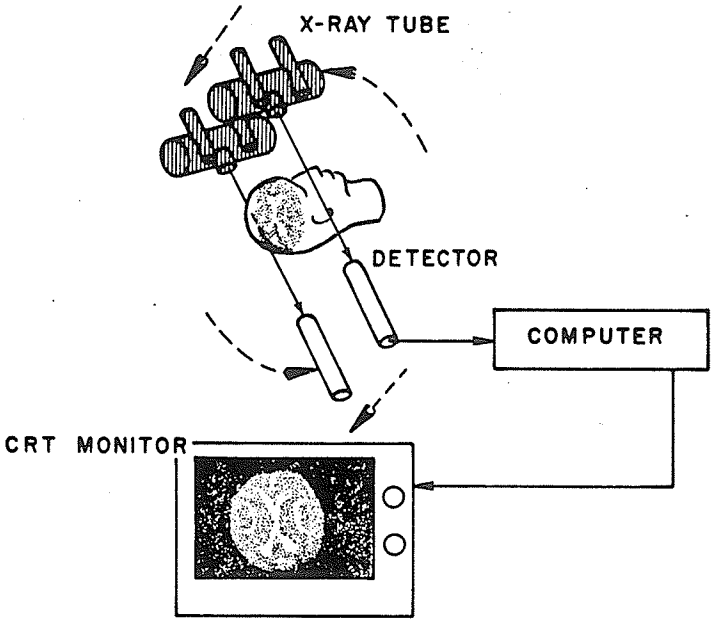

Figure 5: Basic setup for computerized axial tomography

Source: Reference [69]

structure uses a series of projections to yield a transaxial sectional image of the examined part. When several images are put together, a tomograph of the entire brain is produced. CAT scanning distinguishes minute differences in X-ray absorption of different parts of the head. The image reconstructed is a map of the X-ray absorption coefficients.

Absorption coefficients are usually expressed on the Hounsfield scale from -500 units for air to 500 units for bone, with 0 for distilled water. Since absorption coefficients are closely related to tissue density, changes in the density of the tissue will be observed with the CAT scan [69]. When edema occurs, the accumulation of water causes the cerebral density to decrease. An increase of 10 % in water content corresponds approximately to an absorption coefficient drop of only 3 Hounsfield units [40]. Furthermore, the proportions of solids, lipids, water and blood may also change the absorption coefficient. Therefore, an observed reading from the CAT scan cannot be directly attributed to water content. Enhancement of the observation of the edema progression may be achieved through the injection of a contrast fluid into the brain [25]. The extent of the fluid penetration can be assessed by the amount of contrast fluid penetrating into the brain. As CAT scanning is noninvasive, however, it has become the major tool for the nonquantitative observation of edema and for the diagnosis of edema.

1.2.2 Wet-Dry Weight

The wet-dry weight method, unlike CAT scanning, is invasive, requiring opening of the skull and biopsy of tissue [54]. Fresh brain samples are weighed and then dried in a heated oven at approximately 100° C until no further weight loss occurs. The water content of the sample is then calculated by the following formula:

$$\% \text{ tissue water content} = \frac{\text{tissue fresh wt - tissue dry wt}}{\text{tissue fresh wt}} \quad X \quad 100 \qquad (1)$$

This formula assumes that the only volatile component lost during drying is water. Besides being invasive, the wet-dry weight method for measurement of edema has two main disadvantages: 1) samples greater than 25 mg must be used to minimize errors due to evaporation of tissue water, and 2) the drying process requires times of up to three days.

1.2.3 Gravimetric Technique

The gravimetric technique is another physical invasive method of measuring brain water, requiring biopsy of tissue [41]. The specific gravity of the tissue depends on the specific gravity of its dried tissue solids as well as the water content of the sample. As the specific gravity of the dried tissue solids is constant for a particular type of tissue only knowledge of the sample specific gravity is required to mathematically determine the sample water content. This method is based on the principle that the specific gravity of a sample is determined by the depth to which the sample sinks in a linear density gradient column (Figure 6). The column is made up of kerosene and bromobenzene, liquids which do not readily react with the sample. Using the depth and linear density relation, the sample's specific gravity can be determined. The water content can then be determined using the following linear equation [44] between tissue water content and the inverse of its specific gravity:

$$\% \text{ tissue water} = \{ 1 - [(spgr_t - 1)/((1-1/spgr_s) \text{ X } spgr_t)] \} \text{ X } 100 \qquad (2)$$

where $spgr_s$ is the specific gravity of tissue solid and $spgr_t$ is the specific gravity of the sample.

If water is the only substance added to the brain tissue, the specific gravity of normal tissue solid is used. In vasogenic edema, small amounts of proteins and other substances enter the brain which alter the specific gravity of the tissue solid slightly. Thus, a correcting factor must be introduced to (2) to account for this error in these samples

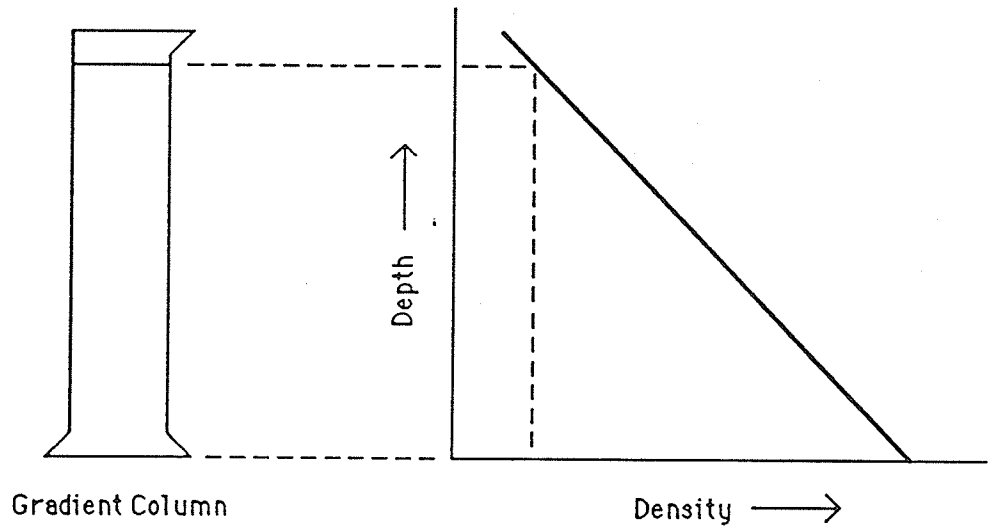

Figure 6: A Linear Density Gradient Column

[42]. The main advantage of this method over the dry-wet weight technique is that the minimum sample size is reduced to approximately 2 mg. In addition, as no weighing is involved, the error from evaporative loss is small and results can be obtained immediately after collection of specimens. Therefore, because of its versatility, the gravimetric technique is most often used to measure water content in animal experiments and clinical practice [7,23,70].

1.3 The Medical Need for Continuous Measurement of Cerebral Edema

In cases of severe edema, a method of continuously measuring the water content of a small tissue volume would be useful in the treatment of edema. A method that precludes the need for repetitive sampling also has the advantage of sparing further damage to cerebral tissue. Continuous monitoring of edema in patients would enable early detection of edema, the assessment of treatment and the prevention of complications. In addition, such a method could be used in clinical research to test the efficacy of experimental drugs to reduce edema. Furthermore, during surgery, it would allow for easier location of injured areas of the brain through recognition of the "balloon like" edematous zone.

1.4 Past Research in Electrical Measurements of Cerebral Tissue

The detection of cerebral edema was first done indirectly by Grant [27], who observed a decrease in the impedance magnitude of white matter at 1 kHz in areas surrounding brain tumours. Decreases in the impedance magnitude at frequencies less than 50 kHz have also been observed after penetration of electrodes into the brain [28]. This may be attributed to the presence of vasogenic edema in and around a cerebral tumour or injured area. This finding has been verified by Fujita [19] and Gazendam [24], who observed a gradual decrease in the impedance of cerebral tissue several hours after the onset of vasogenic edema, produced by the cold lesion technique. However, contrary to these results, increases in impedance have been reported during osmotically induced edema [29].

Van der Veen [72] and Go [26] both attempted to correlate water content of cerebral white matter with impedance magnitude at 10 kHz during vasogenic edema. For each experiment, one electrode was inserted into the brain while a reference electrode was attached to the skin or surface of the brain. Results obtained had a large scatter between impedance magnitude and water content, which may be attributed to the nonhomogeneity of samples measured and the variation of surface resistance among subjects. Both studies verified a decrease in impedance with vasogenic edema. Kao et al [35], however, found strong correlations between water content of canine cerebral white matter in-vitro and the impedance parameters of impedance magnitude and resistance at frequencies between 0.5 and 500 kHz.

Early measurements of the complex dielectric constant of tissues, consisting of the real dielectric constant and loss factor, provided insight into the structure of the biological media. However, limited capability of available instrumentation prevented accurate measurement at higher frequencies. Recently, there has been increased interest in the dielectric properties of tissue at higher frequencies over concern of health hazards due to exposure to radio and microwave frequencies, and the use of these frequencies in hyperthermia, a cancer therapy [61]. Dielectric properties have been used successfully in the detection of the water content in industrial and research applications. Strong relations have been observed between the water content of soil, coal, grain and timber and dielectric parameters [13,36,48,71].

Most studies of the high frequency dielectric properties of tissue have been performed using frequency domain techniques. At lower frequencies, i.e., those below 100 MHz [18,56], impedance measurements are sometimes used to calculate dielectric properties. Higher frequency measurements are based on network analyzers [3,8,18,57,58,60,61], whereby the reflection coefficient of a tissue sample load in a coaxial line is measured and used to calculate the complex dielectric constant. Recently, some researchers have used time domain techniques for measurements of tissue permittivity

[4,12,46]. The complex dielectric constant is calculated from the Fourier transforms of an incident fast rising pulse and its reflected wave from a sample terminating a coaxial line.

The difference in dielectric permittivity in-vivo and in-vitro at the same temperature has been observed to be insignificant at frequencies above 100 MHz. Significantly lower dielectric constants were observed in-vitro above 100 MHz [61]. This was attributed to the Maxwell-Wagner relaxation of membranes, proteins and bound water. Higher frequencies are primarily affected by the relaxation of free water, the ionic conductivity of cytoplasm, and bound water. Based on these results, it would be expected that the complex dielectric constant of tissue is primarily affected by the dielectric nature of the fluid contained in the tissue at higher frequencies. Schepps and Foster [53] have examined the relation between water content and dielectric properties of various types of tissues. It was found that the properties of these tissues fitted to Debye equations above 1-5 GHz correlate well with their water contents. However, their study did not consider variations of water content within one type of tissue. This thesis examined the relation between the dielectric properties of one type of tissue, canine white matter, and its water content.

1.5 Purpose

The purpose of this thesis is to develop a method of continuously measuring cerebral edema. The method investigated measured the complex dielectric constant, consisting of the real dielectric constant and loss factor, of the cerebral tissue. To determine the relationship between these quantities and cerebral edema, the real dielectric constant and loss factor of canine white matter were correlated with its water content during osmotic edema. A preliminary test of the method was also performed using a vasogenic edema progression in a cat.

All dielectric measurements were made using a time domain reflectometer with an open-ended cable to measure the tissue. The small cable size enabled the measurement of a small volume of tissue without the need for biopsy. The frequency window chosen was

100 - 1000 GHz. White matter was chosen as all 4 types of edema, and in particular vasogenic edema, affect this type of tissue.

The theory on which the technique is based is briefly discussed in chapter II, followed by the experimental procedure in chapter III and an analysis of the results in chapter IV.

Chapter II

Theory

The measurement of the complex dielectric constant of brain tissue is accomplished through measurement of its impedance. The tissue was used to terminate an open ended coaxial cable. The terminating impedance presented by the tissue is calculated from the Fourier transforms of the incident and reflected waveforms using a time domain reflectometer. Time domain reflectometry was used as this technique allows the calculation of complex dielectric constant at any frequency within a large window from one set of waveform measurements.

Time domain reflectometry principles are first reviewed followed by a discussion of the measurement system. The chapter concludes with an analysis of system performance. A background review of basic electrical concepts is presented in Appendix A.

2.1 Time Domain Reflectometry (TDR)

A basic time domain reflectometer (TDR) setup is shown in Figure 7. The step generator produces a fast rising voltage step wave, which travels down the transmission line. Typical rise times for this wave are less than 1.0 ns. The wave is detected at the bridging tee by the sampling head and displayed on the oscilloscope. The sampling head has a high input impedance and therefore has very little effect on the observed waveforms. If a line mismatch exists at the load, a reflected wave is produced which propagates back to

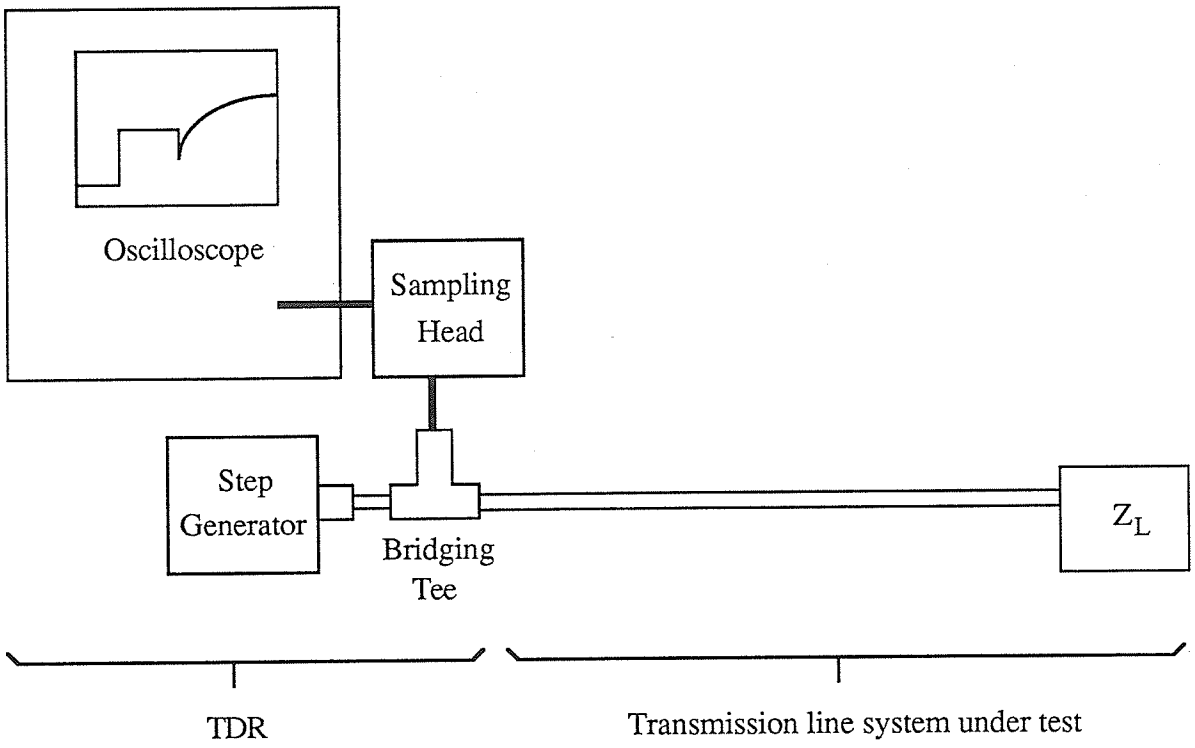

Figure 7: Basic TDR Setup

the generator superimposed on the incident wave. This second waveform is detected on the oscilloscope display when it reaches the bridging tee. The generator impedance is usually line matched, so no reflected wave is produced from the generator (Figure 8).

From an analysis of the incident and reflected waveforms on the oscilloscope, the position, type and magnitude of mismatches composed of linear, passive, frequency independent components may be evaluated. If E_r, the reflected waveform appears a time T after E_i, the initial pulse from the generator, the total distance, D, from the bridging tee to the mismatch is

$$D = \frac{v_p T}{2} \tag{3}$$

where v_p is the "average" or group velocity of propagation of the step pulse. The factor of 1/2 accounts for the wave travelling the distance D to the mismatch and the distance D back.

For a lossless transmission line, the type and magnitude of the linear time-invariant mismatches can also be determined from the shape and magnitude of E_r. Let the incident step pulse be u(t) and the impulse response of the load be h(t). The reflected wave or output, g(t), resulting from the application of u(t) to the load or system is

$$g(t) = h(t) * u(t) \tag{4}$$

where the '*' operator denotes the convolution of the two functions. Transforming (4) into the frequency domain using the Fourier transform yields

$$G(\omega) = H(\omega)\, U(\omega) \tag{5}$$

or,

$$H(\omega) = \frac{G(\omega)}{U(\omega)} \tag{6}$$

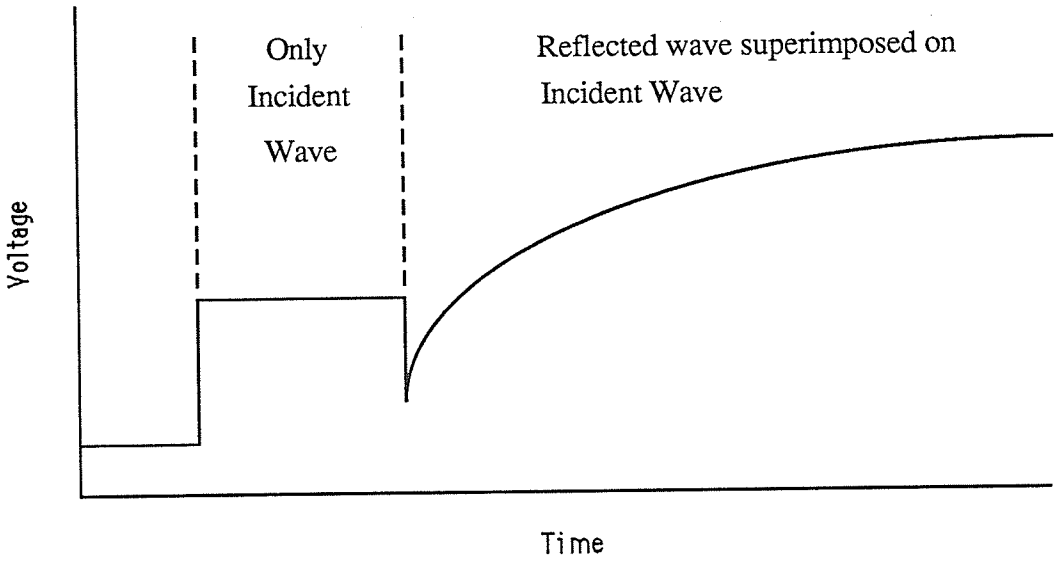

Figure 8: Example of a TDR waveform with line matched Step Generator

$U(\omega)$ can be obtained numerically from the observed waveform, u(t), or may be approximated by assuming that u(t) is an ideal step pulse. $G(\omega)$ can be determined from the observed waveform g(t). Since $G(\omega)$ is the reflected frequency component from $U(\omega)$, $H(\omega)$ is the reflection coefficient, $\rho(\omega)$, of the load. The value of the terminating impedance as a function of frequency is thus known by

$$Z_L(\omega) = Z_0 \frac{1 + H(\omega)}{1 - H(\omega)} . \tag{7}$$

Alternatively, taking the inverse Fourier transform of $H(\omega)$ yields h(t). From either h(t) or $Z_L(\omega)$, an equivalent circuit of the load can be constructed. For real (purely resistive) loads, the equivalent circuit is calculated easily since the reflected waveform is also a step pulse. Reflections from typical real loads are presented in Figure 9. Reflections from typical complex loads are presented in Figure 10.

2.2 Measurement of Complex Dielectric Constant Using TDR

2.2.1 Principle of Operation

The basic setup for measuring the complex dielectric constant, ε_s, of a sample using TDR is shown in Figure 11. A TDR unit is connected to the sample by a uniform transmission line. In some studies, the sample is contained in a sample holder. However, for this study, the open end of the transmission line was used. Samples are measured by applying the open end of the line to the tissue (Figure 12). The result of either configurations is the loading of the transmission line by a complex terminating impedance.

The impedance was calculated using the incident and reflected waveforms, u(t) and g(t), respectively. As a practical matter, the incident waveform was collected as the reflected waveform from an air sample, i.e., an open circuit termination. In addition, taking this waveform as the incident wave eliminated errors due to different time references

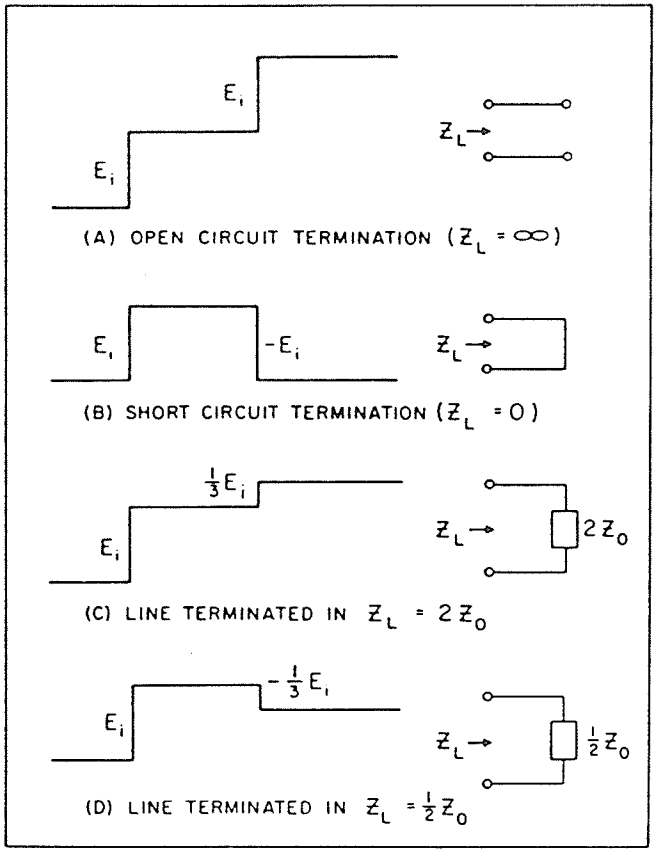

Figure 9: TDR reflections from typical real (resistive) terminating loads

Source: Reference [30]

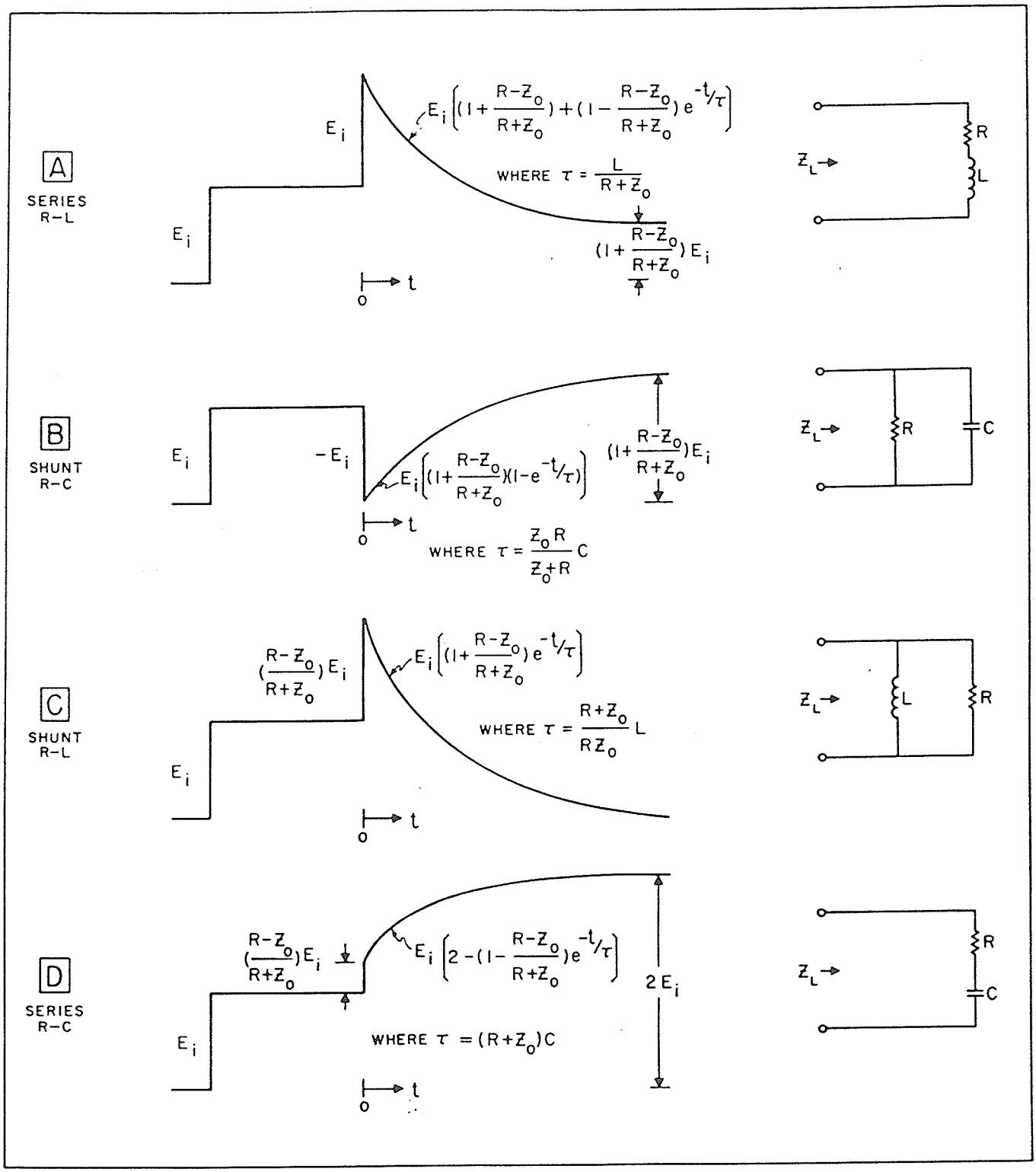

Figure 10: TDR reflections from typical complex loads

Source: Reference [30]

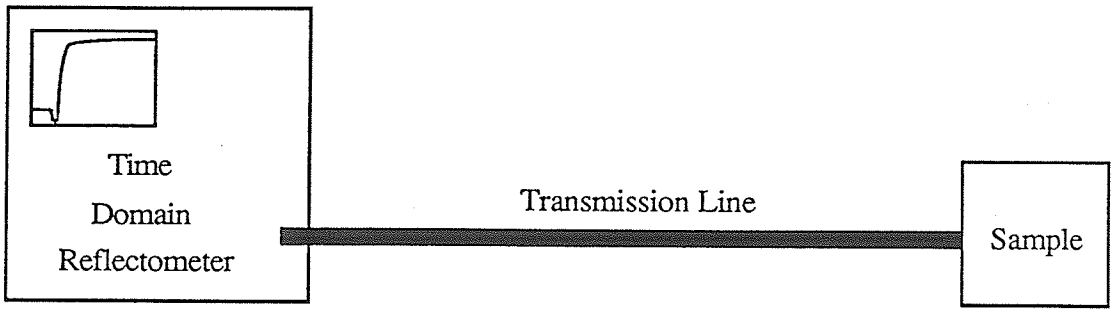

Figure 11: Basic Setup for measuring complex dielectric constant using TDR

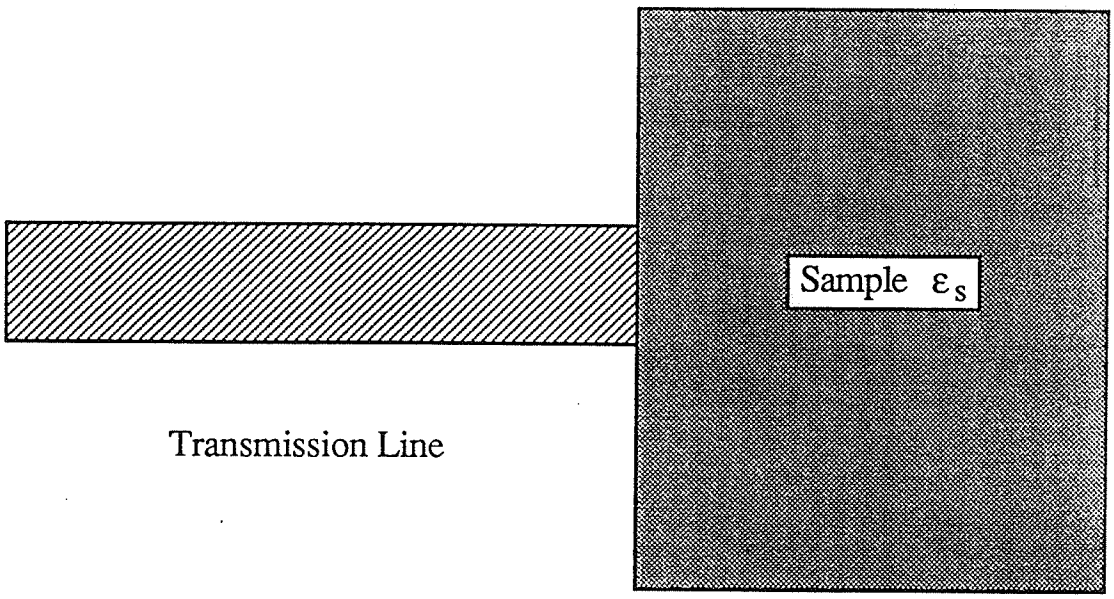

Figure 12: Application of transmission line to a tissue sample

between the waveforms and the attenuation and phase shift due to the length of the cable, as will be discussed. Since the open end of the cable presents an almost infinite impedance, the voltage reflection coefficient, ρ, may be taken as 1. Thus, the reflected waveform at the open end of the cable is identical to that of the incident waveform. This allowed the reflected waveform from tissue samples to be collected over the same time interval as those collected for the incident waveforms. No adjustment of the waveform interval was necessary between the collection of the two types of waveforms. This gave both the incident and reflected waveforms the same time reference, thus eliminating phase differences between the Fourier transforms of the two waveforms. Assuming the initial step had attained a constant voltage level over the collection time interval, the reflected waveform could be calculated by simply subtracting the dc component from the collected waveforms (Figure 13). All collected waveforms included the rise of the pulse, where most high frequency components are contained. From digitized traces of the waveforms on the oscilloscope, the corresponding Fourier transforms, $U(\omega)$ and $G(\omega)$, can be determined numerically.

The voltage reflection coefficient, ρ, can be derived from these transforms. However, the value of ρ depends on the incident and reflected waveforms at the load rather than at the oscilloscope. As each frequency component of a waveform at the oscilloscope is attenuated and out of phase with respect to its value at the load due to the length of the cable, d, $U(\omega)$ and $G(\omega)$ at the oscilloscope may be expressed as

$$\begin{aligned} U(\omega) &= U_L(\omega)\, e^{-\gamma(\omega)\, d} \\ G(\omega) &= G_L(\omega)\, e^{-\gamma(\omega)\, d} \end{aligned} \tag{8}$$

where $U_L(\omega)$ and $G_L(\omega)$ are the respective Fourier transforms at the load of the incident and reflected waveforms and $\gamma(\omega)$ is the propagation constant of the cable. Rearranging (8) yields

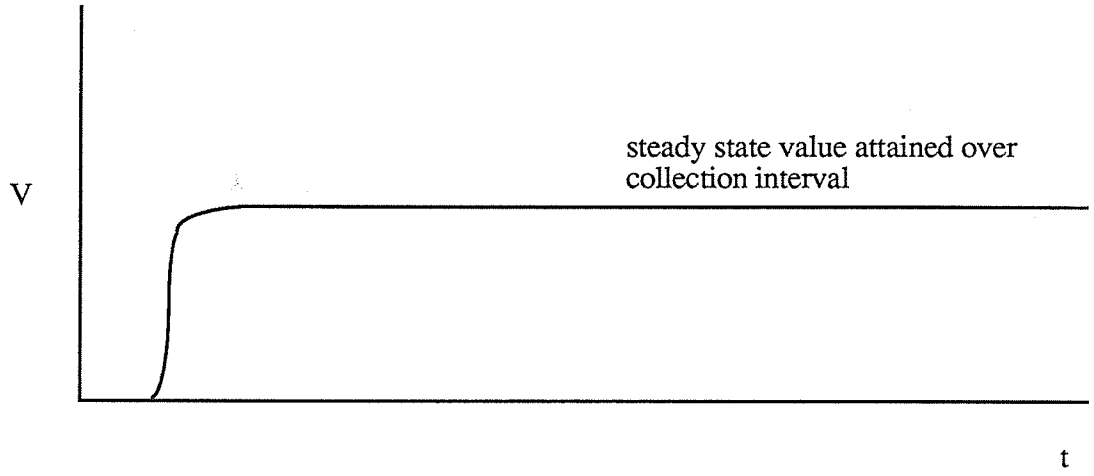

Initial pulse from step generator

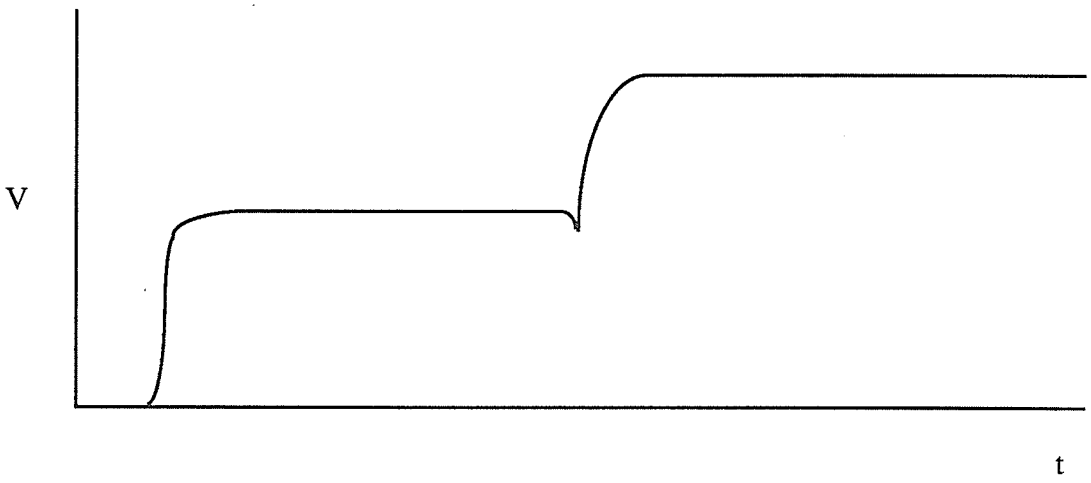

Reflected pulse from load superimposed on constant value

Figure 13: Reflected wave added to a constant value

$$U_L(\omega) = U(\omega)\, e^{+\gamma(\omega)\, d}$$

$$G_L(\omega) = G(\omega)\, e^{+\gamma(\omega)\, d}. \tag{9}$$

The reflection coefficient, $\rho(\omega)$, is then given by

$$\rho(\omega) = \frac{G_L(\omega)}{U_L(\omega)} = \frac{G(\omega)\, e^{+\gamma(\omega)\, d}}{U(\omega)\, e^{+\gamma(\omega)\, d}} = \frac{G(\omega)}{U(\omega)}. \tag{10}$$

Thus, $\rho(\omega)$ may be determined using only the incident and reflected waveforms at the oscilloscope. This eliminated errors due to one of the transforms being attenuated or out of phase with respect to the other due to the length of the cable. Note that in general, ρ is a complex number. Assuming low-loss transmission lines, the value of Z_0 may be considered constant. With ρ defined by (10) the terminating impedance, Z_L, may be determined by

$$Z_L = Z_0 \frac{1 + \rho(\omega)}{1 - \rho(\omega)}. \tag{11}$$

A lumped parameter equivalent circuit was used to model the termination of the coaxial cable with the tissue. Model parameters were determined using the measured load impedance values, Z_L. From this, the relative complex dielectric constant of the sample is obtained. For this study, two equivalent circuits, a two element circuit and a four element circuit, were investigated. In either case, the load impedance could be represented as a simple complex (lossy) capacitance, C_L,

$$C_L = \frac{1}{j\,\omega\, Z_L}. \tag{12}$$

No circuit elements in either circuit were used to represent radiative effects from the tip of the cable as these were assumed negligible over the frequencies considered.

The two element circuit is comprised of two shunt capacitances, C_f and C_t, to represent the fringing field capacitance within the cable dielectric at the open end of the cable and the capacitance of the tissue sample, respectively (Figure 14). The sample capacitance is equal to $\varepsilon_S C_0$ where ε_S is the relative complex dielectric constant of the sample and C_0 is the capacitance of an air sample. Thus, the capacitance, C_L, is equal to

$$C_L = C_f + \varepsilon_S C_0 \tag{13}$$

from which the complex dielectric constant of the sample, ε_S, may be determined. The values C_0 and C_f can be determined from empirical measurements of two samples with known dielectric constants, ε_{S1} and ε_{S2},

$$\begin{aligned} C_{L1} &= C_f + \varepsilon_{S1} C_0 \\ C_{L2} &= C_f + \varepsilon_{S2} C_0. \end{aligned} \tag{14}$$

This system of equations may be solved for the unknown constants, C_0 and C_f,

$$\begin{aligned} C_0 &= \frac{C_{L1} - C_{L2}}{\varepsilon_{s1} - \varepsilon_{s2}} \\ C_f &= C_{L1} + \varepsilon_{S1} C_0. \end{aligned} \tag{15}$$

The sample dielectric constant is determined using (11), (12), and (13),

$$\varepsilon_s(\omega) = \frac{1 - \rho(\omega)}{j\omega Z_0 C_0 (1 + \rho(\omega))} - \frac{C_f}{C_0}. \tag{16}$$

The four element circuit is shown in Figure 15. The two shunt capacitances represent the electric field component tangential to the interface while the two series capacitances represent the electric field normal to the interface [21]. The capacitance, C_L, represented by this circuit may be written as

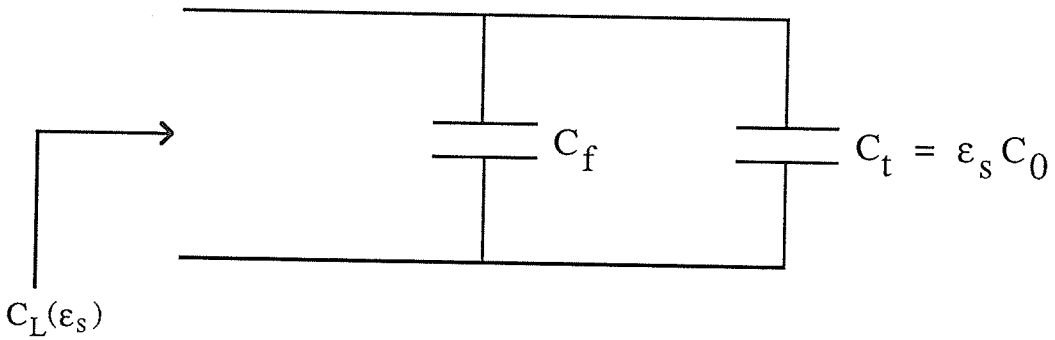

Figure 14: Two element lumped parameter circuit for open-ended cable

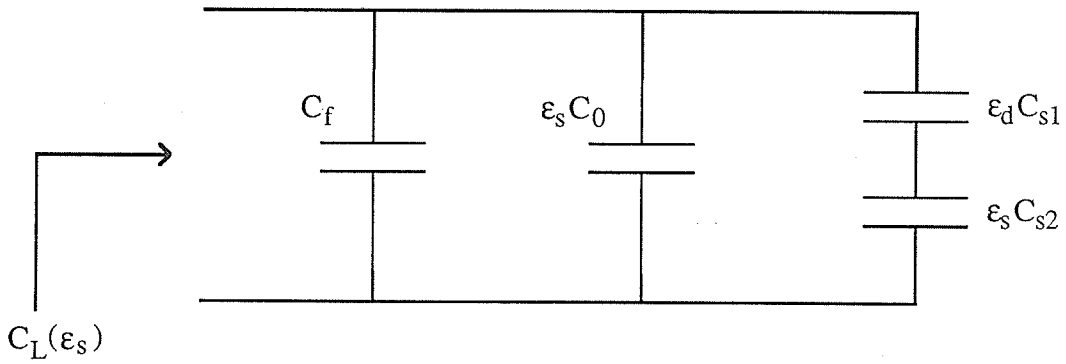

Figure 15: Four element equivalent circuit for the open-ended cable

$$C_L(\varepsilon_s) = C_f + \varepsilon_s C_0 + \frac{\varepsilon_s C_s}{1 + \varepsilon_s k \dfrac{C_s}{\varepsilon_0 (b - a)}} \tag{17}$$

where C_f is the tangential fringing field capacitance in the cable dielectric, C_0 is the tangential fringing field capacitance in the sample , C_s is the equivalent series fringing field capacitance in the sample, and k is a constant. The values of the capacitances normalized to free space permittivity ε_0 and dielectric thickness (b-a) for teflon cables have been determined using the method of moments [21] and are listed in Table 1. With the exception of the last term, (17) is the same as (13) for the 2 element circuit. The last term, when written with the value for $C_s/\varepsilon_0(b-a)$ from Table 1, is

$$\frac{\varepsilon_s C_s}{1 + 0.32\, \varepsilon_s} \tag{18}$$

In comparing this term to the sample capacitance, $C_t = \varepsilon_s C_0$, it is apparent that it is smaller, since by Table 1,

$$| C_0 | > | C_s |$$

which implies

$$| \varepsilon_s C_0 | > | \varepsilon_s C_s |$$

or, since the real dielectric constant, $\mathrm{Re}\{\varepsilon_s\} > 0$,

$$| C_t | = | \varepsilon_s C_0 | > \left| \frac{\varepsilon_s C_s}{1 + 0.32\, \varepsilon_s} \right| . \tag{19}$$

For cerebral white matter, where the real dielectric constant is greater than 30 over the frequencies considered, 100 - 1000 MHz [62], equation (19) becomes approximately

$$| C_t | > \left| \frac{\varepsilon_s C_s}{1 + 0.32\, (30)} \right|$$

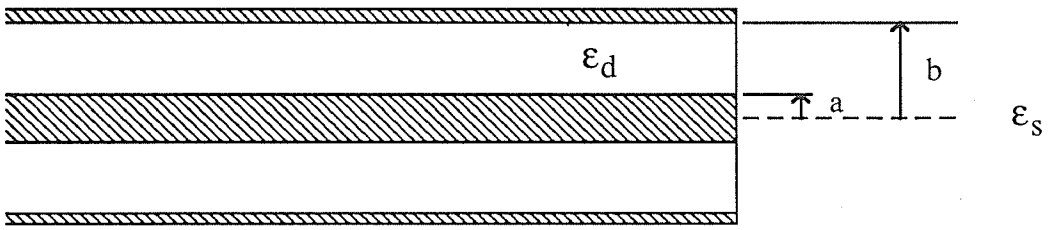

C_f/ε_0(b-a)	C_0/ε_0(b-a)	C_s/ε_0(b-a)	k
0.404	1.953	0.500	0.647

Table 1: Normalized values for 4 element circuit

Source: Reference [21]

$$| C_t | > \left| \frac{\varepsilon_s C_s}{11} \right| . \qquad (20)$$

Thus, for the frequencies and type of tissue considered in this study, this last term is very small compared to the sample capacitance. This circuit may be considered a higher order model than the 2 element model where the last term in (17) represents the truncation error. As all the circuit parameters are known from the cable dimensions and Table 1, (17) may be solved for ε_S. However, of the two solutions obtained from the resulting quadratic equation, only one can be valid. The valid solution has a positive real part.

Accuracy tests were performed by using both equivalent circuits to calculate the dielectric constants of liquids with known dielectric constants, namely distilled water, saline and methanol. The circuit which predicted the dielectric constant closest to the known values was used to analyze data from biological samples.

2.2.2 Numerical Calculation of Fourier Transforms

As mentioned, the determination of the reflection coefficient, $\rho(\omega)$, required the Fourier transforms of the measured incident and reflected waveforms. Here, certain aspects of the numerical determination of the observed waveforms are discussed.

Observed waveforms were digitized to N points (N=512 in this study) spanning T_S (T_S = 5.0 ns) seconds where the constant value from the initial step pulse was subtracted from all collected waveforms. Simpson's rule for numerical integration was then applied to the digitized waveform data in the Fourier transform equation,

$$X(\omega) = \int_{-\infty}^{+\infty} x(t)\, e^{-j\,\omega\, t}\, dt$$

$$= \int_{-\infty}^{+\infty} x(t)\, \cos \omega t\, dt + j \int_{-\infty}^{+\infty} x(t)\, \sin \omega t\, dt \qquad (21)$$

where x(t) is a digitized waveform. However, no information on x(t) is known after the N^{th} digitized point. As the TDR waveform is ideally of infinite duration, the remainder of the waveform was approximated by a step pulse shifted T_S seconds to the right with height equal to that of the N^{th} digitized point in order to eliminate large truncation error (Figure 16). This approximation assumes that the reflected waveform achieved a steady state voltage by T_S seconds. The approximate Fourier transform of the waveform was obtained by adding the Fourier transform of the shifted step pulse to the numerical summation.

2.2.3 Determination of the Frequency Window

The frequency window is defined as the range of frequencies where calculations of complex dielectric constant are accurate. This is limited by the frequency information contained in the collected waveform.

The lower boundary of the window is determined by the minimum frequency which may be resolved from the digitized waveform (Figure 17). This boundary, f_L, may be arbitrarily selected as where half the period of a sinusoid at this frequency equals the time span, T_0, of the collected portion of the step. Thus, f_L may be determined from

$$f_L = \frac{1}{2\,T_0} \tag{22}$$

Note that the shifted step pulse was ignored in the derivation of (22). The effect of the shifted step pulse is to reduce truncation error by supplementing the information stored in the data. Thus , the actual value of f_L is lower than that given by (22) due to the presence of the shifted pulse.

The upper boundary for the frequency window is determined by two factors, the time between digitized points, T, and the rise time, T_r, By the sampling theorem, only bandlimited signals x(t) with $X(\omega)=0$ for $\omega_M > \pi / T$ may be uniquely constructed from its samples taken at every time T. In practice, however, ω_M is often taken as 1/10 its

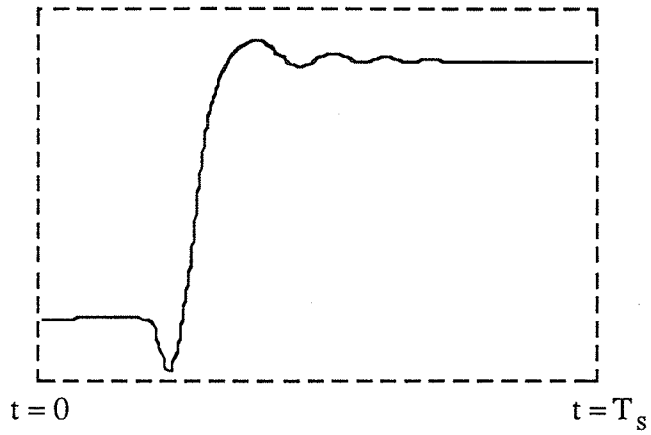

Typical Collected TDR Waveform

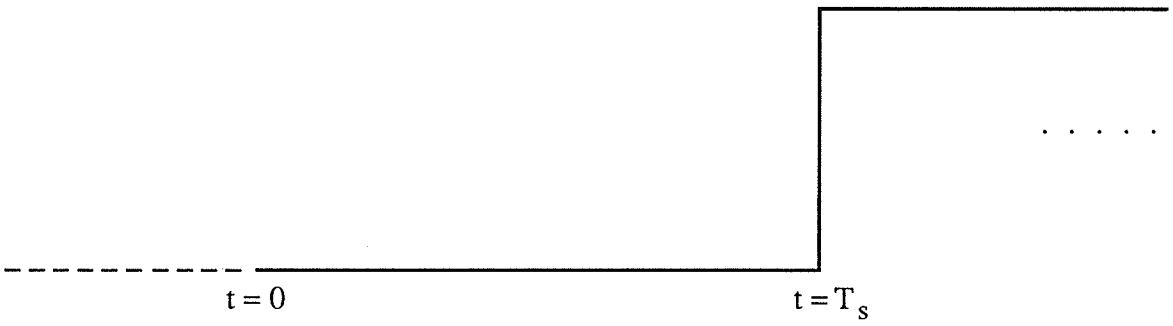

Step Pulse Approximation added to collected waveform

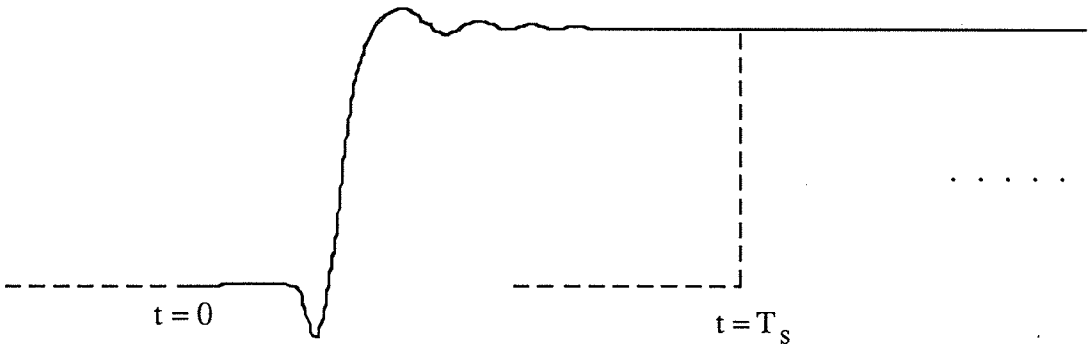

Approximated TDR Waveform

Figure 16: Approximation of TDR waveform from collected data

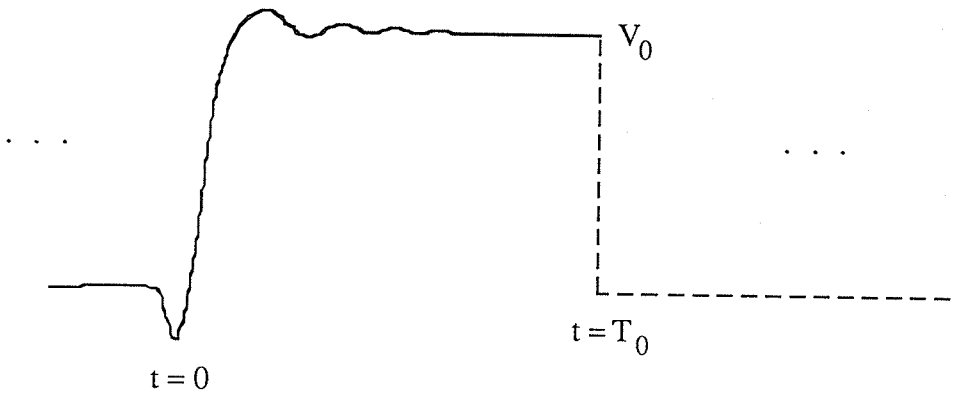

Collected Waveform

Figure 17: Example of a Collected TDR Waveform

theoretical value to ensure no aliasing of the signal occurs. This frequency, $\omega_M/10$, may be considered as an upper frequency boundary limiting calculation due to the digitization of the waveform. The highest frequency component resolveable from a waveform also limits the frequency window. This frequency, f_H, is a limitation of the sampling head of the TDR. A model of an observed waveform and shifted step pulse is given in Figure 18. The shifted step pulse is included since its exclusion would introduce extraneous high frequency components into the analysis. The Laplace transform of y(t) is

$$L\{y(t)\} = Y(s) = \frac{V_0}{s^2 T_r}(1 - e^{-sT_r}) = \frac{V_0}{s}\left[\frac{(1 - e^{-sT_r})}{sT_r}\right]. \tag{23}$$

Y(s) may be considered to be the output of a filter H(s) after an ideal step pulse of height V_0 has been applied to it, where H(s) is defined as

$$H(s) = \frac{(1 - e^{-sT_r})}{sT_r}. \tag{24}$$

At lower frequencies, Y(s) approaches the Fourier transform of a step pulse of height V_0. This can be demonstrated by taking the limit of H(s) as s approaches 0 using L'Hospital's rule,

$$\begin{aligned} \lim_{s\Rightarrow 0} H(s) &= \lim_{s\Rightarrow 0} \frac{(1 - e^{-sT_r})}{sT_r} \\ &= \lim_{s\Rightarrow 0} \frac{T_r e^{-sT_r}}{T_r} \\ &= 1. \end{aligned} \tag{25}$$

Thus, at lower frequencies, the filter passes the step pulse with little distortion. However, as the frequency is increased from 0, the value of H(s) decreases due the factor s in the denominator. At frequencies corresponding to

$$\omega T_r = 2\pi, 4\pi, 6\pi \ldots \tag{26}$$

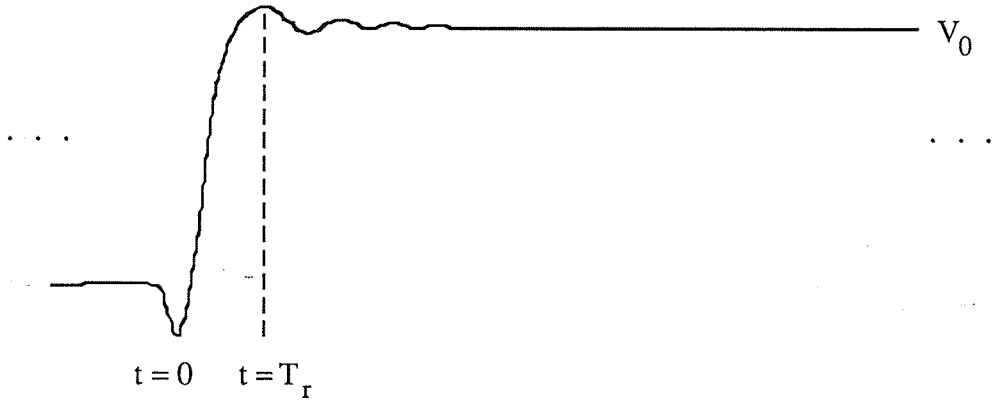

Approximated TDR Waveform

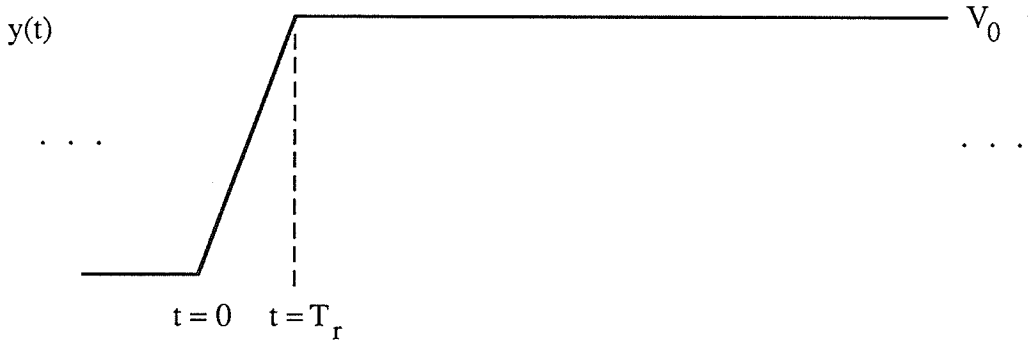

Model of Approximated Waveform

Figure 18: Model of TDR waveform used to determine higher frequency boundary

H(s) equals zero. The upper frequency limit may be considered to occur at the half power point for the filter,

$$\left| \frac{V_0}{s} \frac{(1 - e^{-sT_r})}{sT_r} \right| = \frac{1}{\sqrt{2}} \left| \frac{V_0}{s} \right|$$

or,

$$\left| \frac{(1 - e^{-sT_r})}{sT_r} \right| = \frac{1}{\sqrt{2}} . \tag{27}$$

Solving (27) gives

$$\omega T_r = 2.783$$

or,

$$f_H = \frac{0.443}{T_r} . \tag{28}$$

This upper frequency is determined by the value of T_r. The upper frequency boundary was chosen as the lower of the two values derived above.

The above analysis illustrate the factors which determine the frequency window. The lower boundary may be decreased by increasing the time span of the collected waveform, T_0. The upper boundary may be increased by decreasing the time between samples, T, and decreasing the pulse rise time, T_r.

The rise time is an important factor in determining the frequency window. It is sensitive, however, to the length and type of cable chosen. The attenuation of higher frequencies and dispersion factors increase the value of T_r. Either use of low-distortion cable, such as air cable, or shorter cabling minimizes the deterioration of the rise time.

2.3 System Performance

Sources of error in the technique are described in this section. First, an uncertainty analysis is presented where it is shown that limitations in the equipment affect the accuracy of measurement of some materials. The section concludes with a brief discussion of other possible sources of error.

2.3.1 Uncertainty Analysis

The uncertainty analysis presented gives an indication of the type of materials for which the real dielectric constant, ε', and loss factor, ε'', can be accurately measured using the technique described in section 2.2. Actual uncertainties in the measurements were not estimated for this study.

An uncertainty analysis for the measurement of dielectric constant from its reflection coefficient at one frequency has been derived by Stuchly et al [58] using the 2 element model. It is reasonable to assume that the analysis holds, in general, for the 4 element model since the last term in (17) is very small in comparison to the sample capacitance, $\varepsilon_s C_0$. Thus, (17) reduces to (13) for the 2 element model for the range of dielectric constants considered (see section 2.2.1). The analysis ignored the effects of the fringing capacitance in (13). However, as the value of C_f / C_0 is very small ($C_f / C_0 < 0.3$) in comparison to the measured dielectric constant, this assumption is reasonable. It should be noted that only systematic errors, or uncertainties in measurements due to the equipment used, were modelled. From equation (16), the following equations were obtained for the uncertainties,

$$\frac{\Delta \varepsilon_r'}{\varepsilon_r'} = \left\{ \left(\frac{\Delta C_0}{C_0}\right)^2 + \left(\frac{\Delta Z_0}{Z_0}\right)^2 + \left(\frac{1 - 2|\rho| / \cos\phi + |\rho|^2}{1 + 2|\rho|\cos\phi + |\rho|^2} \times \frac{\Delta\phi}{\tan\phi} \right)^2 + \left(\frac{1 - |\rho|^2}{1 + 2|\rho|\cos\phi + |\rho|^2} \times \frac{\Delta|\rho|}{|\rho|} \right)^2 \right\}^{1/2} \quad (29a)$$

$$\frac{\Delta \varepsilon_r''}{\varepsilon_r''} = \left\{ \left(\frac{\Delta C_0}{C_0}\right)^2 + \left(\frac{\Delta Z_0}{Z_0}\right)^2 + \left(\frac{2|\rho|\sin\phi}{1 + 2|\rho|\cos\phi + |\rho|^2} \times \Delta\phi \right)^2 + \left(\frac{4|\rho| + 2\cos\phi + 2|\rho|^2\cos\phi}{\left(1 - |\rho|^2\right)\left(1 + 2|\rho|\cos\phi + |\rho|^2\right)} \times \Delta|\rho| \right)^2 \right\}^{1/2} \quad (29b)$$

where $|\rho|$ and ϕ are respectively the magnitude and the phase angle of the reflection coefficient, ρ, at the frequency considered respectively. The uncertainty in ε_r' depends primarily on the value of ϕ. For values of ϕ approaching - 180^0, and $|\rho|$ approaching 1 (i.e., samples which are good conductors at the frequency considered where $\varepsilon_r'' \gg \varepsilon_r'$), the uncertainty approaches infinity due to the tan ϕ factor in the denominator of the 3rd term of (29a). As ϕ approaches 90^o in (29a), the uncertainty falls rapidly. The uncertainty in ε_r'' depends primarily on the value of $\Delta|\rho|$ and $|\rho|$ for all values of ϕ. As ϕ approaches 0^0 and $|\rho|^2$ approaches 1, or alternatively as $|\rho|$ approaches 1, (i.e., samples which present a very high impedance at the frequency considered) the 4th term in (29b) approaches infinity. The $\Delta|\rho|$ factor, however, affects the rate at which this term approaches infinity.

If a lossless material ($\varepsilon_r' \gg \varepsilon_r'' \approx 0$ at the frequency considered) is measured, then $|\rho|$ approaches 1 and $-180^0 < \phi < 0^0$ (see equation A.13 in Appendix A). The uncertainties for such materials are thus

$$\frac{\Delta \varepsilon_r'}{\varepsilon_r'} = \left\{ \left(\frac{\Delta C_0}{C_0} \right)^2 + \left(\frac{\Delta Z_0}{Z_0} \right)^2 + \left(\frac{2 - 2/\cos\phi}{2 + 2\cos\phi} \times \frac{\Delta\phi}{\tan\phi} \right)^2 \right\}^{1/2} \tag{30a}$$

$$\frac{\Delta \varepsilon_r''}{\varepsilon_r''} = \left\{ \begin{array}{c} \left(\frac{\Delta C_0}{C_0} \right)^2 + \left(\frac{\Delta Z_0}{Z_0} \right)^2 + \left(\frac{\sin\phi}{1+\cos\phi} \times \Delta\phi \right)^2 \\ + \left(\frac{2}{\left(1 - |\rho|^2\right)} \times \Delta|\rho| \right)^2 \end{array} \right\}^{1/2} \tag{30b}$$

The uncertainty in ε_r' is least for low permittivity materials (ϕ approaches 0^0). For high permittivity materials (ϕ approaches -180^0), the uncertainty approaches infinity due to the $\tan\phi$ factor in the denominator of the 3rd term of (30a). The uncertainty in ε_r'', however, approaches infinity regardless of the value of ϕ as a result of $|\rho|$ tending to 1. Thus, measurements of low loss materials will contain larger uncertainties in loss factor than those for more lossy materials.

The type of substances which may be measured accurately is restricted to those which are lossy materials, but not good conductors over the range of frequencies considered. Such materials include soft biological tissue and saline. However, the measured impedance must be large enough to ensure the reflection coefficient does not approach 1. For the open-ended cable configuration used in this study, the diameter of the cable directly affects the value of the measured impedance since a larger dielectric thickness increases the value of C_0 in both (13) and (17). For lossless materials, the uncertainty is

least for low permittivities though loss factor measurements would contain higher uncertainties then more lossy materials.

2.3.2 Practical Limitations to the Accuracy of Measurements

Several practical limitations affect the accuracy of measurements. These include noise present in the collected waveform, drift, radiation of signal energy from the open-ended cable, unwanted reflections and errors in obtaining the TDR waveforms from the digitized data. These factors are briefly discussed in this section.

Noise

Noise is the result of signal channel noise in the sampler and time-base circuitry jitter [10]. Noise present in a digitized waveform affect mostly the high frequency accuracy of the technique. The effects of noise may be greatly reduced by time averaging several signals [10], as was performed for waveform collection in this study.

Drift

Over long periods of time, a TDR waveform may drift by several picoseconds. Incident and reflected waveforms collected between such times will contain a time shift due to the drift, thus introducing phase errors into the Fourier transform of the signal. Again, the higher frequency components are affected most. This effect may be reduced by allowing the TDR unit a warmup time and minimizing the time between the collection of the incident and reflected waveforms. Both these procedures were used in the collection of waveform data.

Radiation of the TDR signal from the open-ended cable

For lower frequencies, where the dimensions of the line are small compared with the wavelength, the open end of the cable radiates very little energy. Almost all of the energy is stored in the fringe field emanating from the end of the cable. At higher frequencies, energy is radiated into the sample. The effect of this radiation is to cause the value C_0 to become a function of frequency [39]. In addition, a shunt resistance

representing the energy lost in the sample must be included along with the sample impedance in the equivalent circuit for the terminating impedance. If these parameters are not considered at these higher frequencies, errors in the evaluation of the complex dielectric constant occur. For the size of cable used in this study (0.141" outer diameter), it has been shown that radiation may be considered insignificant over the range over the frequencies considered of 100 - 1000 MHz [59].

Unwanted Reflections

Extraneous reflections from discontinuities such as connectors and line mismatches affect the observed waveform. Appropriate lengths of cable were chosen to place large reflections outside the time window. However, a smaller reflection was included in the time window to avoid the use of long cables, as will be discussed in chapter III. Long cabling increases the rise time of the waveform and lowers the upper frequency boundary, f_L, as was noted in section 2.2.3. In addition, all connections were cleaned in order to reduce mismatch.

Errors in Obtaining TDR Waveforms from the Digitized Data

Errors in the TDR waveform result from the the subtraction of the constant level of the initial step from all collected waveforms. The initial step has some variation over the time window. However, for this study this variation was observed to be less than 1 % of the height of the reflected waveform. Thus, errors introduced by this factor are relatively small. Truncation error also introduces error into the measurements. To determine the Fourier transform of a TDR waveform, it was assumed that the voltage had attained a constant level by the end of the time window. The Fourier transform of a shifted step pulse was added to that of the collected waveform to approximate the Fourier transform of the infinite TDR waveform. The terminating impedance may be modelled as a resistance and a capacitance in shunt. Thus, after the application of the step pulse, the voltage reflected from the sample would rise indefinitely approaching a constant. At the end of the time window, the voltage would not have reached a constant value. However, as the time

constants of the samples measured in this thesis were small, the voltage would be very close to the final value.

Chapter III

Materials and Method

The experimental apparatus and the procedure for dielectric constant measurement are first presented in this chapter. This is followed by the method for preparation of tissue samples.

3.1 Experimental Setup

High frequency complex dielectric constant was measured in all samples using a Time Domain Reflectometer (TDR) connected to an open-ended coaxial transmission line. The TDR unit consisted of a Tektronix 7854 oscilloscope with 7S12 TDR/ Sampler plug-in unit. An S-52 pulse generator and an S-2 sampling head were used for step pulse generation and signal detection, respectively. A Tektronix GURU package installed in an IBM personal computer was used to retrieve digitized waveforms from the oscilloscope.

The transmission line consisted of 60 cm of flexible RG58A cable connected through an SMA connector to 30 cm of 50 Ω semirigid 0.141" coaxial cable (0.0359 ± 0.0005 inches inner conductor outer diameter, 0.1175 ± 0.001 inches dielectric outer diameter). All connections were cleaned with circuit cleaner to reduce the effects of any discontinuities introduced by the connector. The open end of the semirigid cable was slightly rounded so as to reduce the possibility of air being trapped beneath the cable during measurements.

The S-2 sampling head does not have a high input impedance. Its 50 Ω input impedance reduced the height of the incident wave by 1/ 3. Moreover, the sampling head was not line matched and caused multiple reflections in the transmission line. The total length of the line was chosen to completely avoid measurement of multiple reflections of the step pulse. The lengths of cable making up the transmission line were calculated to place reflections from the SMA connector approximately 3.0 ns after the beginning of the pulse. This time was chosen since it placed reflections away from the step rise, or high frequency portion of the waveform while keeping the cable length as short as possible to minimize rise time.

3.2 Determination of Complex Dielectric Constant

3.2.1 Collection of Waveform Data

Prior to all measurements, the TDR unit was allowed a warmup time of 2 - 6 hours in order to minimize drift. The time window and voltage scale were set and were not altered throughout an entire experiment. Collected waveforms spanned 5.0 ns and began approximately 0.5 ns before the pulse. The voltage scale was adjusted to fit the waveform to the full screen. The rise time of an incident pulse collected from the oscilloscope was measured to be approximately 100 ps. One hundred signals were averaged by the oscilloscope in order to minimize observed noise on the waveforms. Individual waveforms were displayed using the high resolution function on the TDR unit. The averaged waveforms were digitized to 512 points and transferred using a GURU package to an IBM personal computer for storage. Each point was stored as its vertical distance from the bottom of the oscilloscope grid, in hundredths of millimeters.

3.2.2 Calculation of Complex Dielectric Constant

Listings of the programs to calculate the complex dielectric constant using the 2 element and the 4 element models are given in Appendix B.

The frequency window was calculated from the measured waveform parameters to determine the frequencies where complex dielectric constant could be measured accurately. By (22), the lower frequency boundary, f_L, was 111.1 MHz. As noted, due to the presence of the shifted step pulse added to each waveform, f_L is lower than this value. The upper frequency boundary determined by the digitization of the signal was $f_M / 10 =$ 5110 MHz while the upper boundary determined by the rise time of the pulse was 4429.5 MHz. The upper boundary, f_H, was thus taken as 4429.5 MHz giving a total frequency range of 4318.4 MHz. Based on this frequency window, the complex dielectric constant was calculated at 100.0, 250.0, 500.0, 750.0 and 1000.0 MHz.

Analysis of the waveforms was performed using double precision FORTRAN. In order to calculate their Fourier transforms, both incident and reflected waveforms had to be adjusted to the same voltage level and time reference. This was accomplished by setting zero voltage (the steady state dc level of the initial step) and zero time as occurring at the 6^{th} digitized point (49 ps after the first digitized point). This location was chosen as the first 5 points of each waveform occasionally contained noise and thus were not included in the data analysis. The value of the 6^{th} point was first subtracted from each digitized point. Fourier transforms of the waveforms were evaluated by applying Simpson's rule for numerical integration to the remaining data in the Fourier transform equation. The Fourier transform of a step pulse with height equal to that of the 512^{th} point and shifted by 4.94 ns to the right was added to the numerical summation to reduce the truncation error of approximating the infinite TDR pulse (see Section 2.2.2). No multiplicative factors were introduced to the waveforms to scale them to their actual voltage values. This was unnecessary since only the ratio of the transforms is needed to calculate the voltage reflection coefficient, ρ, in (10) rather than the actual transform values. Once ρ had been calculated, Z_L and C_L could be determined using (11) and (12), respectively. From C_L, the complex dielectric constant could be calculated using either the 2 element or the 4 element lumped parameter circuit.

The constants C_0 and C_f required in (16) for the calculation of complex dielectric constant using the 2 element model were determined using measurements of air and of distilled water taken at 100.0, 250.0, 500.0, 750.0 and 1000.0 MHz. Measurements for the capacitance of the cable in air were taken from published data for the capacitance of an open-ended 0.141" coaxial line [39]. The total capacitance of the open-ended cable was taken as constant since its variation over the frequencies considered was less than 0.03 % [39]. Since the real dielectric constant of distilled water is much greater than its loss factor from 100 to 1000 MHz [6], this substance was taken as lossless. Thus, based on the uncertainty analysis given in section 2.2.3, loss factor measurements were considered inaccurate over this frequency range. Consequently, only the capacitive component of C_L in (12) was used to determine the values of C_0 and C_f. The real dielectric constant of distilled water was linearly interpolated as a function of the log of the measuring frequency from tabulated data [6]. Five measurements of distilled water were performed at each frequency. For each measurement, the tip of the cable was cleaned with distilled water, dried and the incident waveform collected. The open end of the transmission line was then lowered vertically to a depth of 1.0 cm into 200 ml of fluid contained in a 250 ml beaker (Figure 19), after which the reflected waveform was collected. Care was taken to ensure no air was trapped beneath the cable. The temperature at which measurements were performed was also recorded. C_0 and C_f were calculated at each frequency using (14), where C_{L1} equals 22.4 pF, ε_{s1} equals 1.0 for air, C_{L2} is the average capacitance measured at frequency f and ε_{s2} is the dielectric constant of water at frequency f. The constants C_0 and C_f used to analyze data were the averages of the values obtained at each frequency. This procedure was repeated with the open end of the cable applied to the surface of the liquid (Figure 20). The complex dielectric constant of a sample was calculated using these averaged values in equation (16).

Constants C_f, C_0 and C_s for the 4 element method were calculated from Table 1 and the appropriate cable dimensions. For the chosen cable, they are

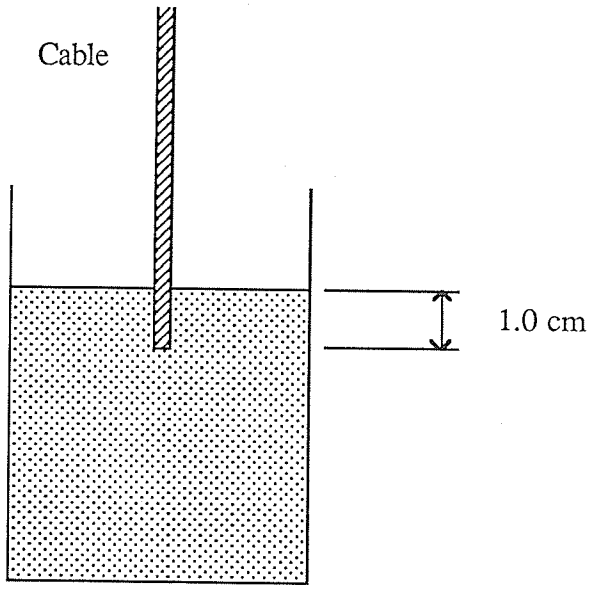

Figure 19: Cable Submerged in Liquid for Tests

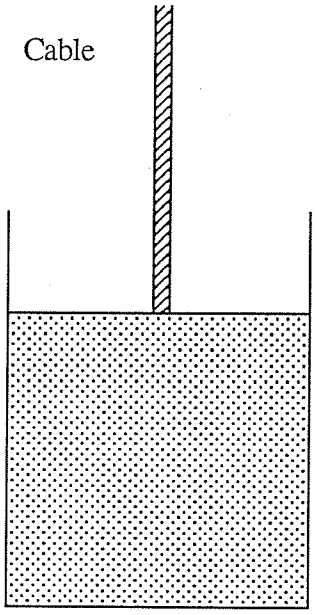

Figure 20: Cable Placed at Surface of Liquid for Tests

$$C_f = 0.371 \text{ pF}$$
$$C_s = 4.588 \text{ pF} \quad (29)$$
$$C_0 = 17.920 \text{ pF}$$

These values were used in (17) to solve for the complex dielectric constant of a sample where as noted, only the solution giving a positive real part, or positive real dielectric constant, is valid.

3.3 Accuracy Tests

The accuracy of both equivalent circuits was assessed by measurement of the complex dielectric constant of three known liquids, namely distilled water, methanol, and saline. Before each measurement, the tip of the cable was cleaned with methanol, dried and the incident waveform collected. The head was then lowered vertically to a depth of 1.0 cm into 200 ml of fluid contained in a 250 ml beaker (Figure 19) after which the reflected waveform was measured. Care was taken to ensure no air was trapped beneath the cable. This procedure was repeated 5 times for each liquid. The temperature at which measurements were conducted was recorded The average complex permittivities and standard errors for each liquid were calculated at 100.0, 250.0, 500.0, 750.0 and 1000.0 MHz for comparison with published data. An accuracy test following the same procedure was performed for the application of the cable to the surface of the liquid (Figure 20). The equivalent circuit which best agreed with published data was used to analyze measurements from biological tissues.

3.4 Minimum Sample Size

Minimum sample size was established for saline and distilled water using the more accurate equivalent circuit determined from the accuracy test. For this purpose, the cable was lowered vertically into a petri dish filled to a depth of 10 mm with liquid (Figure 21).

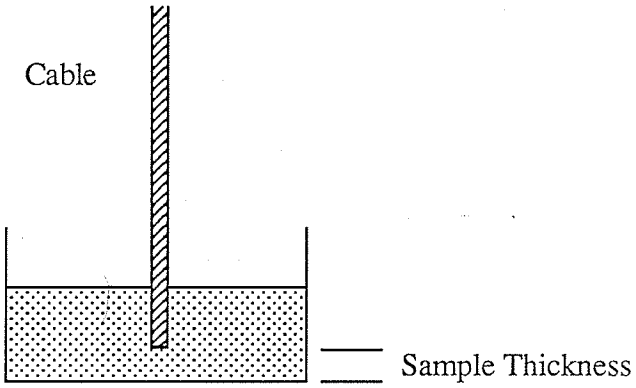

Figure 21: Setup to Measure Minimum Sample Thickness with Cable Submerged

The distance from the tip of the cable to the bottom of the dish, or sample thickness, was altered from 5.0 mm to 1.0 mm in steps of 1.0 mm. At each thickness, 5 measurements were performed following the same procedure for cable preparation and waveform collection as in the accuracy test. The averages and standard errors of dielectric constant and loss factor were calculated at 100.0, 250.0, 500.0, 750.0 and 1000.0 MHz for comparison with values established by the accuracy test. The minimum sample thickness, z, for a dielectric parameter was taken as the largest thickness for which any of its averages at each frequency changed by more than 5 %. The above procedure was repeated for the configuration with the cable at the surface of the liquid. Sample thicknesses were varied by altering the depth of saline in the petri dish (Figure 22). The minimum sample thickness was taken as the largest value z, determined for either distilled water or saline, with an added margin of error. The minimum sample volume was taken as the volume of tissue within a distance z from the center of the head.

3.5 Preparation of In-Vitro Samples

3.5.1 In-Vitro Production of Osmotic Edema

Thirteen dogs were sacrificed either through intravenous injection of sodium chloride, overdose of sodium pentobarbital (Nembutal) or blood vasation. The cerebral hemispheres were removed immediately. For nine dogs, the hemispheres were placed within thick plastic containers and frozen for tissue preservation at -30^{o} C. Within one week of removal, these brains were thawed at room temperature and measured. For the remaining four brains, the cerebral hemispheres were removed immediately and measured within six hours. For measurement, each brain was cut into 8 coronal slices (Figure 23). Control specimens were kept normal while experimental specimens were made edematous. In-vitro cerebral osmotic edema was produced by immersion of slices in distilled water. Different water contents were achieved by soaking the samples for different times. Slices from the right hemisphere were immersed in water while those from the left hemisphere

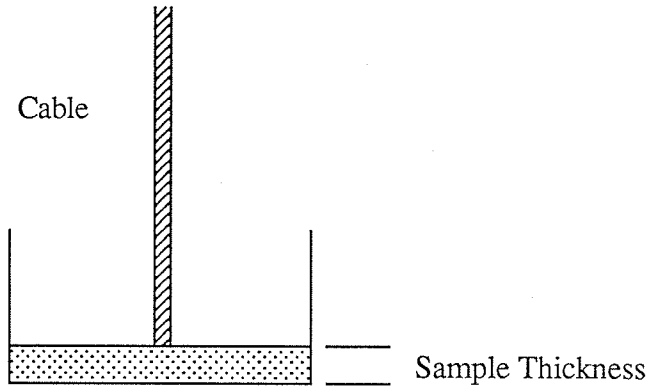

Figure 22: Setup for Measuring Minimum Sample Thickness with Cable at Surface of Test Liquid

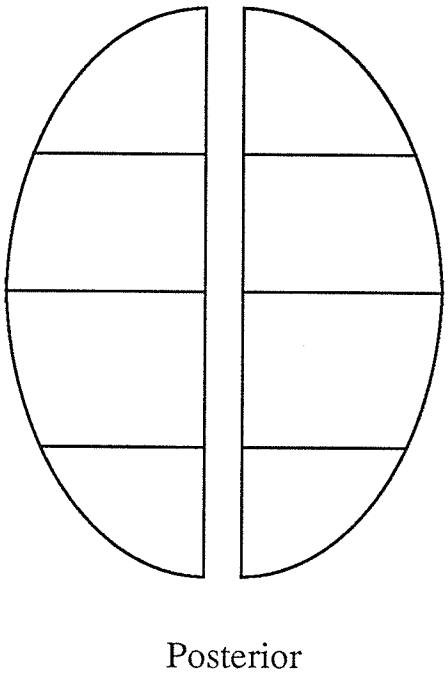

Figure 23: Schematic of Cutting of the Brains

were kept normal. Comparison of the water contents from the two hemispheres allowed verification of the production of edema. Soaking times were varied between 1 and 6 hours in seven of the frozen brains and the four fresh brains. The remaining two frozen brains were kept normal.

3.5.2 In-Vivo Production of Osmotic Edema

Cerebral osmotic edema was produced in-vivo in 8 adult mongrel dogs using the technique described by Herschkowitz [29]. Each dog was anesthetized first using sodium pentobarbital (Nembutal). Pitressin was then administered intraperitoneally at 0.01 units/ kg. After 5 minutes, pyrogenic-free water was intravenously infused at 50 ml/ kg into the femoral vein for periods between 10 and 20 minutes. The dog was sacrificed 30 minutes after infusion by intravenous injection of sodium chloride (KCl), after which the cerebral hemispheres were removed immediately. For 6 dogs, the hemispheres were placed within thick plastic containers and frozen for tissue preservation at -30^{o} C. Within one week of removal, these brains were thawed at room temperature and measured. For the remaining 2 dogs, the hemispheres were removed immediately and measured. In preparation for measurement, each brain was cut into 8 coronal slices.

3.5.3 Cable Preparation and Water Content Measurement

To measure each sample, the tip of the cable was first cleaned with distilled water and dried. The incident waveform was then collected. An area of white matter on the sample was selected and any blood or water on the surface was removed with gauze. The tip of the cable was introduced to the white matter area at a depth of 1.0 mm and a reflected waveform was collected. Immediately following the measurements, a sample of white matter was taken from directly beneath the cable and placed in a gravimetric column to measure its water content. A description of the preparation of a gravimetric column is given in Appendix C. Equilibrium depths of the samples were taken at 2 minutes after

entry in the column. The temperature at which samples were measured was also recorded. To ensure that only the complex dielectric constant of white matter was measured, only samples with no gray matter within the minimum sample volume of the cable were reported for this thesis.

3.6 Production and Measurement of Vasogenic Edema

The changes in the dielectric properties of cerebral white matter with water content may differ between in-vitro and in-vivo samples. A preliminary test of the technique in-vivo was performed by monitoring a vasogenic edema progression in cerebral white matter.

One adult female cat was anesthetized with sodium pentobarbital. The dura overlying the parasagittal portion of the posterior gyrus of the left cerebral hemisphere was exposed. A cold lesion was produced by placing a 5 by 10 mm probe, cooled to approximately -50° C by dry ice, for 10 minutes to the exposed dura. The right hemisphere was left unaffected. The tip of the cable was then introduced into the white matter immediately anterior to the lesion at a 6 mm depth and was left untouched throughout the experiment.

Immediately before the cable was inserted into the brain, an incident waveform was acquired from 1000 averaged signals digitized to 512 points. Following the placement of the cable, reflected waveforms were collected every 15 minutes for 375 minutes after which the cat was sacrificed. Each reflected waveform was the average of 100 individual signals digitized to 512 points. Since no incident waveform could be collected with this setup, it was assumed that the incident waveform collected prior to cable insertion could be used in the calculation of the complex dielectric constant for all waveforms. The production of edema was verified from measurement of the specific gravity of white matter taken from respective areas on the fixated left and right cerebral hemispheres.

Chapter IV

Results and Discussion

An analysis of the results from the tests and experiments is presented in this chapter. This is followed by a discussion of possible sources of error in the measurement of biological samples and the use of this technique for the measurement of cerebral edema.

4.1 Capacitance Values for the 2 Element Equivalent Circuit

The values of C_0 and C_f with the open end of the cable submerged in distilled water was found to be 21.5 ± 0.3 SE fF and 0.9 ± 0.3 SE fF respectively. The values of C_0 and C_f with the open end of the cable at the surface of the distilled water were 20.2 ± 0.7 SE fF and 2.2 ± 0.7 SE fF respectively. The difference between these two values may be accounted by a fringing field in the air surrounding the cable. The presence of this field models results in a 4 element model for the terminating impedance as in Figure 15, where $\varepsilon_s C_0$ and C_f represent the total fringing field capacitances rather than the normal fringing field capacitances, in the sample and cable dielectric, respectively. The two series capacitances represent the total fringing capacitances due to the field through the air surrounding the cable and the sample. However, the series fringing capacitance in air is probably much smaller than the fringing field capacitance in the samples measured in this study, as the dielectric constant of air is 1 while those of the tissue samples are in the range

30 - 50 [62]. Thus, the equivalent capacitance of the 2 series capacitors is very close to the value of the fringing field capacitance in air. This air capacitance may be taken as constant, thus reducing the 4 element circuit to the 2 element circuit of Figure 14, where C_f is the sum of the fringing field capacitances in the surrounding air and the cable dielectric, and $\varepsilon_s C_0$ is the fringing field capacitance in the sample. The greater standard errors observed with the cable at the surface of the liquid may be due to the difficulty of placing the cable tip exactly at the surface of the liquid.

The values for C_0 and C_f at the surface of the sample are in agreement with the values of C_0 = 22.0 fF and C_f = 1 fF found by Stuchly et al for the same cable position [59]. The relationship between these parameters and dielectric thickness, (b-a), may be assessed by the ratio C_0/ C_f. From the values determined in this study, the ratio for 0.141" cable is 9.2. The value of C_0/ C_f for 0.325" cable is 5.1 based on values found by Stuchly et al [58]. The differences imply that C_0 and C_f are not linear functions of the parameter (b-a).

4.2 Accuracy and Minimum Sample Thickness Tests

The accuracy of the technique was assessed from measurements of methanol, distilled water and saline. The minimum sample thickness was established using samples of distilled water and saline of varying thicknesses.

4.2.1 Accuracy Tests

Dielectric measurements of methanol, distilled water and saline with the open end of the cable submerged in each liquid are listed in Tables 2, 3 and 4 respectively. The averages and standard errors from analysis using the 2 and 4 element equivalent circuits are listed. As can be seen , in every measurement, the 2 element circuit predicts dielectric parameters much closer to the published data.

Table 2

Dielectric Measurements of Methanol

for the Open End of the Cable Submerged

Real Dielectric Constant

frequency (MHz)	ε_r' (from equation given for 25^0 C in reference [6])	ε_r' * (measured this study at 24.2^0 C using 2 element circuit)	ε_r' * (measured this study at 24.2^0 C using 4 element circuit)
100	32.6	33.8 ± 1.4	39.9 ± 1.7
250	32.5	33.3 ± 1.2	39.2 ± 1.4
500	32.1	32.5 ± 1.1	38.3 ± 1.3
750	31.3	32.0 ± 1.1	37.7 ± 1.3
1000	30.4	30.2 ± 1.1	35.5 ± 1.3

Loss Factor

frequency (MHz)	ε_r'' (from equation given for 25^0 C in reference [6])	ε_r'' * (measured this study at 24.2^0 C using 2 element circuit)	ε_r'' * (measured this study at 24.2^0 C using 4 element circuit)
100	0.8	1.4 ± 0.9	1.6 ± 1.1
250	2.0	2.3 ± 0.2	2.8 ± 0.2
500	4.0	5.4 ± 0.2	6.5 ± 0.2
750	5.8	6.8 ± 0.2	8.2 ± 0.2
1000	7.4	8.2 ± 0.1	9.9 ± 0.2

* values are averages ± standard error

Table 3

Dielectric Measurements of Distilled Water

for the Open End of the Cable Submerged

Real Dielectric Constant

frequency (MHz)	ε_r' (from measurements given at 25^0 C in reference [6])	ε_r' ** (measured this study at 24.2^0 C using 2 element circuit)	ε_r' ** (measured this study at 24.2^0 C using 4 element circuit)
100	78.0	76.6 ± 0.5	91.2 ± 0.5
250	77.6 *	78.0 ± 0.6	92.9 ± 0.7
500	77.3 *	77.6 ± 0.6	92.4 ± 0.8
750	77.2 *	78.6 ± 0.7	93.6 ± 0.9
1000	77.1 *	76.4 ± 0.8	90.9 ± 0.9

Loss Factor

frequency (MHz)	ε_r'' (from measurements given at 25^0 C in reference [6])	ε_r'' ** (measured this study at 24.2^0 C using 2 element circuit)	ε_r'' ** (measured this study at 24.2^0 C using 4 element circuit)
100	0.4	-2.3 ± 0.6	-2.7 ± 0.8
250	1.1 *	2.8 ± 0.2	3.4 ± 0.2
500	3.6 *	5.4 ± 0.1	6.5 ± 0.1
750	5.5 *	4.5 ± 0.2	5.4 ± 0.2
1000	6.9 *	4.7 ± 0.1	5.7 ± 0.1

* points interpolated from data given at 100, 300 and 3000 MHz

** values are averages ± standard error

Table 4

Dielectric Measurements of Saline

for the Open End of the Cable Submerged

Real Dielectric Constant

frequency (MHz)	ε_r' (from equation given for 25^0 C in reference [55])	ε_r' * (measured this study at 24.2^0 C using 2 element circuit)	ε_r' * (measured this study at 24.2^0 C using 4 element circuit)
100	75.6	74.3 ± 1.0	88.4 ± 1.2
250	75.6	76.9 ± 1.1	91.6 ± 1.3
500	75.6	73.7 ± 1.1	87.8 ± 1.3
750	75.5	75.7 ± 1.1	90.2 ± 1.4
1000	75.4	73.8 ± 1.3	87.9 ± 1.5

Loss Factor

frequency (MHz)	ε_r'' (from equation given for 25^0 C in reference [55])	ε_r'' * (measured this study at 24.2^0 C using 2 element circuit)	ε_r'' * (measured this study at 24.2^0 C using 4 element circuit)
100	274.0	276.8 ± 0.9	332.2 ± 1.1
250	110.4	113.9 ± 0.4	136.7 ± 0.5
500	56.6	61.4 ± 0.3	73.7 ± 0.4
750	39.2	42.8 ± 0.3	51.3 ± 0.4
1000	31.0	32.5 ± 0.3	39.0 ± 0.4

* values are averages ± standard error

Dielectric measurements of methanol, distilled water and saline with the open end of the cable at the surface of each liquid are listed in Tables 5, 6 and 7 respectively. In most measurements, the 2 element equivalent circuit dielectric parameters are much closer to the published data. Values predicted by the 4 element circuit with the cable at the surface are closer to the published data than corresponding values with the cable submerged. This suggests that parameters in the 4 element model are dependent on the depth of the tip of the cable in the liquid.

The 2 element circuit was used to analyze data from biological samples, since the results from the accuracy tests indicate this circuit predicts dielectric properties more accurately. The C_0 and C_f values for the cable submerged in the liquid were used in the analysis of the vasogenic edema progression in the cat, where the cable was inserted in cerebral tissue. The values for the cable at the surface of the liquid were used in the analysis of in-vitro samples, where the cable was applied to the surface of the tissue.

It should be noted that the higher errors observed for the 4 element circuit do not necessarily imply that a 4 element circuit does not model the terminating impedance accurately. As discussed in section 4.1, the existence of a fringing field in the air surrounding the cable suggests a 4 element model describes the terminating impedance. However, a 2 element circuit can be used to approximate this 4 element circuit. The errors observed using the 4 element model are probably due to the errors in the determination of C_f, C_0 and C_s. C_f, C_0 and C_s are probably not linearly related to the dielectric thickness, (b-a) due to the finite conductance of the cable conductors and the skin effect in these conductors.

4.2.2 Minimum Sample Thickness

The dielectric parameters measured at varying thicknesses of distilled water and saline with the cable submerged are listed in Tables 8 and 9. All the measurements of the real dielectric constant of distilled water deviate more than 5 % from their values established

Table 5

Dielectric Measurements of Methanol

for the Open End of the Cable at the Liquid Surface

Real Dielectric Constant

frequency (MHz)	ε_r' (from equation given for 25^0 C in reference [6])	ε_r' * (measured this study at 23.5^0 C using 2 element circuit)	ε_r' * (measured this study at 23.5^0 C using 4 element circuit)
100	32.6	34.7 ± 1.5	38.4 ± 1.7
250	32.5	33.4 ± 1.3	37.0 ± 1.5
500	32.1	32.5 ± 1.3	35.9 ± 1.4
750	31.3	32.4 ± 1.2	35.8 ± 1.4
1000	30.4	31.1 ± 1.4	34.3 ± 1.5

Loss Factor

frequency (MHz)	ε_r'' (from equation given for 25^0 C in reference [6])	ε_r'' * (measured this study at 23.5^0 C using 2 element circuit)	ε_r'' * (measured this study at 23.5^0 C using 4 element circuit)
100	0.8	1.1 ± 0.8	1.2 ± 0.9
250	2.0	4.3 ± 0.1	4.8 ± 0.1
500	4.0	5.3 ± 0.3	6.0 ± 0.3
750	5.8	7.0 ± 0.2	7.9 ± 0.2
1000	7.4	8.8 ± 0.1	9.8 ± 0.2

* values are averages ± standard error

Table 6

Dielectric Measurements of Distilled Water

for the Open End of the Cable at the Liquid Surface

Real Dielectric Constant

frequency (MHz)	ε_r' (from measurements given at 25^0 C in reference [6])	ε_r' ** (measured this study at 23.5^0 C using 2 element circuit)	ε_r' ** (measured this study at 23.5^0 C using 4 element circuit)
100	78.0	82.3 ± 1.1	91.9 ± 1.3
250	77.6 *	74.7 ± 1.2	83.3 ± 1.3
500	77.3 *	75.8 ± 1.0	84.6 ± 1.1
750	77.2 *	77.6 ± 1.1	86.6 ± 1.2
1000	77.1 *	76.9 ± 1.2	85.8 ± 1.3

Loss Factor

frequency (MHz)	ε_r'' (from measurements given at 25^0 C in reference [6])	ε_r'' ** (measured this study at 23.5^0 C using 2 element circuit)	ε_r'' * (measured this study at 23.5^0 C using 4 element circuit)
100	0.4	3.6 ± 0.5	4.1 ± 0.5
250	1.1 *	6.1 ± 0.5	6.9 ± 0.5
500	3.6 *	4.1 ± 0.1	4.6 ± 0.1
750	5.5 *	4.2 ± 0.2	4.8 ± 0.2
1000	6.9 *	4.9 ± 0.1	5.5 ± 0.1

* points interpolated from data given at 100, 300 and 3000 MHz

** values are averages ± standard error

Table 7

Dielectric Measurements of Saline

for the Open End of the Cable at the Liquid Surface

Real Dielectric Constant

frequency (MHz)	ε_r' (from equation given for 25^0 C in reference [55])	ε_r' * (measured this study at 23.5^0 C using 2 element circuit)	ε_r' * (measured this study at 23.5^0 C using 4 element circuit)
100	75.6	76.1 ± 1.3	84.9 ± 1.4
250	75.6	74.2 ± 1.1	82.8 ± 1.3
500	75.6	74.7 ± 1.2	83.3 ± 1.3
750	75.5	76.1 ± 1.0	84.9 ± 1.1
1000	75.4	75.2 ± 1.2	83.9 ± 1.3

Loss Factor

frequency (MHz)	ε_r'' (from equation given for 25^0 C in reference [55])	ε_r'' * (measured this study at 23.5^0 C using 2 element circuit)	ε_r'' * (measured this study at 23.5^0 C using 4 element circuit)
100	274.0	275.5 ± 1.4	309.8 ± 1.5
250	110.4	110.7 ± 0.6	124.5 ± 0.7
500	56.6	57.2 ± 0.4	64.4 ± 0.5
750	39.2	40.6 ± 0.4	45.6 ± 0.4
1000	31.0	31.9 ± 0.4	35.8 ± 0.4

* values are averages ± standard error

Table 8

Minimum Sample Thickness of Distilled Water

Real Dielectric Constant *

frequency (MHz)	Accuracy Test	5 mm	4 mm	3 mm	2 mm	1 mm
100.0	76.6	76.8	76.4	76.2	75.5	71.1
250.0	78.0	77.8	77.8	77.6	76.7	72.5
500.0	77.6	77.5	77.8	77.4	76.6	72.3
750.0	78.6	78.2	78.8	78.3	77.4	73.1
1000.0	76.4	76.1	76.8	76.2	75.1	70.9

Loss Factor *

frequency (MHz)	Accuracy Test	5 mm	4 mm	3 mm	2 mm	1 mm
100.0	-2.3	-2.3	-3.3	-3.2	-2.7	-3.0
250.0	2.8	2.6	2.6	2.8	2.7	2.6
500.0	5.4	5.5	5.6	5.7	5.7	5.4
750.0	4.5	4.2	4.3	4.4	4.3	4.1
1000.0	4.7	3.4	3.6	3.7	3.4	3.1

* all measurements at 24.2^0 C

Table 9

Minimum Sample Thickness of Saline

Real Dielectric Constant *

frequency (MHz)	Accuracy Test	5 mm	4 mm	3 mm	2 mm	1 mm
100.0	74.3	73.9	73.7	74.0	72.2	67.8
250.0	76.9	75.8	75.9	76.1	74.9	70.5
500.0	73.7	74.9	75.0	75.3	74.1	69.7
750.0	75.7	75.6	75.6	76.0	74.9	70.2
1000.0	73.8	73.4	73.6	73.9	72.7	68.2

Loss Factor *

frequency (MHz)	Accuracy Test	5 mm	4 mm	3 mm	2 mm	1 mm
100.0	276.8	273.4	272.1	271.3	267.1	249.5
250.0	113.9	112.5	112.2	111.5	110.7	103.5
500.0	61.4	58.7	58.6	58.3	58.0	54.1
750.0	42.8	41.4	41.3	41.1	40.8	37.9
1000.0	32.5	31.5	31.4	31.4	30.8	28.4

* all measurements at 24.2^0 C

by the accuracy test at a sample thickness of 1 mm. Measurements at other thicknesses were within 5 % of the accuracy test values. Due to the uncertainty in the measurement of the loss factor of distilled water, this parameter was not included in the determination of minimum sample thickness. Again, all measurements of the real dielectric constant of saline deviate by more than 5 % at a thickness of 1 mm. The measurements at other thicknesses were within 5 % of the accuracy test values. Measurements of the loss factor of saline deviate by more than 5 % at thicknesses of 2 mm or less, while deviations at greater thicknesses were less than this amount.

The field at the tip of the cable at the surface of the liquid would be expected to be similar to that for the cable submerged in the liquid. Data for the tip of the cable at the surface of the liquid, which are not reported in this thesis, support this argument as the same results for the minimum sample thicknesses were obtained.

The minimum sample thickness of a tissue sample may be taken as the greatest minimum sample thickness measured for distilled water or saline, 2 mm. Including a margin of error, this value was taken as 3 mm for the collection of tissue data. Reliable results may thus be expected if all the tissue within a 3 mm radius of the tip of the cable was of the same type.

4.3 Results from In-Vitro Measurements

4.3.1 Measurements on Normal Canine White Matter

Twenty-nine normal samples were collected with average specific gravity equal to 1.0435 ± 0.0015 SE (water content = 68.709 ± 0.972 SE %) at temperatures between 20^0 C and 22^0 C. The specific gravity of brain samples are in close agreement with the value of 1.0437 for canine centrum semiovale (white matter) reported by Inaba et al [31].

The average and standard errors of real dielectric constant and loss factor at each frequency are listed in Table 10. Figures 24 and 25 contain graphs of this data and results for normal canine white matter reported by Schepps and Foster [53] at 37^0 C versus

Table 10

Measured Dielectric Properties of Normal Canine Cerebral White Matter *

frequency (MHz)	ε'	ε''
100.0	49.1 ± 3.2	53.9 ± 5.8
250.0	37.4 ± 2.5	26.5 ± 2.3
500.0	34.2 ± 2.3	15.7 ± 1.3
750.0	33.5 ± 2.3	11.3 ± 1.0
1000.0	32.0 ± 2.1	9.2 ± 2.9

* all measurements at 20^0 - 22^0 C

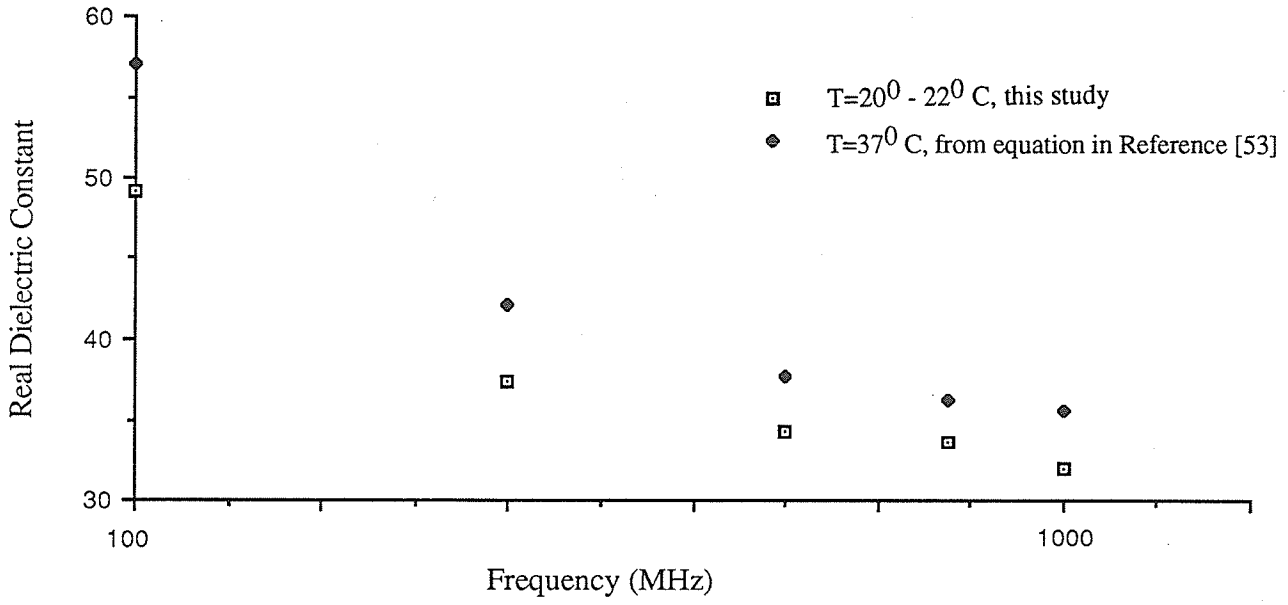

Figure 24: Real Dielectric Constant of Normal Canine White Matter vs. Frequency

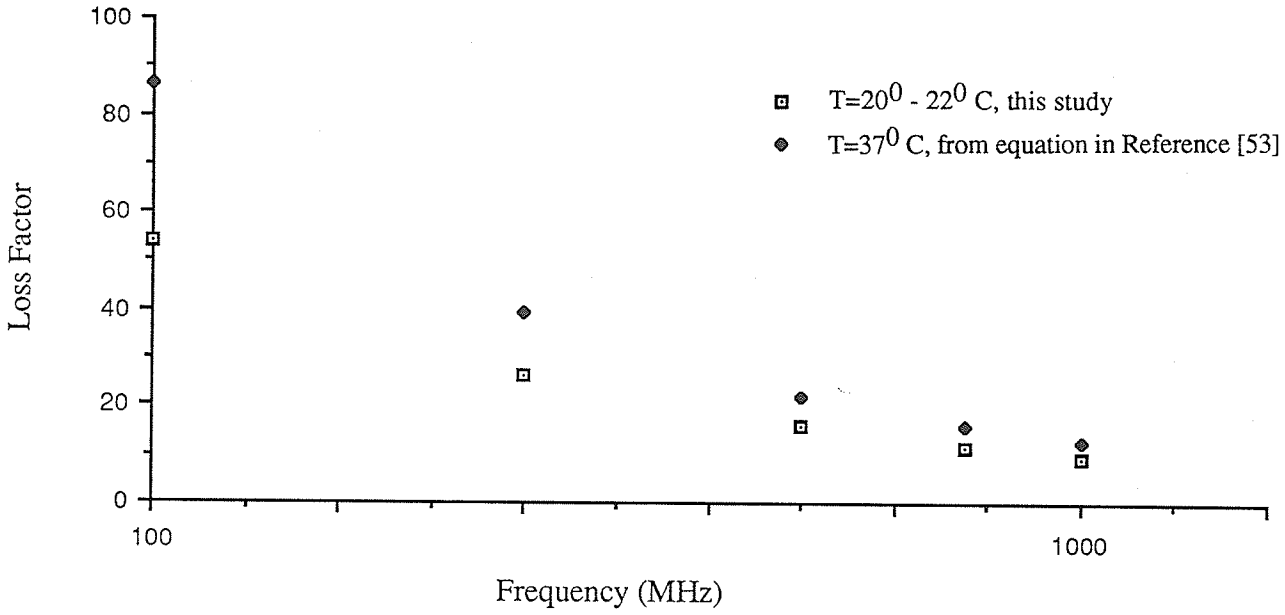

Figure 24: Loss Factor of Normal Canine White Matter vs. Frequency

frequency. The trends observed with frequency and temperature are in agreement with trends observed by Foster and Schepps [18] for canine white matter between 100 and 1000 MHz.

4.3.2 In-Vitro Production of Osmotic Edema

Graphs of the real dielectric constant and loss factor of edematous samples and normal samples at each frequency are given in Appendix D. With each frequency, a least squares fit of the measured parameter and water content is graphed. The correlation coefficient, R, and the linear equation are also given. Twenty-seven edematous samples were measured at temperatures between 20^0 C and 22^0 C, giving a total of 56 points per graph. The average water content of the edematous samples was 75.319 ± 2.836 SE % with a maximum water content of 80.526 %.

The real dielectric constant of cerebral samples increased with increasing water content at each frequency. The value of R was least at 100 MHz with a value of 0.76. For the remaining frequencies, the correlation was stronger with $0.87 \leq R \leq 0.89$. The change in dielectric constant with water content, or the slope of the fitted line was least at 100 MHz with a value of 0.895 units/ % water content. The slope increased at 250 MHz to 1.503 units/ % water content and for the higher frequencies was approximately 1.7 units/ % water content. The above results suggest water content is best measured using the real dielectric constant at higher frequencies. Better correlations with water content and a higher sensitivity of measurements to this parameter are observed at these frequencies. The lowest correlation observed at 100 MHz may reflect the increased contribution of the relaxation of cell membranes. The relaxation of the membranes is a function of the time since excision [61] and may vary from animal to animal.

The loss factor of the samples decreased with increasing water content at each frequency. At all frequencies, the correlation coefficient was in the range $0.81 \leq R \leq 0.84$. The change in loss factor with water content, unlike permittivity, was greatest at 100 MHz

with a magnitude of 2.373 units/ % water content and declined with increasing frequency to 0.357 units/ % water content at 1000 MHz. From the above observations, water content would best be measured using loss factor at lower frequencies due to its high sensitivity in this range.

The above observations may be explained by modelling the increase in water content as the "dilution" of a mixture of water and the proteins present in dried tissue. At the frequencies considered, cellular membranes have extremely low impedance, and the tissue may be treated as a suspension of proteins in water [53]. From measurements of normal canine white matter, it is observed that the real dielectric constant of normal canine white matter is less than that of distilled water in the frequency range 100 - 1000 MHz. The expected effect of the addition of water to the white matter is to increase its real dielectric constant. Similarly, since the loss factor of normal white matter is greater than that of water in this frequency range, the addition of water to the tissue would cause this parameter to decrease. These effects on the dielectric parameters with the addition of distilled water were observed. Based on the above argument, it would be expected that as the water content of the tissue approaches 100 %, both the real dielectric constant and loss factor should approach that of distilled water. The permittivity and loss factor should approach that of dried tissue as the water content approaches 0 %. A linear mixture model might describe the dielectric parameters of tissue with its water content,

$$\varepsilon_{\text{tissue}} = \varepsilon_{\text{dried tissue}} + \frac{\varepsilon_{\text{water}} - \varepsilon_{\text{dried tissue}}}{100} \times \text{Water Content (\%)} \qquad (30)$$

where ε represents either the permittivity or loss factor of the tissue. Rewriting (30) for normal tissue parameters,

$$\varepsilon_{\text{tissue}} = \varepsilon_{\text{normal tissue}} + \frac{\varepsilon_{\text{water}} - \varepsilon_{\text{normal tissue}}}{100 - (\text{Normal Water Content})} \times$$

$$(\text{Water Content (\%)} - \text{Normal Water Content}) \qquad (31)$$

As can be seen from (31), the slope of the line is directly proportional to the value of $\varepsilon_{water} - \varepsilon_{normal\ tissue}$. The real dielectric constant of water may be taken as approximately constant while that of normal tissue decreases with increasing frequency over 100 - 1000 MHz. Thus, the slope of the line relating real dielectric constant and water content should be positive and increase with frequency, as was observed. The loss factor of water is less than that of normal white matter over 100 - 1000 MHz. The loss factor of water increases while that of normal tissue decreases as frequency is increased over 100 - 1000 MHz. The slope of the line relating loss factor and water content should therefore be negative, and its magnitude decrease with frequency, which was observed.

The validity of this model may be determined from the linear equations fitted to the data at each frequency. As mentioned above, at 0 % water content, the complex dielectric constant of tissue should approach that of dried tissue whereas at 100 % water content, it should approach that of water. The predicted values of the dielectric parameters at 0 % and 100 % water content may be used to test the model. Table 11 gives the predicted real dielectric constant and loss factor values at 0 % and 100 % water content at each frequency. A water content of 0 % results in impossible negative real dielectric constants. At a water content of 100 %, dielectric constant is predicted with a maximum error of 10 dielectric units while the loss factor is predicted with an error of 9 to 22 dielectric units. These results demonstrate that the model is not valid over the full water content range from 0 to 100 %. However, the relatively low errors observed at 100 % water content suggest that this model predicts the approximate behavior of complex dielectric constant between normal and 100 % water content. Below this range, the relations between the dielectric parameters and water content are most likely nonlinear.

Errors in this model may be accounted for by proteins in the tissue. The large number of proteins of different shapes and sizes and their interactions with one another and the water solute may affect their individual contributions to the complex dielectric constant at different water contents. At lower water contents, proteins are closer to each other and

Table 11

Predicted Dielectric Properties of Canine White Matter

at 0 % and 100 % Water Content

frequency	0 %		100 %	
(MHz)	ε'	ε"	ε'	ε"
100	-12.1	215.2	77.4	-22.1
250	-65.1	104.9	85.2	-10.5
500	-81.5	59.2	88.2	-4.9
750	-86.4	42.3	89.5	-3.4
1000	-86.2	33.5	87.3	-2.2

less water is present in the tissue. The interactions between the protein molecules and the lack of interaction between these molecules and water may cause a nonlinear relationship between dielectric parameters and water content. As water content is increased, these interactions are less prominent and interactions with water molecules contribute more to the dielectric constant . At higher water contents, interactions of protein molecules with themselves contribute less to complex dielectric constant while interactions with water molecules approach a constant. Thus, with higher water contents, the material would be expected to behave closer to the model.

4.3.3 In-Vivo Production of Osmotic Edema

Graphs of the real dielectric constant and loss factor of edematous and normal samples at each frequency are given in Appendix E. With each graph, the least squares linear fit and correlation coefficient, R, are given. Forty-one edematous samples were measured at temperatures between 20^0 C and 22^0 C for a total of 70 data points in each graph. The average water content of the edematous samples was 69.599 ± 1.224 % SE with a maximum water content of 71.746 % measured . The average water content of the edematous samples and the average water content of normal samples were within 1 standard error of each other. Thus, the method of water intoxication used in this thesis was not successful in producing significant cerebral edema, i.e., normal and edematous populations were practically identical.

The inability of the water intoxication technique to produce more edema in the white matter may be attributed to the species of animal used. Herschkowitz et al whose method of water intoxication was employed in this thesis used monkeys and rabbits in their study of water intoxication and achieved increases in water content of up to 4.5 % [29]. The canine species, though, may be more resistant to the drop in blood osmolarity associated with water intoxication and therefore less edema was produced.

Weak correlations were observed of dielectric constant with increasing tissue water content at each frequency ($0.26 \leq R \leq 0.28$). However, the fitted linear equations do predict an increase in dielectric constant with increasing water content. The weak correlations reflect the small increase in the water content of the edematous samples as they suggest measurements may have been from the same normal population.

Almost a zero correlation was observed of loss factor with increasing water content at each frequency ($0.03 \leq R \leq 0.09$ for all frequencies except 100 MHz). Again, these low correlations reflect the small amount of edema produced and suggest measurements were from the same normal population.

The above results demonstrate that this technique cannot be used to reliably detect changes of the order of 1 % from a single measurement of white matter. The uncertainty in a single measurement prevents measurement to this accuracy. Note that changes of 1 % might be detected with continuous monitoring since the change in water content can be calculated from the change in dielectric properties. The spread of the measurements is not present in this situation and thus does not introduce uncertainty.

4.4 Measurement of Vasogenic Edema

The dielectric constant and loss factor from measurements of cat brain are graphed with time at each frequency in Appendix F. The production of edema was verified from specific gravities of samples taken from the fixated brain and a visual examination of the hemispheres. The specific gravities of samples taken from respective areas on the fixated right and left hemispheres were 1.0376 for the experimental left hemisphere and 1.0405 for the control right hemisphere. The lower specific gravity for the left hemisphere suggests a higher water content and thus the production of edema in this hemisphere.

The cable probably did not measure purely white matter as the thickness of the white matter in front of the cable was approximately 1.0 mm, less than the minimum

sample thickness of 3.0 mm established from the tests. Thus, it would be expected that the complex dielectric constant of a mixture of gray and white matter was measured.

Both real dielectric constant and loss factor were observed to change significantly with time. At 0 time, it may be assumed the edema front had not reached the tip of the cable and the measured dielectric parameters were those of normal tissue. With time, both real dielectric constant and loss factor increased from normal. The behaviour of dielectric constant with increasing water content is the same as that observed for osmotic edema. This fact may be used to estimate the approximate increase in the water content of the tissue. However, the behaviour of loss factor is opposite to that observed for osmotic edema. This may be explained by the protein composition of the edematous fluid introduced into the brain.

4.4.1 Normal values of Cat Tissue

Dielectric properties measured for the cerebral tissue at time 0 are listed in Table 12 along with normal values reported by Stuchly et al [57] for feline gray and white matter. It may be assumed that the vasogenic edema front had not reached the cable by time 0. Thus, these measured values were taken as those for normal tissue.

The real dielectric constants obtained in this study are in general between the ranges previously reported for gray and white matter, suggesting a mixture of both gray and white matter. The measured data, however, is closer to values for white matter, which implies that mostly white matter was measured. Loss factor values are mostly in the lower range previously reported for gray matter or between the ranges for gray and white matter. This again implies that a mixture of gray and white matter was measured.

4.4.2 Changes of Real Dielectric Constant with Time

From examination of the graphs of real dielectric constant with time listed in Appendix F, it is apparent that the shape of these graphs is similar over all the frequencies

Table 12

Measured Dielectric Properties of Normal Cat Cerebral Tissue *

Real Dielectric Constant

frequency (MHz)	ε_r' (gray matter measured at $33^0 \pm 0.5^0$ C by Stuchly et al [57])	ε_r' (white matter measured at $33^0 \pm 0.5^0$ C by Stuchly et al [57])	ε_r' (measured this study at body temperature)
100	65 - 80	58 - 64	66.0
250	55 - 60 *	46 - 47	46.8
500	48 - 52	39 - 40	42.6
750	47 - 51 **	38 - 39	42.0
1000	47 - 51	37.5 - 38.5	39.6

Loss Factor

frequency (MHz)	ε_r' (gray matter measured at $33^0 \pm 0.5^0$ C by Stuchly et al [57])	ε_r' (white matter measured at $33^0 \pm 0.5^0$ C by Stuchly et al [57])	ε_r' (measured this study at body temperature)
100	93.5 - 152.8	86.3 - 91.7	103.8
250	43.1 - 59.7 *	38.1 - 38.5	45.8
500	25.5 - 33.4	21.9 - 22.3	26.1
750	19.2 - 25.3 **	17.0 - 17.4	19.1
1000	16.0 - 21.0	14.6 - 14.7	15.5

* average of measurements betweeen 200 and 300 MHz

** average of measurements between 700 and 800 MHz

considered. The real dielectric constant of the cat tissue increased from normal with the advancement of the vasogenic edema front. The maximum value achieved by this parameter occurred at approximately 255 minutes. Fluctuation in the real dielectric constant with time might be attributed to the accidental movement of the cable.

The results of measurements of the real dielectric constant of in-vitro osmotic edema samples and in-vivo vasogenic edema suggest that dielectric constant increases with tissue water content. It may be assumed that the changes of dielectric constant with water content determined for in-vitro samples (Appendix D) hold for in-vivo samples. Note however, that this assumption might not be valid since the data in Appendix D is for canine white matter measured in-vitro between 19^0 C and 22^0 C while the sample here is for the feline species, a mixture of gray and white matter, in-vivo and at body temperature. These differences may change the value of the slope.

Nonetheless, using the fitted slopes from Appendix D, the predicted maximum increase at each frequency is listed in Table 13. With the exception of the value at 100 MHz, the average maximum increase is 9.5 ± 1 SE %. This is in agreement with increases in water content reported in the area of a cold lesion by Reulen et al [52] of 11 %. The value at 100 MHz is much greater than the other estimates. This may reflect the relaxation of cell membranes which are more prominent in-vivo [61] at 100 MHz.

4.4.3 Changes of Loss Factor with Time

From examination of the graphs of loss factor with time listed in Appendix F, it is seen that the shape of these graphs are similar over all frequencies. The loss factor appears to increase with the increasing water content associated with vasogenic edema. This is in sharp contrast to the decrease in loss factor observed with increasing water content during in-vitro osmotic edema (section 4.3.2). This may be explained by the nature of the edematous fluid introduced into the tissue during both edemas. During vasogenic edema, the accumulated fluid is close in composition to blood plasma. Measurements of the loss

Table 13

Predicted Maximum Increases in Water Content

in Vasogenic Edema Progression

frequency (MHz)	Predicted Increase (%)
100	20.12
250	10.74
500	9.51
750	8.27
1000	9.42

factor of human blood serum over 100 - 500 MHz at 23^0 C [62] suggest that the loss factor is close to that of saline. This same relation may be extended to feline blood plasma over 100 -1000 MHz. Thus, the loss factor of feline blood would be greater than that of the feline cerebral tissue measured for this experiment (Table 12). By the mixture model discussed in section 4.3.2, the loss factor should approach that of the accumulated edematous fluid as water content is increased. Thus, it would be expected that with the introduction of the edematous fluid in vasogenic edema, loss factor would increase, as was observed. As mentioned earlier, the introduction of distilled water, which has a loss factor lower than that of cerebral tissue over the frequencies considered, would cause tissue loss factor to decrease, as was observed. It should be noted that loss factor, in general, increases with the concentration of ions and proteins dissolved in the solution.

4.5 The Use of TDR in Measurements of Cerebral Edema

4.5.1 Errors in Measurements of Biological Samples

Variation in the collected data may be accounted for by systematic errors and practical limitations in the method, as discussed in section 2.3.2. Factors in the measurement of biological samples may contribute to variation, such as gray matter contamination in samples, nonuniform water content distribution in the sample and errors in the determination of water content gravimetrically. These factors are discussed in this section.

Gray Matter Contamination in Samples

Gray matter contamination in the samples likely had some effect on the in-vitro results. Approximately 40 % of all the in-vitro samples were rejected because gray matter was within the minimum sample volume. It is possible that some samples contained small unobserved amounts of gray matter. The sample of feline cerebral tissue measured in the vasogenic edema experiment contained gray matter. It is not known exactly how much this

factor would affect measurements of the complex dielectric constant though it would decrease the specific gravity of the sample. Since gray matter has a lower specific gravity than white matter, this would cause overestimation of water content.

Nonuniform Distribution of Water Content in the Sample

The nonuniform distribution of water content in the tissue most likely affected the results. With the in-vitro production of osmotic edema, a water content gradient was probably formed with its maximum at the surface of the tissue. Thus, samples measured were not homogeneous. It is not known how much this factor affected complex dielectric constant measurements, but it does change the estimate of water content. The thickness of the sample taken for the gravimetric column would affect its specific gravity, and therefore its water content. Thicker samples (those containing more tissue from the interior of the cerebral slice) would have lower estimates of the water content as specific gravity of the whole sample is measured. Samples taken for this study had approximately the same thickness and volume. For the vasogenic edema progression, the water content gradient established by the lesion produced water content variation in front of the cable as well.

Errors in the Gravimetric Determination of Sample Water Content

Errors in the gravimetric technique may have contributed to errors in water content estimation. Variations in the specific gravity of normal tissue affect the linear relation between water content and the inverse of tissue specific gravity. However, the variation in the water content and specific gravity of normal samples is not very large, as is demonstrated by the values of normal canine white matter established in this study of 68.709 ± 0.973 SE % and 1.0435 ± 0.0015 SE respectively.

4.5.2 Complex Dielectric Constant in the Measurement of Cerebral Edema

The results of this study suggest that the dielectric constant is primarily affected by the water content of the tissue while loss factor is primarily affected by the loss factor of the tissue fluid over the frequency range 100 - 1000 MHz. However, the loss factor of an aqueous solution, in general, increases with the concentration of proteins and ions. This might therefore enable the detection of all types of edemas using the real dielectric constant of the tissue. As the loss factor would reflect the concentration of proteins and ions, the type of edema might also be determined from the measurements.

The use of TDR in-vivo for the detection of cerebral edema presents several problems. Changes in the dielectric parameters with water content in-vivo must be established as changes of dielectric parameters with water content may be different from in-vivo to in-vitro. Factors which may limit the accuracy the measurement of this relation of biological samples were discussed in section 4.5.1. Variation in the dielectric parameters may not allow resolution of the water content to accuracies of 1 % from a single measurement. However, as changes of 3 - 4 % might be the minimum change considered significant clinically, this factor may not be important. Continuous monitoring to 1 % accuracy, however, may still be possible since changes in dielectric parameters could be attributed to changes in water content. Ideally, smaller diameter cable is preferable for in-vivo measurements to minimize further damage to the brain. The smaller cable also decreases the complex capacitance of the sample, thereby increasing its impedance. From the uncertainty analysis given in section 2.3.1, uncertainty in measurements would increase since the reflection coefficient, ρ, would tend to a magnitude of 1 and a phase angle of 0^0. The smaller sample volume associated with the smaller diameter would make measurements more sensitive to local variations in water content, especially changes in the tissue due to damage from the cable itself. In addition, measurements in-vivo would be sensitive to any collection of blood or cerebrospinal fluid at the tip of the cable. As these substances are very high in water content, erroneous estimates of water content would result. Lastly, the

electric field at the tip of the cable increases as the diameter of the cable decreases. Care must be taken to ensure that no damage to the cerebral tissue occurs in the vicinity of the open end occurs as a result of excessive high frequency irradiation [34].

Chapter V

Conclusions

Time domain reflectometry may be used to determine the complex dielectric constant of a small sample placed at the end of a coaxial transmission line. For the cable used (0.141" diameter), estimated accuracies of less than 5 % were achieved with a minimum sample thickness of 3 mm. All calculations of complex dielectric constant were between 100 and 1000 MHz. The real dielectric constant of canine white matter was observed to increase while its loss factor decreased with increasing water content during in-vitro osmotic edema. However, a preliminary test of the technique found that both the real dielectric constant and loss factor of feline cerebral tissue increase with increasing water content during vasogenic edema. These results suggest that the real dielectric constant of tissue is sensitive to the water content of the tissue while tissue loss factor is sensitive to the loss factor of the accumulated edematous fluid over the frequency range 100 - 1000 MHz. The technique may enable the detection of all types of edema using the real dielectric constant of the tissue. As the tissue loss factor reflects the concentration of proteins and ions, the type of edema might also be determined from measurements.

Future in-vivo experiments must establish the changes in dielectric properties of tissue with water content, as they may differ from in-vitro changes. Uncertainties in the measurements may not allow resolution of water content to within 1 % from a single measurement of the tissue though this small error may not be significant clinically.

Continuous monitoring of the brain may allow resolution of changes in water content to 1 % as changes in dielectric parameters may be attributed to changes in water content.

Bibliography

[1] M. Adachi and I. Feigin, "Cerebral Oedema and the Water Content of Normal White Matter," J.Neurol. Neurosurg. Psychiat., vol. 29, pp.446-450, 1966.

[2] L. Anderson, S. S. Stuchly and G.B. Gajda, "Parallel-Plate Coaxial Sensor for Dielectric Measurements - Further Analysis," IEEE Trans. Instrum. Meas., vol. IM-35, no. 1, pp.89-91, 1986.

[3] T. W. Athey, M.A. Stuchly, "Measurement of Radio Frequency Permittivity of Biological Tissues with an Open-Ended Coaxial Line: Part 1," IEEE Trans. Microwave Theory Tech., vol. MTT-30, no.1, pp.82-86, 1982.

[4] T.K. Bose, A.M. Bottreau, and R. Chahine, "Development of a Dipole Probe for the Study of Dielectric Properties of Biological Substances in Radiofrequency and Microwave Region woth Time-Domain Reflectometry," IEEE Trans. Instrum. Meas., vol-IM-35, no. 1, pp.56-60, 1986.

[5] M. Brodwin and J. Benway, "Experimental Evaluation of a Microwave Transmission Moisure Sensor, " J. Microwave Power, vol. 15, no.4, pp.261-265, 1980.

[6] F. Buckley and A.A. Maryott, "Tables of Dielectric Dispersion Data for Pure Liquids and Dilute Solutions," National Bureau of Standards Circular 589, Nov. 1958.

[7] R. Bullock, R. Smith, J. Favier, M. du Trevou, and G. Blake, "Brain Specific Gravity and CT Scan Density Measurements after Human Head Injury," J. Neurosurg., vol. 63, pp. 64-68, 1985.

[8] E.C. Burdette, F.L. Cain, and J. Seals, "In Vivo Probe Measurement Technique at VHF through Microwave Frequencies," IEEE Trans. Microwave Theory Tech., vol. MTT-28, no. 4, pp.414-427, 1980.

[9] E.C. Burdette, P.G. Friederich, R.L. Seaman, and L.E. Larsen, "In Situ Permittivity of Canine Brain: Regional Variations and Postmortem Changes," IEEE Trans. Microwave Theory Tech., vol. MTT-34, no.1, pp.38-50, 1986.

[10] R.H. Cole, "Time Domain Reflectometry," Ann. Rev. Phys. Chem., vol. 28, pp.283-300, 1977.

[11] R.H. Cole, "Time-Domain Spectroscopy of Dielectric Materials," IEEE Trans. Instrum. Meas., vol. IM-25, no.4, pp. 371-375, 1976.

[12] A.W.J. Dawkins, C.Gabriel, R. J. Sheppard and E.H. Grant, "Electrical properties of Lens Material at Microwave Frequencies," Phys. Med. Biol., vol. 26, no. 1, pp.1-9, 1981.

[13] A. J. Delaney and S.A. Arcone, "A Large-Size Coaxial Waveguide Time Domain Reflectometry Unit for Field Use," IEEE Trans. Geoscience and Remote Sensing, vol. GE-22, no.5, pp.428-431, 1984.

[14] C. Eyzaguirre and S. Fidone, Physiology of the Nervous System. Chicago: Year Book Medical Publishers, 1969, pp. 395-396.

[15] R. Ferszt, H. Hahm, and J. Cervos-Navarro, "Measurement of the Specific Gravity of the Brain as a Tool in Brain Edema Research," Adv. Neurol., vol. 28, pp.15-26, 1980.

[16] R.A. Fishman, "Brain Edema," The New England Journal of Medicine, vol. 293, no.14, pp.706-711, 1975.

[17] K.R. Foster, J. L. Schepps, and H. P. Schwan, "Microwave Dielectric Relaxation in Muscle: A Second Look," Biophys. J., vol. 29, pp.271-282, 1980.

[18] K.R. Foster, J. L. Schepps, R.D. Stoy and H. P. Schwan, "Dielectric Properties of Brain Tissue between 0.01 and 10 GHz," Phys. Med. Biol., vol.24, no.6, pp.1177-1187, 1979.

[19] S. Fujita, T. Ueda, and M. Yagi, "Detection of Experimental and Clinical Brain Edema Using an Electrical Impedance Method," J. Neurosurg., vol. 37, pp. 156-163, 1972.

[20] C. Gabriel, R.J. Sheppard and E.H. Grant, "Dielectric Properties of Ocular Tissues at 37^0 C," Phys. Med. Biol., vol. 28, no.1, pp.43-49, 1983.

[21] G. Gajda and S.S. Stuchly, "An Equivalent Circuit of an Open-Ended Coaxial Line," IEEE Trans. Instrum. Meas., vol.IM-32, no.4, pp. 506-508, 1983.

[22] G.B. Gajda and S.S. Stuchly, "Numerical Analysis of Open-Ended Coaxial Lines," IEEE Trans. Microwave Theory and Tech., vol. MTT-31, no.5, pp.380-385, 1983.

[23] S. Galbraith, E. R. Cardoso, and J. Patterson, "The Water Content of White Matter after Head Injury in Man," in Recent Progress in the Study and Theory of Brain Edema. New York: Plenum Press, 1984, pp. 323-329.

[24] J. Gazendam, K.G. Go, J.J. Van der Meer and F. Zuiderveen, "Changes of Electrical Impedance in Edematous Cat Brain during Hypoxia and after Intracerebral Oubain Injection," Exp. Neurol., vol. 66, pp. 78-87, 1979.

[25] K.G. Go, "Physical Methods for Study of Brain Edema," Adv. Neurol., vol.28, pp. 1-8, 1980.

[26] K.G. Go, P.H. Van der Veen, E. J. Ebels, and F. van Woudenberg, "A Study of Electrical Impedance of Oedematous Cerebral Tissue During Operations," Acta. Neurochir., vol. 27, pp. 113- 124, 1972.

[27] F.C. Grant, "Localization of Brain Tumours," JAMA, vol. 81, pp. 2169-2171, 1923.

[28] H.D. Hermann, W. Hort, F. Loew and H. Palleske, "The Determination of Specific Tissue Impedance - A Simple Method of Measuring the Experimental Cerebral Edema," Cesk. Neurol., vol. 31, pp. 105-111, 1968.

[29] N. Herschkowitz, B.B. MacGillivray, and J.N. Cumings, "Biochemical and Electro-physiological Studies in Experimental Cerebral Oedema," Brain, vol.88, pp.557-584, 1965.

[30] Hewlett-Packard Application Note 62, "Time Domain Reflectometry," 1964.

[31] Y. Inaba, H. Hiratsuka, M. Tsuyumu, H. Tabata, and S. Tsuruoka, "Evaluation of Periventricular Hypodensity in Clinical and Experimental Hydrocephalus in Metrizamide Computed Tomographt," in Recent Progress in the Study and Therapy of Brain Edema. New York: Plenum Press, pp. 299-310.

[32] M.F. Iskander and S.S. Stuchly, "A Time-Domain Technique for Measurement of the Dielectric Properties of Biological Substances," IEEE Trans. Instrum. Meas., vol. IM-21, no.4, pp.425-429, 1972.

[33] M. F. Iskander and S.S Stuchly, "Fringing Field Effect in the Lumped-Capacitance Method for Permittivity Measurement," IEEE Trans. Instrum. Meas. vol. IM-27, no.1, pp.107-109, 1978.

[34] D.R. Justeson, "Microwave Irradiation and the Blood-Brain Barrier," Proc. IEEE, vol. 68, no. 1, pp.60-67, 1980.

[35] H.P. Kao, E.R. Cardoso, and E. Shwedyk, "Electrical Measurement of Cerebral Edema," submitted for publication.

[36] A. Klein, "Microwave Determination of Moisture in Coal: Comparison of Attenuation and Phase measurement," J. Microwave Power, vol. 16, no. 3&4, pp.289-304, 1981.

[37] A. Kraszewski, "Microwave Aquametry - A Review," J.Microwave Power, vol. 15, no.4, pp.209-220, 1980.

[38] A. Kraszewski, S. Kulinski, J. Madziar and K. Zielkowski, "Microwave On-Line Moisture Content Monitoring in Low-Hydrated Organic Materials," J. Microwave Power, vol. 15, no.4, pp.267-275, 1980.

[39] A. Kraszewski and S.S. Stuchly, "Capacitance of Open-Ended Dielectric-Filled Coaxial Lines - Experimental Results," IEEE Trans. Instrum. Meas.,vol. IM-32, no.4, pp.517-519, 1983.

[40] W. Lanksch, W. Oettinger, A. Baethman and E. Kazner, "CT Findings in Brain Edema Compared with Direct Chemical Analysis of Tissue Samples," in Dynamics of Brain Edema. New York: Springer-Verlag, 1976, pp. 283-287.

[41] A. Marmarou, W. Poll, K. Shulman, and H. Bhagavan, "A Simple Gravimetric Technique for Measurement of Cerebral Edema," J. Neurosurg., vol.49, pp.530-537, 1978.

[42] A. Marmarou, K. Tanaka, and K. Shulman, "An Improved Gravimetric Measure of Cerebral Edema," J. Neurosurg., vol.56, pp.246-253, 1982.

[43] F.I. Mopsik, "Precision Time-Domain Dielectric Spectrometer," Rev. Sci. Insrtum., vol. 55, no. 1, pp 79-87, 1984.

[44] S.R. Nelson, M.L. Mantz, and J.A. Maxwell, "Use of Specific Gravity in the Measurement of Cerebral Edema," J. Appl. Physiol., vol. 30, no. 2, pp.268-271, 1971.

[45] A.M. Nicolson, "Measurement of the Intrinsic Properties of Materials by Time-Domain Techniques," IEEE Trans. Instrum. Meas., vol. IM-19, no. 4, pp. 377-382, 1970.

[46] N.R.V. Nightingale, A.W.J. Dawkins, R.J. Sheppard, E.H. Grant, V.D. Goodridge, and J.L. Christie, "The Use of Time Domain Spectroscopy to Measure the Dielectric Properties of Mouse Brain at Radiowave and Microwave Frequencies," Phys. Med. Biol., vol.25, no.6, pp.1161-1165, 1980.

[47] S.C. Olsen and M.F. Iskander, "A New In Situ Procedure for Measuring the Dielectric Properties of Low Permittivity Materials," IEEE Trans. Intrum. Meas., vol . IM-35, no.1, pp. 2-6, 1986.

[48] S. Okamura, "High-Moisture Content Measurement of Grain by Microwaves," J. Microwave Power, vol. 16, no. 3&4, pp. 253-256, 1981.

[49] D.E. Patterson and M. W. Smith, "The Measurement of Unfrozen Water Content by Time Domain Reflectometry: Results from Laboratory Tests," Can. Geotech. J., vol. 18, 1981, pp.131-144, 1981.

[50] C. Pilcher "Experimental Cerebral Trauma: The Fluid Content of the Brain after Trauma to the Head," Arch. Surg., vol. 35, p. 522, 1937.

[51] S.I. Rapoport, Blood-Brain Barrier in Physiology and Medicine. New York: Raven Press, 1976, pp. 117-119.

[52] H.J. Reulen, R. Graham, M. Spatz, and I. Klatzo, "Role of Pressure Gradients and Bulk Flow in Dynamics of Vasogenic Brain Edema," J. Neurosurg., vol. 46, pp. 24-35, 1977.

[53] J.L. Schepps and K.R. Foster, "The UHF and Microwave Dielectric Properties of Normal and Tumour Tissues: Variation in Dielectric Properties with Tissue Water Content," Phys. Med. Biol., vol.25, no.6, pp.1149-1159, 1980.

[54] A.M. Stewart, "A Biochemical Study of Cerebral Edema and the Changes in Cerebral Edema," Brain, vol.62, pp. 426-438, 1939.

[55] A. Stogryn, "Equations for Calculating the Dielectric Constant of Saline Water," IEEE Trans. Microwave Theory Tech., vol. MTT-19, pp. 733-736, 1971.

[56] R.D. Stoy, K.R. Foster, and H.P. Schwan, "Dielectric Properties of Mammalian Tissues from 0.1 to 100 MHz: A Summary of Recent Data," Phys. Med. Biol., vol. 27, no. 4, pp. 501-513, 1982.

[57] M.A. Stuchly, T.W. Athey, S.S. Stuchly, G.M. Samaras, and G. Taylor, "Dielectric Properties In Vivo at Frequencies 10 MHz-1 GHz," Bioelectromag., vol. 2, pp. 93-103, 1981.

[58] M.A. Stuchly, T.W. Athey, S.S. Stuchly, G.M. Samaras, and G. Taylor, "Measurement of Radio frequency Permittivity of Biological Tissues with an Open-Ended Coaxial Line: Part II - Experimental Results," IEEE Trans. Microwave Theory Tech., vol. MTT-30, no. 1, pp. 87-92, 1982.

[59] M.A. Stuchly, M.M. Brady, S.S. Stuchly, and G. Gajda, " Equivalent Circuit of an Open-Ended Coaxial Line in a Lossy Dielectric," IEEE Trans. Instrum. Meas., vol. IM-31, pp. 116-119, 1982.

[60] M.A. Stuchly, A. Kraszewski, S.S. Stuchly and A.M. Smith, "Dielectric Properties of Animal Tissues at Radio and Microwave Frequencies: Comparison between Species," Phys. Med. Biol., vol. 27, no. 7, pp. 927-936, 1982.

[61] M.A. Stuchly and S.S. Stuchly, "Permittivity of Mammalian Tissues In Vivo and In Vitro: Advances in Experimental Techniques and Recent Results," Int. J. Electronics, vol. 56, no. 4, pp. 443-456, 1984.

[62] M.A. Stuchly and S.S. Stuchly, "Dielectric Properties of Biological Substances - Tabulated," J. Microwave Power, vol. 15, no. 1, pp.19-26, 1980.

[63] M.A. Stuchly and S.S. Stuchly, "Coaxial Line Reflection Methods for Measuring Dielectric Properties of Biological Substances at Radio and Microwave Frequencies - A Review," IEEE Trans. Instrum. Meas., vol. IM-29, no. 3, pp. 176-183, 1980.

[64] S.S. Stuchly, G. Gajda, L. Anderson and A. Kraszewski, "A New Sensor for Dielectric Measurements," IEEE Trans. Instrum. Meas., vol. IM-35, no. 2, pp.138-141, 1986.

[65] S.S. Stuchly, A. Kraszewski, and M.A. Stuchly, "Uncertainties in Radiofrequency Dielectric Measurements of Biological Substances," IEEE Trans. Instrum. Meas., vol. IM-36, no.1, pp. 67-70, 1987.

[66] S.S. Stuchly, J. Mladek, M.A. Stuchly and B. Parisien, " A Method for Measurement of the Permittivity of Thin Samples," vol. 14, no. 1, pp.7-13, 1979.

[67] S.S. Stuchly, M.A. Rzepecka, and M.F. Iskander, "Permittivity Measurements at Microwave Frequencies Using Lumped Elements," IEEE Trans. Instrum. Meas., vol. IM-23, no. 1, pp.56-62, 1974.

[68] Suggett, A., "Time Domain Methods," Dielectr. Relat. Mol. Processes, vol. 1, pp. 100-120, 1972.

[69] M.M. Ter-Pogossian, "Computerized Cranial Tomography: Equipment and Physics," Sem. Roentgen., vol. 12, no. 1, pp.13-25, 1977.

[70] R.M. Torack, H. Alcala, and M. Gado, "Water, Specific Gravity and Histology as Determinants of Diagnostic Computerized Cranial Tomography (CCT)," in Dynamics of Brain Edema. New York: Springer-Verlag, 1976, pp.271-277.

[71] M. Tiuri, K. Jokela, and S. Heikkila, "Microwave Instrument for Accurate Moisture and Density Measurement of Timber," J. Microwave Power, vol. 15, no. 4, pp.251-254, 1980.

[72] P.H. Van der Veen, K.G. Go, F. Zuiderveen, D. Buiter, and J. Van der Meer, "Electrical Impedance of Cat Brain with Cold-Induced Edema," Exp. Neurol., vol. 40, pp. 675-682, 1973.

[73] C.G. Wasterlain and J.B. Posner, "Cerebral Edema in Water Intoxication: I. Clinical and Chemical Observations," Arch. Neurol., vol. 19, pp. 71-78, 1968.

[74] C.G. Wasterlain and J.B. Posner, "Cerebral Edema in Water Intoxication: II. An Ultrastructural Study," Arch. Neurol., vol. 19, pp. 79-87, 1968.

Appendix A

Review of Basic Electrical Concepts

This appendix includes a review of the definition of complex dielectric constant and the basic transmission line theory for the operation of time domain reflectometers.

A.1 Complex Dielectric Constant

When a vacuum capacitor (Figure A1) is connected to a sinusoidal voltage source, V, a sinusoidal current, I, which leads the voltage by 90° flows through it. The phasor voltage, **V**, and the phasor current, **I**, are related by the susceptance of the capacitor, Y_C,

$$Y_C = \frac{\mathbf{I}}{\mathbf{V}} = j\omega C_0 \qquad (A.1)$$

where $\omega=2\pi f$ and C_0 is the capacitance of the capacitor. When the capacitor is filled with a substance, the capacitance changes by a positive factor of ε_r'

$$C = \varepsilon_r' \times C_0 \qquad (A.2)$$

This factor, ε_r', is called the relative real dielectric constant or, the permittivity of the substance. The real dielectric constant ε' of a material is defined as

$$\varepsilon' = \varepsilon_r' \times \varepsilon_o \qquad (A.3)$$

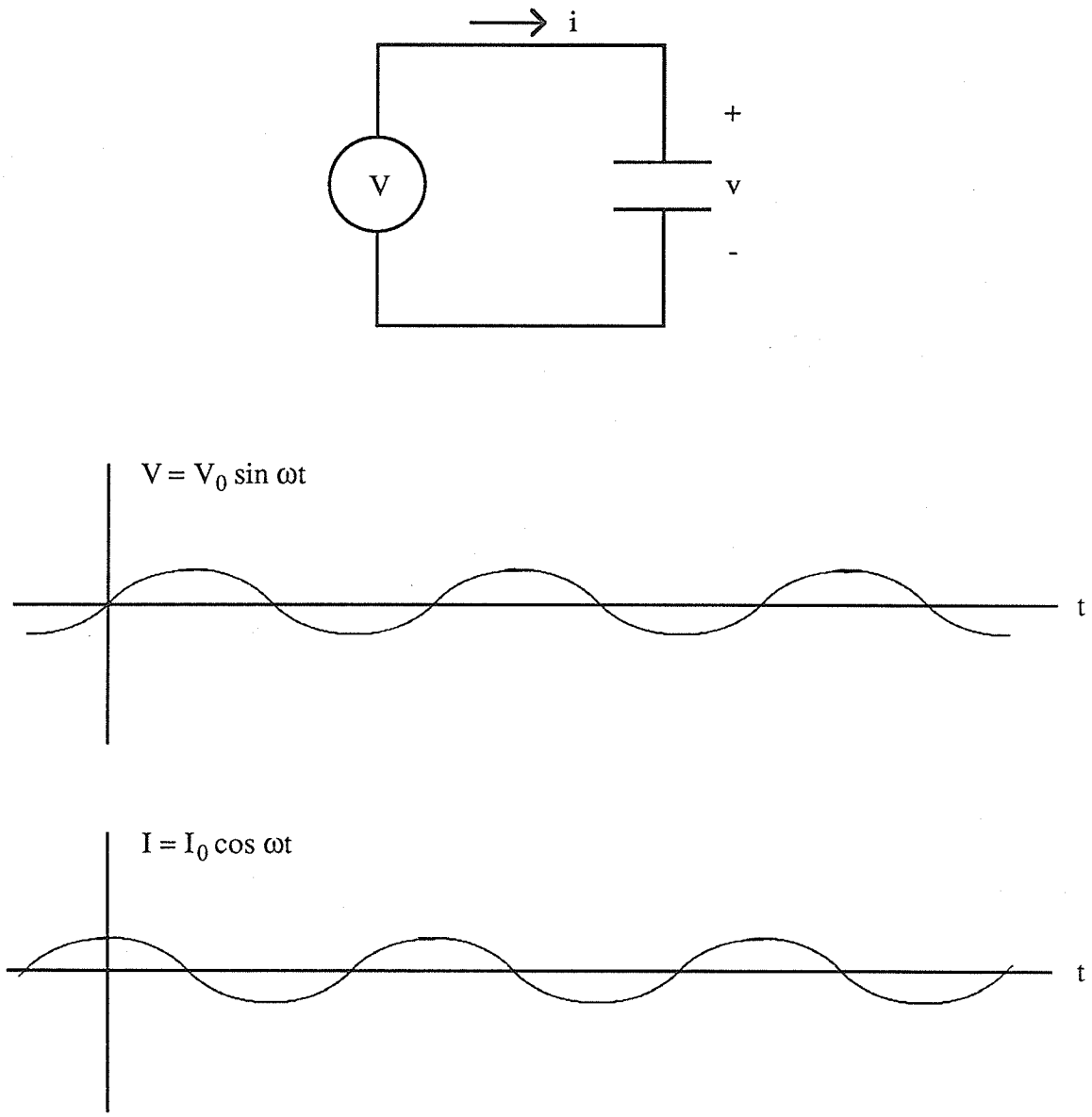

Figure A1: Voltage and current relations for a capacitor

where ε_0 is the dielectric constant of vacuum. In actual materials, the current and voltage can never attain an exact phase difference of 90°. This is accounted for by the presence of a loss current in the material due to energy consuming processes brought about by the applied voltage, such as migration of charge carriers or molecular rotation. In some materials, energy loss is negligible and the phase angle is practically 90°. A resistor placed in shunt with the capacitor is used to model the energy loss in the equivalent circuit of the capacitor (Figure A2). To describe this loss current, a negative imaginary component, ε'', is introduced to the dielectric constant called the loss factor. The dielectric constant with the loss factor is called the complex dielectric constant, ε^*,

$$\varepsilon^* = \varepsilon' - j\varepsilon'' = (\varepsilon_r' - j\varepsilon_r'') \times \varepsilon_0 \qquad (A.4)$$

where ε_r^* is the relative complex dielectric constant and ε_r'' is the relative loss factor. The value C in (A.2) is then rewritten as a complex capacitance,

$$C = (\varepsilon_r' - j\varepsilon_r'') \times C_0 \qquad (A.5)$$

Insertion of ε_r^* in (A.1) yields the following values for R and C in Figure A2,

$$\begin{aligned} C &= \varepsilon_r' \times C_0 \\ R &= \frac{1}{\omega \varepsilon''_r C_0} \end{aligned} \qquad (A.6)$$

Thus, knowledge of the equivalent conductance and capacitance of a material in a vacuum capacitor enables the calculation of the complex dielectric constant.

A.2 Transmission Lines

A transmission line is a device for transmitting or guiding energy from one point to another. Basically, it consists of two terminals into which power is transmitted and two terminals into which power is received. Thus, a transmission line can be considered as a

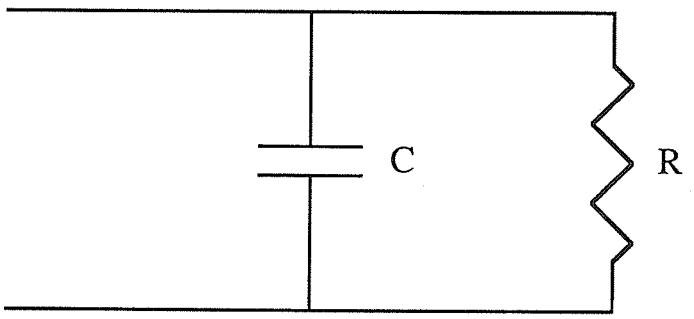

Figure A2: Equivalent Circuit of a dielectric filled vacuum capacitor

four terminal device for connecting electrical devices. An example of a transmission line is the coaxial cable (Figure A3).

Uniform transmission lines can be modelled as being made up of a chain of units of resistances (R), conductances (G), inductances (L) and capacitances (C) defined per unit length of cable (Figure A4). These cable parameters are determined by the physical dimensions and the dielectric of the cable. The characteristic impedance of the line, Z_0, is a property of the uniform transmission line. It is a function of the frequency of the sinusoidal voltage wave in the line and the line electrical characteristics. If the line is infinitely long, Z_0 is defined as

$$Z_0 = \sqrt{\frac{R + j\omega L}{G + j\omega C}} \tag{A.7}$$

where $\omega=2\pi f$, f being the frequency of the sinusoidal voltage wave in the line. Another property of uniform transmission lines is the propagation constant. A single frequency voltage travels down an infinite line at a finite velocity. As every material has some electrical losses associated with it, the voltage will be attenuated by an amount α per unit length. The phase of this voltage also lags behind that induced at the generator by an amount β radians per unit length. This attenuation and phase shift are described by the propagation constant, γ,

$$\begin{aligned} \gamma &= \alpha + j\beta \\ &= \sqrt{(R + j\omega L)(G + j\omega C)} \end{aligned} \tag{A.8}$$

where α is the attenuation in nepers per unit length and β is the phase shift in radians per unit length. This constant can be used to determine the phasor voltage, $\mathbf{E}_i$, and the phasor current, $\mathbf{I}_i$, at any distance x along an infinitely long line by the relations

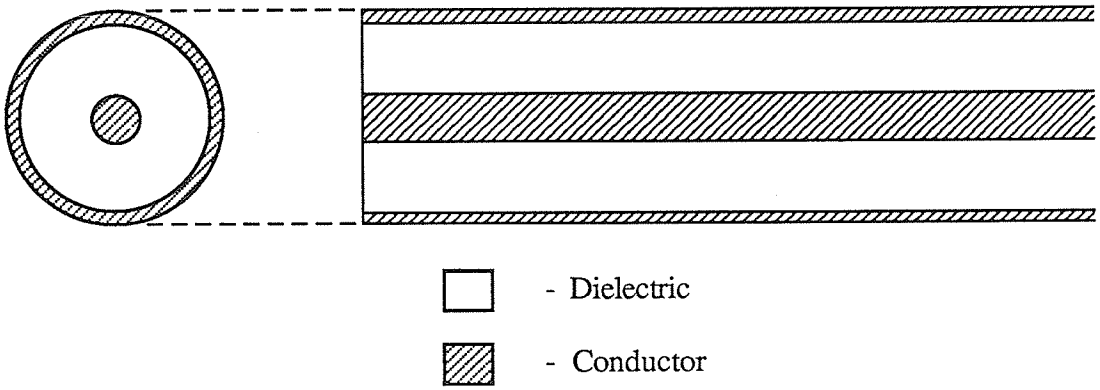

Figure A3: A Coaxial Cable

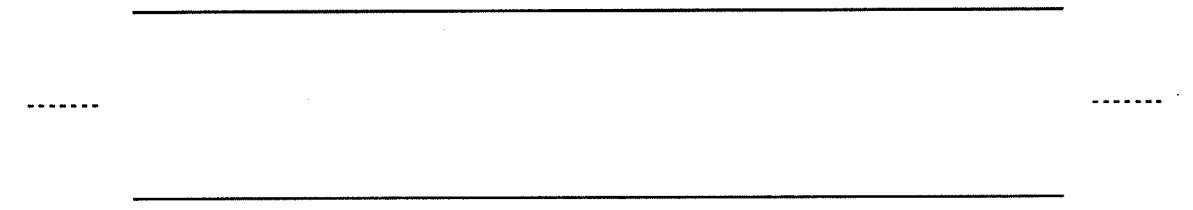

(a)

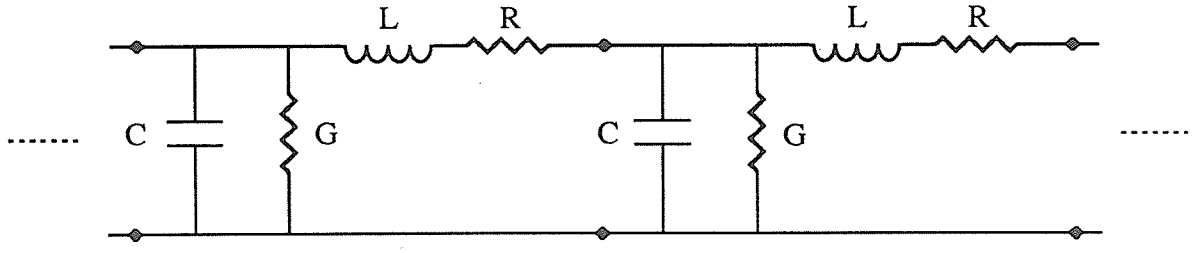

(b)

Figure A4: (a) Circuit Notation, and (b) Equivalent Circuit for a transmission line

$$E_i = E_0 e^{-\gamma x}$$
$$I_i = I_0 e^{-\gamma x} \qquad (A.9)$$

where zero reference in the x direction is arbitrarily defined. At any point along the line, the voltage and current are related by the characteristic impedance of the line,

$$Z_0 = \frac{E_i}{I_i}. \qquad (A.10)$$

Transmission lines terminated in a complex impedance, $Z_L=R_L+jX_L$, may change the infinite line situation, depending on the value of Z_L (Figure A5). The generator, E_S, produces a single frequency voltage in the line which propagates toward the load. If the transmission line is finite in length and is terminated in a load, Z_L, equal to the characteristic impedance of the line, Z_0, then equations (A.9) - (A.10) hold for the length of the line to x=d. For this case, the line is said to be line matched. However, if Z_L is different from Z_0, or line mismatched, a second wave must be considered which originates at the load and propagates toward the generator. This second wave is the reflected wave from the load consisting of the energy not delivered to the load. In the transmission line, the first and second waves add by superposition. Equations determining the voltage and current of the reflected wave are derived similarly to the infinite line equations by assuming the wave originates from a source at the end of the line,

$$E_r = E_d e^{-\gamma(d-x)}$$
$$I_r = I_d e^{-\gamma(d-x)} \qquad (A.11)$$

where E_d and I_d are the voltage and current phasors at the load. At the load, the ratio of reflected to incident voltages is found from (A.9) and (A.11),

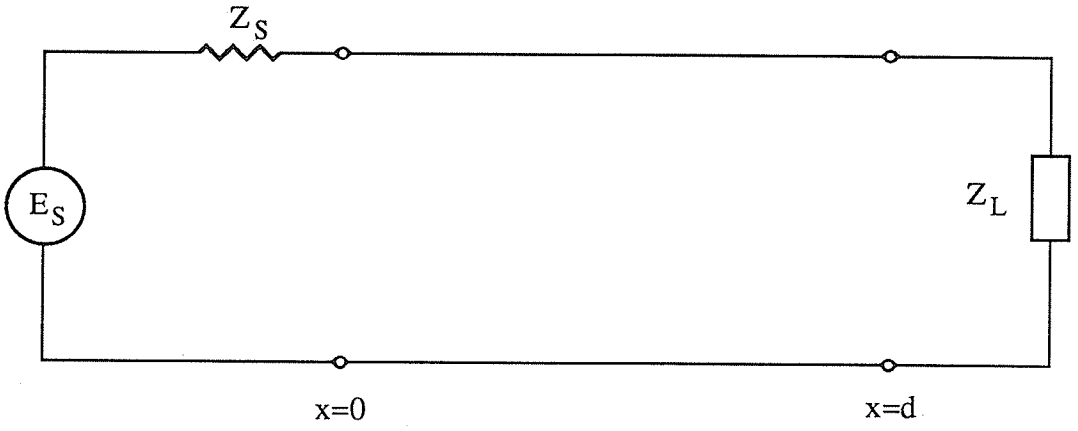

Figure A5: Transmission line circuit terminated in load Z_L

$$\rho = \frac{E_r}{E_i} = \frac{E_d}{E_0} e^{-\gamma(d-2x)} . \qquad (A.12)$$

This ratio, ρ, is known as the voltage reflection coefficient and is frequency dependent. This ratio is also dependent on Z_0 and Z_L

$$\rho = \frac{Z_L - Z_0}{Z_L + Z_0} . \qquad (A.13)$$

Determination of ρ and knowledge of Z_0 allows for the calculation of Z_L. Similarly, the generator impedance, Z_S, may be regarded as a load impedance for the reflected wave. If Z_S is line mismatched, a second reflected wave is produced from the first reflected wave. This wave, too, adds by superposition to the first two waves in the transmission line. This process of continually reflecting waves would continue indefinitely if no line matches exist on the line.

For many transmission lines, attenuation of the signal is negligible, or R and G may be assumed equal to 0, over the lengths of line considered. With this simplification, equations (A.7) and (A.8) can be reduced to, respectively,

$$Z_0 = \sqrt{\frac{L}{C}} \qquad (A.14)$$

$$\gamma = j\omega\sqrt{LC} = j\beta. \qquad (A.15)$$

In these cases, the transmission line is called a low-loss transmission line. This assumption greatly reduces the amount of mathematical calculation required in many transmission line problems.

There are several factors affecting the use of transmission lines. Attenuation is present in all transmission lines. If the line is long enough, serious attenuation of any signal will result. Amplification is necessary after the signal has passed through a certain amount of line in order to be detected at the receiving point. Dispersion is another factor which limits the use of transmission lines. Signal carrying information is usually comprised of a group of frequencies. The phase velocity is the velocity of a single frequency signal in a transmission line. If the line contains a nondispersive dielectric, such as vacuum, the phase velocity of different frequencies are the same. If the line contains a dispersive dielectric, such as teflon, the phase velocities varies with the frequency. A multifrequency signal travelling down a dispersive transmission line is distorted since its different components travel at different velocities. For a typical transmission line, higher frequency components travel faster than lower ones. Thus, shorter lines are preferred to reduce any signal distortion. Lastly, the frequency response of transmission line dielectrics limit transmission of high frequency signals. The dielectric absorbs high frequencies from the signal, thus distorting the signal. Thus, only frequencies up to a certain limit as determined by the line dielectric can be transmitted efficiently.

Appendix B

Program Listings

2 element program

```
C
C*************************************************************************
C*                                                                       *
C*   This program will  calculate the  complex  dielectric  constant of a *
C*   from time domain reflectometry (TDR) measurements on a sample.  Only *
C*   data  obtained  from  probes with 3.6 mm  outer  conductor  diameter  *
C*   can be  inputted to the  program.  This  may be  altered for  other   *
C*   probe  sizes by  adjusting the  constants C0 and CF.  CF and C0 are   *
C*   must be placed in the program.  Data  for  the capacitance of  some   *
C*   open-ended coaxial lines are listed in the reference below.           *
C*                                                                       *
C*   Note, the  program is user  interactive, prompting  the user for the *
C*   number and names of data files and data titles.                       *
C*                                                                       *
C*   This program was written by Hung Pin KAO,  Department of  Electrical *
C*   Engineering, University of Manitoba, June, 1989.                      *
C*                                                                       *
C*   Important Program Variables                                         *
C*   ===========================                                         *
C*                                                                       *
C*           INPUT       -       Vector containing incident waveform     *
C*           FNT         -       Vector containing reflected waveform    *
C*           FINT        -       Complex value of fourier transform of the *
C*                               incident waveform at a prescribed frequency *
C*           FFNT        -       Complex value of fourier transform of the *
C*                               reflected waveform at a prescribed frequency *
C*           PERIOD      -       Time length of the waveforms            *
C*           POINTS      -       Number of digitized points              *
C*           C0,CF       -       Variables needed to calculate the sample *
C*                               impedance                               *
C*           CT          -       Complex sample capacitance              *
C*           Z0          -       Characteristic impedance of coaxial cable *
C*           F0          -       First frequency at which the dielectric *
C*                               constant is calculated                  *
C*           FINC        -       Incremental frequency at which dielectric *
C*                               constant is calculated.  Note, the second *
C*                               frequency used is FINC, the third is 2*FINC, *
C*                               and so on.                              *
C*           MAX         -       Number of frequencies to be calculated  *
C*                                                                       *
C*   Reference for total capacitance of a 3.6 mm line                    *
C*   ================================================                    *
C*                                                                       *
C*   A. Kraszewski and S.S. Stuchly, "Capacitance of Open-Ended Dielectric- *
C*   Filled Coaxial Lines - Experimental Results,"  IEEE  Trans.  Instrum. *
C*   Meas., vol. IM-32, no. 4, pp. 517-519, Dec. 1983.                   *
C*                                                                       *
C*************************************************************************
C
      REAL*8 INPUT(512),FNT(512),PERIOD,T,C0,CF,Z0,W,F,F0,FINC,PI,ZEROI,
     *       ZEROF,ZERO
      INTEGER POINTS,MAX,I,M,K
      COMPLEX*16 FINT,FFNT,P,CT,E,CFREQ
      CHARACTER*25 JUNK
      CHARACTER*64 FNAME,TITLE
C
C Set program constants.
C
      PERIOD=5D-9
```

```
      POINTS=512
      POINTS=POINTS-1
      T=PERIOD/POINTS
      CF=0.89077D-15
      Z0=50.0
      F0=100.0
      FINC=250.0
      MAX=5
      ZERO=0.0
      PI=3.141592654
C
C Prompt user for name of file to contain dielectric constant data and open
C file.
C
      WRITE (*,500)
      READ(*,510) FNAME
      OPEN(1,FILE=FNAME)
C
C Prompt user for number of samples to be calculated.
C
      WRITE(*,520)
      READ(*,*) M
C
C Adjust first page spacing.
C
      WRITE(1,*) ' '
C
C Begin calculations.
C
      DO 10 K=1,M
C
C Prompt user for new waveform files and open the files.
C
         WRITE(*,530)
         READ(*,510) FNAME
         OPEN(2,FILE=FNAME)
C
         WRITE(*,540)
         READ(*,510) FNAME
         OPEN(3,FILE=FNAME)
C
C Prompt user for title of sample dielectric constants.
C
         WRITE(*,550)
         READ(*,510) TITLE
C
C Read in data from waveform files into INPUT and FNT.
C
         READ(2,510) JUNK
         DO 20 I=1,512
            READ(2,*) INPUT(I)
20        CONTINUE
C
         READ(3,510) JUNK
         DO 30 I=1,512
            READ(3,*) FNT(I)
30       CONTINUE
C
C Adjust zero level of waveform files.
C
```

```
          ZEROI=INPUT(6)
          ZEROF=FNT(6)
          DO 40 I=6,512
              INPUT(I)=INPUT(I)-ZEROI
              FNT(I)=FNT(I)-ZEROF
40        CONTINUE
C
C Write title onto screen and output file.
C
          WRITE(*,*) ' '
          WRITE(1,*) ' '
          WRITE(*,*) ' '
          WRITE(1,*) ' '
          WRITE(*,*) TITLE
          WRITE(1,*) '       ', TITLE
          WRITE(*,*) ' '
          WRITE(1,*) ' '
          WRITE(*,560)
          WRITE(1,570)
C
C Calculate sample dielectric constant at each frequency.
C
          F=F0
          DO 50 I=1,5
             W=2*PI*F*1E6
C
C Find fourier transform of each waveform at frequency W.
C
             CALL FORIER(W,INPUT,FINT,T,POINTS)
             CALL FORIER(W,FNT,FFNT,T,POINTS)
C
C Determine the reflection coefficient at frequency W and complex capacitance,
C CT.
C
             P=FFNT/FINT
             CFREQ=DCMPLX(ZERO,W)
             CT=(1-P)/(Z0*(1+P)*CFREQ)
C
C Calculate dielectric constant from complex capacitance.
C
             C0=21.50911D-15
             E=(CT-DCMPLX(CF,ZERO))/C0
C
C Write results onto screen and into output file.
C
             WRITE(*,*) ' '
             WRITE(1,*) ' '
             WRITE(*,580) F,E
             WRITE(1,590) F,E
C
C Increment frequency.
C
             F=FINC*I
C
50        CONTINUE
C
C Close waveform files.
C
          CLOSE(2)
          CLOSE(3)
```

```
C
C Set page skip.
C
         IF (MOD(K,4).EQ.0) THEN
            WRITE(1,600) CHAR(12)
         END IF
C
10     CONTINUE
C
       STOP
500    FORMAT(' Name of file to contain dielectric constants: '\)
510    FORMAT(A)
520    FORMAT(' How many samples to be calculated ? '\)
530    FORMAT(' Incident Waveform Filename: '\)
540    FORMAT(' Reflected Waveform Filename: '\)
550    FORMAT(' Set Title of Data: '\)
560    FORMAT(9X,'Frequency (MHz)',10X,'Dielectric Constant',6X,
      *'Loss Factor')
570    FORMAT(12X,'Frequency (MHz)',10X,'Dielectric Constant',6X,
      *'Loss Factor')
580    FORMAT(12X,F6.1,18X,f10.3,12X,F10.3)
590    FORMAT(15X,F6.1,18X,F10.3,12X,F10.3)
600    FORMAT(A1)
       END
C
       SUBROUTINE FORIER(W,FUNC,FFUNC,T,POINTS)
C
C   This subroutine will determine the value of the fourier transform of a
C   digitized step pulse at radian frequency, W.  The digitized portion of
C   the waveform is  contained in vector FUNC and the complex value of the
C   transform is contained in FFUNC.   The value of T is the time distance
C   between the points.  Calculation of the transform is by Simpson's rule
C   of  numerical  integration,  adding to the sum the value of a  delayed
C   step pulse with height equal to the value of the last digitized point.
C
C   Note that the beginning of the waveform is  assumed to be at the sixth
C   digitized point.
C
       INTEGER I,POINTS,UPPER
       REAL*8 W,FUNC(512),ANGLE,T,ZERO,XTEMP,YTEMP
       COMPLEX*16 FIRST,LAST,SUM1,SUM2,FFUNC,TEMP1,TEMP2
C
C Calculate incremental sums from first and last sections.
C
       ANGLE=W*T
       ZERO=0.0
       FIRST=DCMPLX(FUNC(6),ZERO)
       XTEMP=DCOS(506*ANGLE)
       YTEMP=-DSIN(506*ANGLE)
       TEMP1=DCMPLX(XTEMP,YTEMP)
       LAST=FUNC(512)*TEMP1
C
C Compute sums needed to determine remaining areas.
C
       SUM1=(0.0,0.0)
       SUM2=(0.0,0.0)
C
       UPPER=POINTS-6
       DO 30 I=1,UPPER,2
          XTEMP=DCOS(I*ANGLE)
```

```
         YTEMP=-DSIN(I*ANGLE)
         TEMP1=DCMPLX(XTEMP,YTEMP)
         SUM1=SUM1+TEMP1*FUNC(I+6)
30     CONTINUE
C
       UPPER=POINTS-7
       DO 40 I=2,UPPER,2
         XTEMP=DCOS(I*ANGLE)
         YTEMP=-DSIN(I*ANGLE)
         TEMP1=DCMPLX(XTEMP,YTEMP)
         SUM2=SUM2+TEMP1*FUNC(I+6)
40     CONTINUE
C
C Determine transform of waveform.
C
       XTEMP=DCOS(W*T*506)
       YTEMP=-DSIN(W*T*506)
       TEMP1=DCMPLX(XTEMP,YTEMP)
       TEMP2=DCMPLX(ZERO,W)
       FFUNC=T/3*(FIRST+4*SUM1+2*SUM2+LAST)+TEMP1/TEMP2*FUNC(512)
C
       RETURN
       END
```

4 element program

```
C
C*************************************************************************
C*                                                                       *
C*   This program will  calculate the  complex  dielectric  constant of a *
C*   from time domain reflectometry (TDR) measurements on a sample.  Only *
C*   data  obtained  from  probes with 3.6 mm  outer  conductor  diameter  *
C*   can be  inputted to the  program.   This  may be  altered  for  other *
C*   probe  sizes by  adjusting the  constants C0, CF and CS according to *
C*   equations  given in the  reference below.    The time  length of the *
C*   waveforms and the number of digitized points may also be adjusted.   *
C*                                                                       *
C*   Note, the  program is user  interactive, prompting  the user for the *
C*   number and names of data files and data titles. Should a discrepancy *
C*   occur  in  the data, and error  message will be  generated.  ERROR 1 *
C*   indicates  two  solutions for the  complex  dielectric constant were *
C*   found with  negative real  dielectric constants (ie., two impossible *
C*   sulutions were encountered).   ERROR 2  incicates that two  possible *
C*   solutions were encountered.                                         *
C*                                                                       *
C*   This program was written by Hung Pin KAO,  Department of  Electrical *
C*   Engineering, University of Manitoba, June, 1989.                    *
C*                                                                       *
C*   Important Program Variables                                         *
C*   ===========================                                         *
C*                                                                       *
C*            INPUT       -       Vector containing incident waveform  *
C*            FNT         -       Vector containing reflected waveform *
C*            FINT        -       Complex value of fourier transform of the *
C*                                incident waveform at a prescribed frequency *
C*            FFNT        -       Complex value of fourier transform of the *
C*                                reflected waveform at a prescribed frequency *
C*            PERIOD      -       Time length of the waveforms         *
C*            POINTS      -       Number of digitized points           *
C*            C0,CS,CF    -       Variables needed to calculate the sample *
C*                                impedance                            *
C*            CT          -       Complex sample capacitance           *
C*            Z0          -       Characteristic impedance of coaxial cable *
C*            F0          -       First frequency at which the dielectric *
C*                                constant is calculated               *
C*            FINC        -       Incremental frequency at which dielectric *
C*                                constant is calculated.  Note, the second *
C*                                frequency used is FINC, the third is 2*FINC, *
C*                                and so on.                           *
C*            MAX         -       Number of frequencies to be calculated *
C*                                                                     *
C*   Reference for equations of C0, CF and CS                          *
C*   ========================================                          *
C*                                                                     *
C*   G. Gajda and S.S. Stuchly, "Equivalent Circuit of an Open-Ended Coaxial *
C*   Cable," IEEE Transactions on Instrumentation and Measurement,     *
C*   vol. IM-32, pp. 506-508, December 1983                            *
C*                                                                     *
C*************************************************************************
C
      REAL*8 INPUT(512),FNT(512),PERIOD,T,C0,CF,CS,Z0,W,F,F0,FINC,PI,ZEROI,
     *       ZEROF,ZERO,TEMP1,TEMP2,XTEMP,YTEMP
      INTEGER POINTS,MAX,I,M,K
      COMPLEX*16 FINT,FFNT,A,B,C,CONST,P,CT,E,E1,E2,CFREQ
      CHARACTER*25 JUNK
```

```
      CHARACTER*64 FNAME,TITLE
C
C Set program constants.
C
      PERIOD=5D-9
      POINTS=512
      POINTS=POINTS-1
      T=PERIOD/POINTS
      C0=1.792034306D-14
      CS=4.587901449D-15
      CF=3.707024371D-16
      Z0=50.0
      F0=100.0
      FINC=250.0
      MAX=5
      ZERO=0.0
      PI=3.141592654
      XTEMP=0.3235*C0
      A=DCMPLX(XTEMP,ZERO)
      XTEMP=C0+CS+0.3235*CF
      CONST=DCMPLX(XTEMP,ZERO)
C
C Prompt user for name of file to contain dielectric constant data and open
C file.
C
      WRITE (*,500)
      READ(*,510) FNAME
      OPEN(1,FILE=FNAME)
C
C Prompt user for number of samples to be calculated.
C
      WRITE(*,520)
      READ(*,*) M
C
C Adjust first page spacing.
C
      WRITE(1,*) ' '
C
C Begin calculations.
C
      DO 10 K=1,M
C
C Prompt user for new waveform files and open the files.
C
        WRITE(*,530)
        READ(*,510) FNAME
        OPEN(2,FILE=FNAME)
C
        WRITE(*,540)
        READ(*,510) FNAME
        OPEN(3,FILE=FNAME)
C
C Prompt user for title of sample dielectric constants.
C
        WRITE(*,550)
        READ(*,510) TITLE
C
C Read in data from waveform files into INPUT and FNT.
C
        READ(2,510) JUNK
```

```
          DO 20 I=1,512
             READ(2,*) INPUT(I)
20         CONTINUE
C
          READ(3,510) JUNK
          DO 30 I=1,512
             READ(3,*) FNT(I)
30        CONTINUE
C
C Adjust zero level of waveform files.
C
          ZEROI=INPUT(6)
          ZEROF=FNT(6)
          DO 40 I=6,512
              INPUT(I)=INPUT(I)-ZEROI
              FNT(I)=FNT(I)-ZEROF
40        CONTINUE
C
C Write title onto screen and output file.
C
          WRITE(*,*) ' '
          WRITE(1,*) ' '
          WRITE(*,*) ' '
          WRITE(1,*) ' '
          WRITE(*,*) TITLE
          WRITE(1,*) '       ', TITLE
          WRITE(*,*) ' '
          WRITE(1,*) ' '
          WRITE(*,560)
          WRITE(1,570)
C
C Calculate sample dielectric constant at each frequency.
C
          F=F0
          DO 50 I=1,5
             W=2*PI*F*1E6
C
C Find fourier transform of each waveform at frequency W.
C
             CALL FORIER(W,INPUT,FINT,T,POINTS)
             CALL FORIER(W,FNT,FFNT,T,POINTS)
C
C Determine the reflection coefficient at frequency W and complex capacitance,
C CT.
C
             P=FFNT/FINT
             CFREQ=DCMPLX(ZERO,W)
             CT=(1-P)/(Z0*(1+P)*CFREQ)
C
C Calculate dielectric constant from complex capacitance.
C
             B=CONST-0.3235*CT
             C=CF-CT
             E1=(-B+CDSQRT(B**2-4*A*C))/(2*A)
             E2=(-B-CDSQRT(B**2-4*A*C))/(2*A)
C
C Check if discrepancies exist in result.
C
             TEMP1=CDABS(CDEXP(E1))
             TEMP2=CDABS(CDEXP(E2))
```

```
            IF (TEMP1.GE.1.0) THEN
               E=E1
            ELSE
               E=E2
            END IF
            IF (TEMP1.LE.1.0 .AND. TEMP2.LE.1.0) WRITE(*,*) 'ERROR 1'
            IF (TEMP1.GE.1.0 .AND. TEMP2.GE.1.0) WRITE(*,*) 'ERROR 2'
C
C Write results onto screen and into output file.
C
            WRITE(*,*) ' '
            WRITE(1,*) ' '
            WRITE(*,580) F,E
            WRITE(1,590) F,E
C
C Increment frequency.
C
            F=FINC*I
C
50       CONTINUE
C
C Close waveform files.
C
         CLOSE(2)
         CLOSE(3)
C
C Set page skip.
C
         IF (MOD(K,4).EQ.0) THEN
            WRITE(1,600) CHAR(12)
         END IF
C
10    CONTINUE
C
      STOP
500   FORMAT(' Name of file to contain dielectric constants: '\)
510   FORMAT(A)
520   FORMAT(' How many samples to be calculated ? '\)
530   FORMAT(' Incident Waveform Filename: '\)
540   FORMAT(' Reflected Waveform Filename: '\)
550   FORMAT(' Set Title of Data: '\)
560   FORMAT(9X,'Frequency (MHz)',10X,'Dielectric Constant',6X,
     *'Loss Factor')
570   FORMAT(12X,'Frequency (MHz)',10X,'Dielectric Constant',6X,
     *'Loss Factor')
580   FORMAT(12X,F6.1,18X,f10.3,12X,F10.3)
590   FORMAT(15X,F6.1,18X,F10.3,12X,F10.3)
600   FORMAT(A1)
      END
C
      SUBROUTINE FORIER(W,FUNC,FFUNC,T,POINTS)
C
C   This subroutine will determine the value of the fourier transform of a
C   digitized step pulse at radian frequency, W.  The digitized portion of
C   the waveform is  contained in vector FUNC and the complex value of the
C   transform is contained in FFUNC.   The value of T is the time distance
C   between the points.  Calculation of the transform is by Simpson's rule
C   of  numerical  integration,  adding to the sum the value of a  delayed
C   step pulse with height equal to the value of the last digitized point.
C
```

```
C   Note that the beginning of the waveform is  assumed to be at the sixth
C   digitized point.
C
      INTEGER I,POINTS,UPPER
      REAL*8 W,FUNC(512),ANGLE,T,ZERO,XTEMP,YTEMP
      COMPLEX*16 FIRST,LAST,SUM1,SUM2,FFUNC,TEMP1,TEMP2
C
C Calculate incremental sums from first and last sections.
C
      ANGLE=W*T
      ZERO=0.0
      FIRST=DCMPLX(FUNC(6),ZERO)
      XTEMP=DCOS(506*ANGLE)
      YTEMP=-DSIN(506*ANGLE)
      TEMP1=DCMPLX(XTEMP,YTEMP)
      LAST=FUNC(512)*TEMP1
C
C Compute sums needed to determine remaining areas.
C
      SUM1=(0.0,0.0)
      SUM2=(0.0,0.0)
C
      UPPER=POINTS-6
      DO 30 I=1,UPPER,2
         XTEMP=DCOS(I*ANGLE)
         YTEMP=-DSIN(I*ANGLE)
         TEMP1=DCMPLX(XTEMP,YTEMP)
         SUM1=SUM1+TEMP1*FUNC(I+6)
30    CONTINUE
C
      UPPER=POINTS-7
      DO 40 I=2,UPPER,2
         XTEMP=DCOS(I*ANGLE)
         YTEMP=-DSIN(I*ANGLE)
         TEMP1=DCMPLX(XTEMP,YTEMP)
         SUM2=SUM2+TEMP1*FUNC(I+6)
40    CONTINUE
C
C Determine transform of waveform.
C
      XTEMP=DCOS(W*T*506)
      YTEMP=-DSIN(W*T*506)
      TEMP1=DCMPLX(XTEMP,YTEMP)
      TEMP2=DCMPLX(ZERO,W)
      FFUNC=T/3*(FIRST+4*SUM1+2*SUM2+LAST)+TEMP1/TEMP2*FUNC(512)
C
      RETURN
      END
```

Appendix C

Preparation of Gravimetric Columns

The gravimetric method requires the use of a mixture, or gradient column, contained in a graduated cylinder to measure the specific gravity of tissue samples. The specific gravity of the liquid decreases as the distance from the bottom of the graduated cylinder increases. To construct the gradient, two mixtures of kerosene and bromobenzene are prepared (Figure B1). The upper flask, A, contains liquid with specific gravity $SPGR_A$, while the lower flask, B, contains a denser liquid with specific gravity $SPGR_B$. The position of the flasks is such that hydrostatic pressure would cause the outflow of lighter liquid ($SPGR_A$) from A to B to be half that of the mixture from B to the cylinder. A drop or two of liquid is then siphoned out of flask A using connecting tube 1, after which the tube is clamped. Next, the double outflow tubes, 2, from solution B into the cylinder are siphoned and clamped. All 3 tubes are then simultaneously unclamped, allowing the cylinder to slowly fill with a linear density gradient. Care was taken to ensure severe tube crimping did not occur. To allow for uniform mixing, a mixer constantly stirs the contents of flask B. The mechanical stage shown raised the flasks in order maintain hydrostatic pressure constant. The time required to load a column of 0.5 liters is approximately 1.5 hours plus 1 hour to allow the column to settle.

The specific gravity at the bottom of the column (depth=0) equals the initial specific

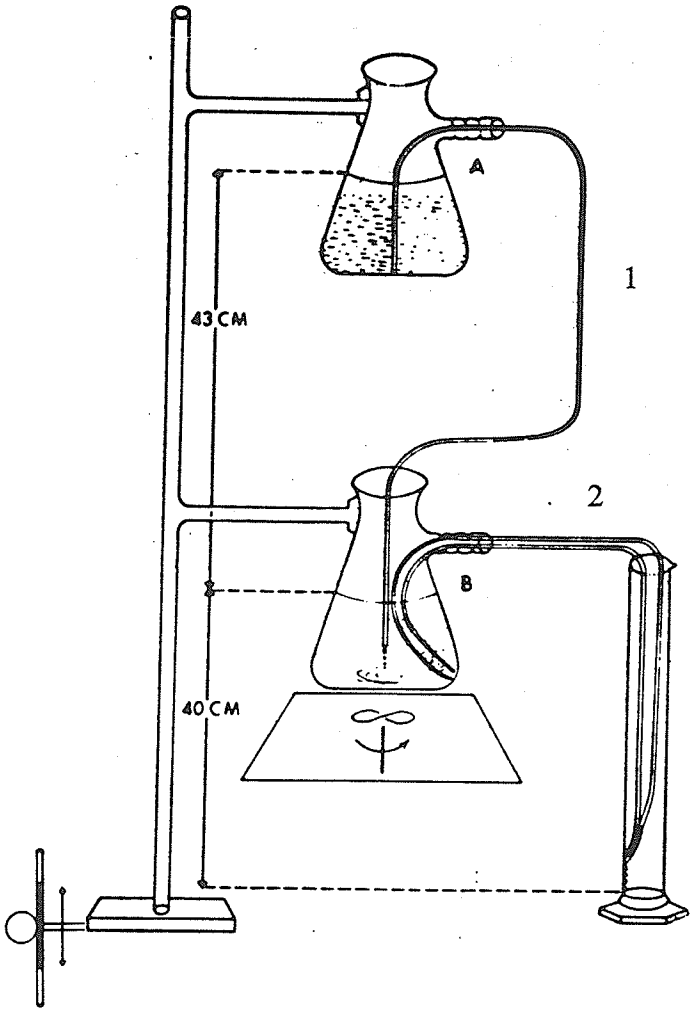

Figure B1: Setup for the preparation of a Gravimetric Column

Source: Reference [41]

gravity of flask B, $SPGR_B$. At the top of the cylinder, the specific gravity equals the average of the initial specific gravities of the two flasks. The volumes of kerosene (specific gravity = 0.78734), K, and bromobenzene (specific gravity = 1.49716), BB, required to produce stocks A and B can be found from the following equations (for 1000 ml of solution):

$$\text{ml of BB} = \frac{\text{desired spgr - spgr K}}{\text{spgr BB - spgr K}} \times 1000 \qquad \text{(B.1)}$$

$$\text{ml of K} = 1000 - \text{ml of BB} \qquad \text{(B.2)}$$

The linearity of the column was tested when completed using specific gravity standards made of potassium sulfate and distilled water. One drop of each standard was gently placed in the column using a small syringe and its depth of equilibrium was recorded at 2 minutes. The specific gravity at this depth was that of the standard solution.

Small tissue samples (less than 5 mg) can be measured by dropping them in the column and recording its equilibrium depth at two minutes. From a least squares linear fit between specific gravity standard values and their depths, the sample specific gravity may be found. If water is the only substance to enter the brain, as in osmotic edema, then equation (2) relating the inverse of the specific gravity of cerebral tissue with its water content may be used to determine the water content of the sample. For canine white matter, the specific gravity of normal tissue has been found to be 1.0437 [31] while the normal water content has been found to be 68.6 % [50]. The equation to calculate the water content of cerebral tissue from its specific gravity may be determined from the linear interpolation between the specific gravity of 1.0437 for a water content of 68.6 % and the specific gravity of 1.0000 for a water content of 100.0 % in equation (2).

Appendix D

Real Dielectric Constant and Loss Factor

vs.

Water Content

for In-Vitro Production of Osmotic Edema

Dielectric Constant vs. Water Content

Frequency = 100 MHz

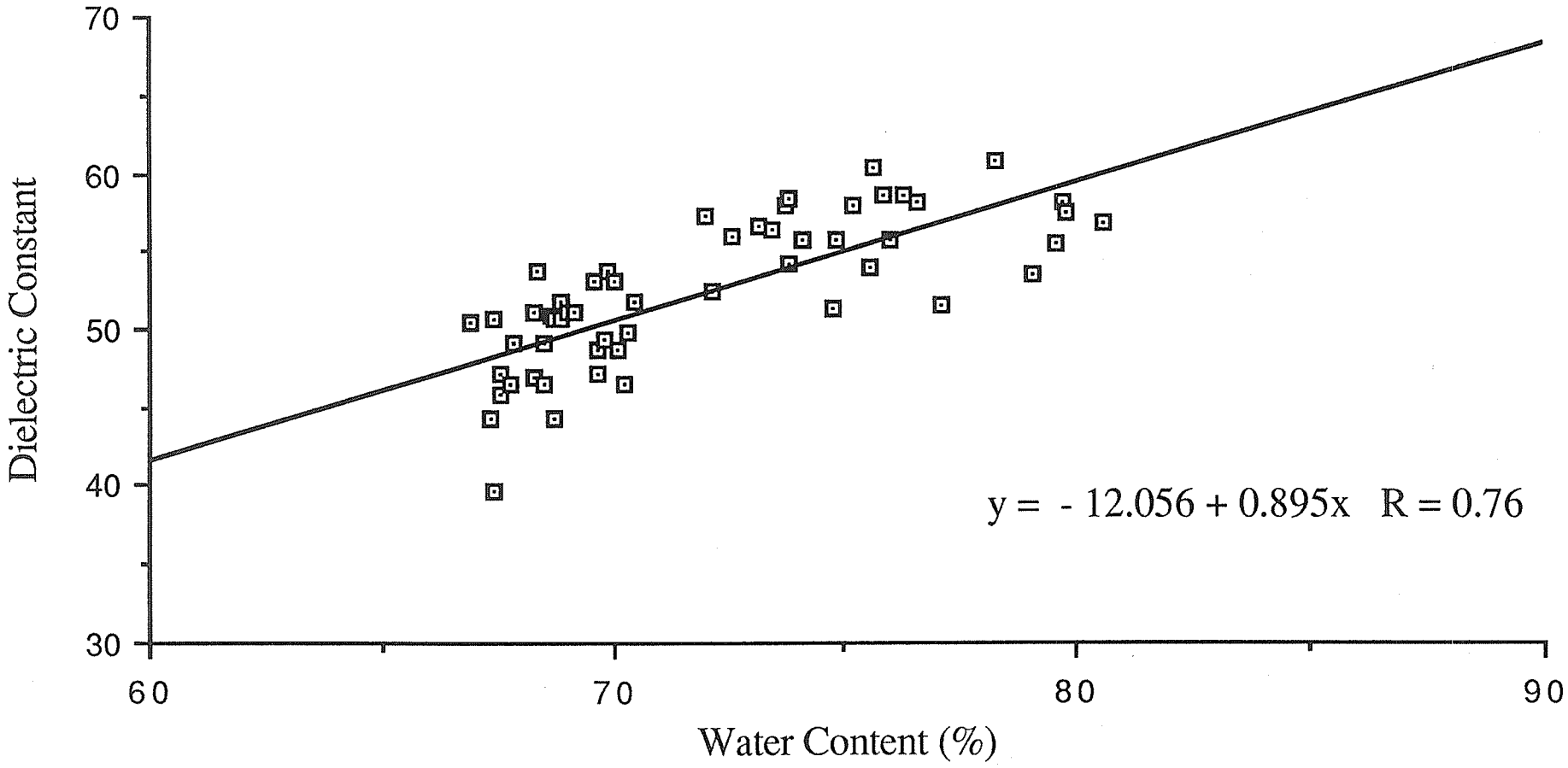

Dielectric Constant vs. Water Content

Frequency = 250 MHz

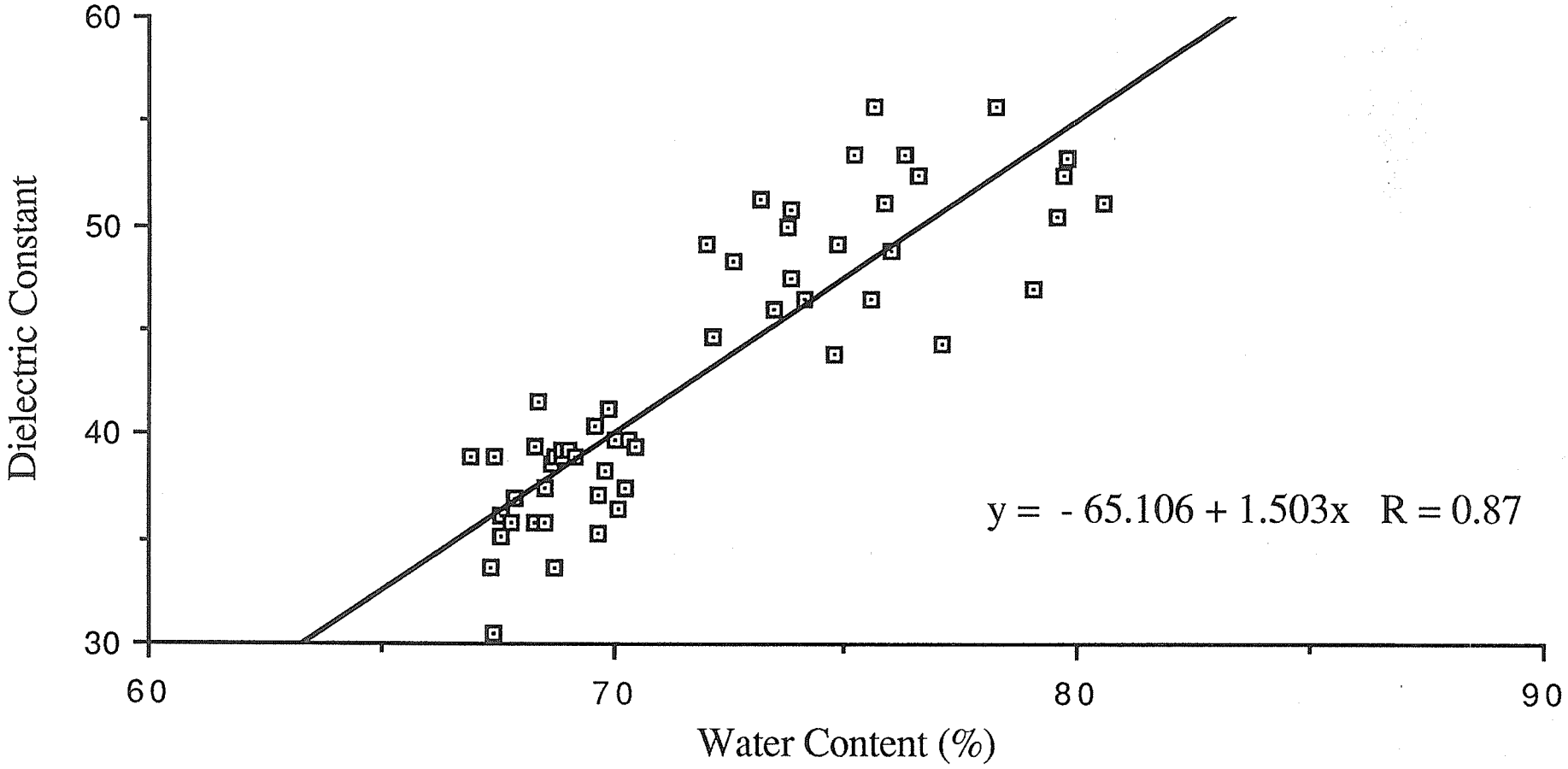

Dielectric Constant vs. Water Content

Frequency = 500 MHz

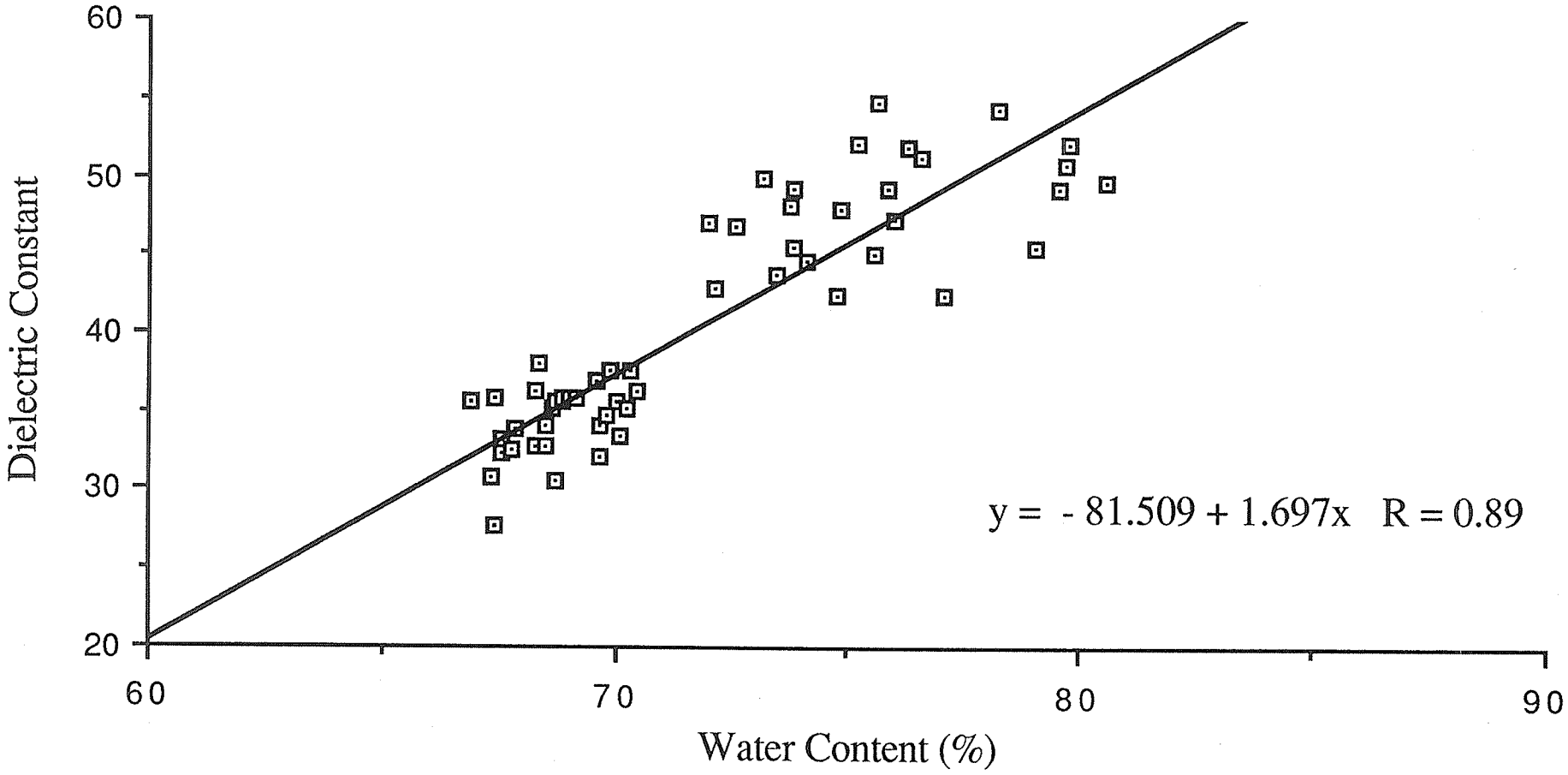

Dielectric Constant vs. Water Content

Frequency = 750 MHz

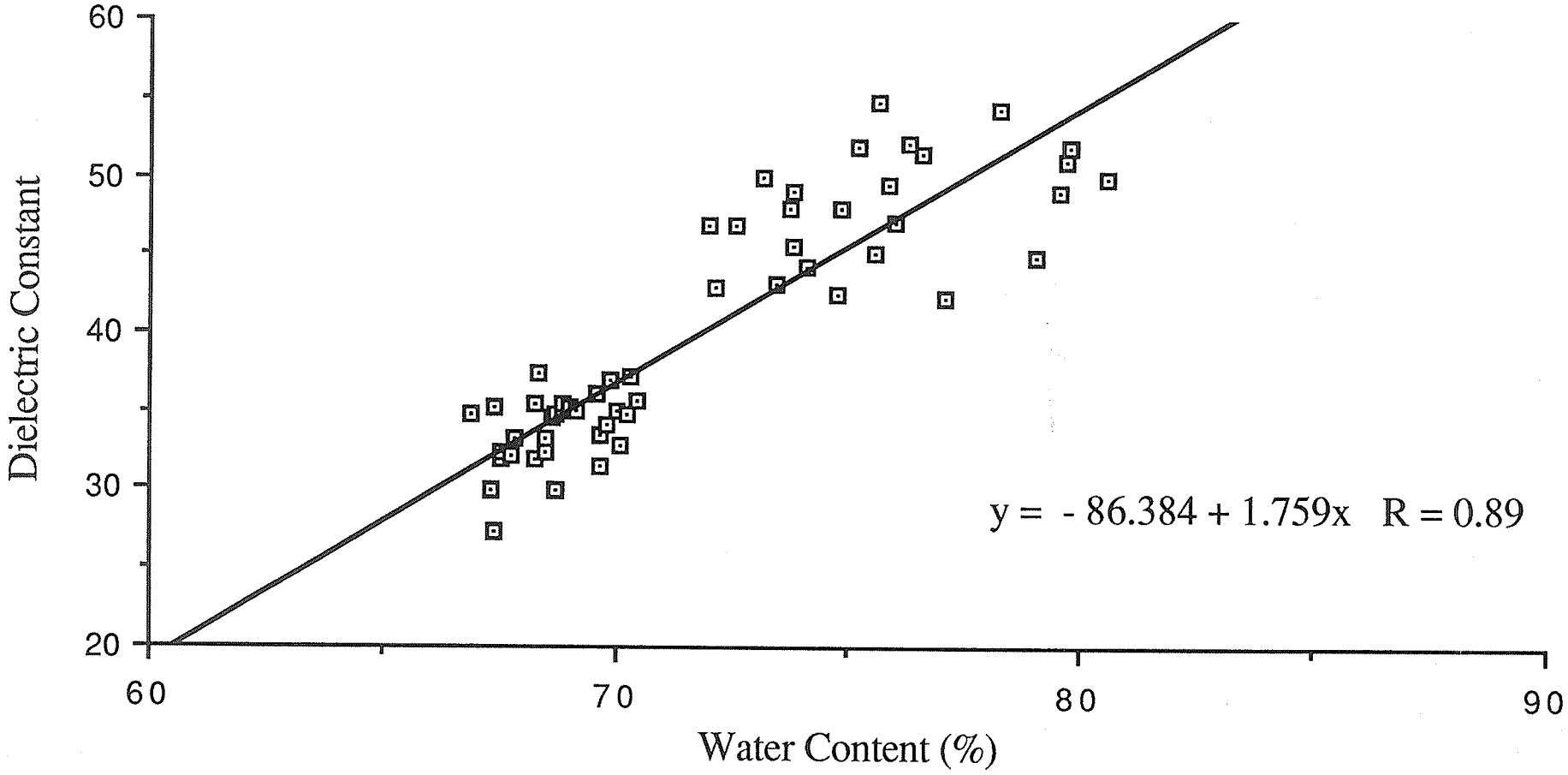

Dielectric Constant vs. Water Content

Frequency = 1000 MHz

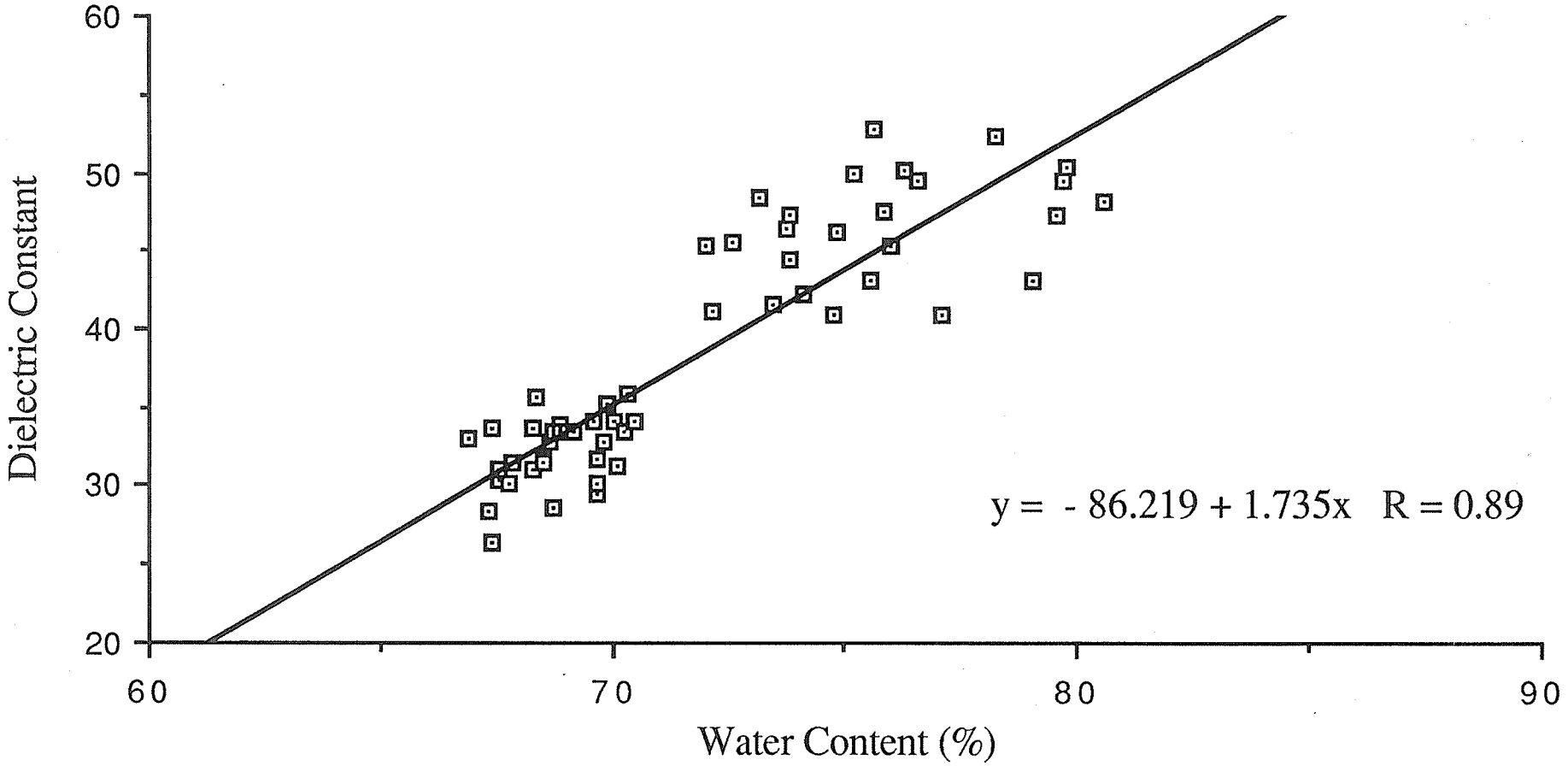

Loss Factor vs. Water Content

Frequency = 100 MHz

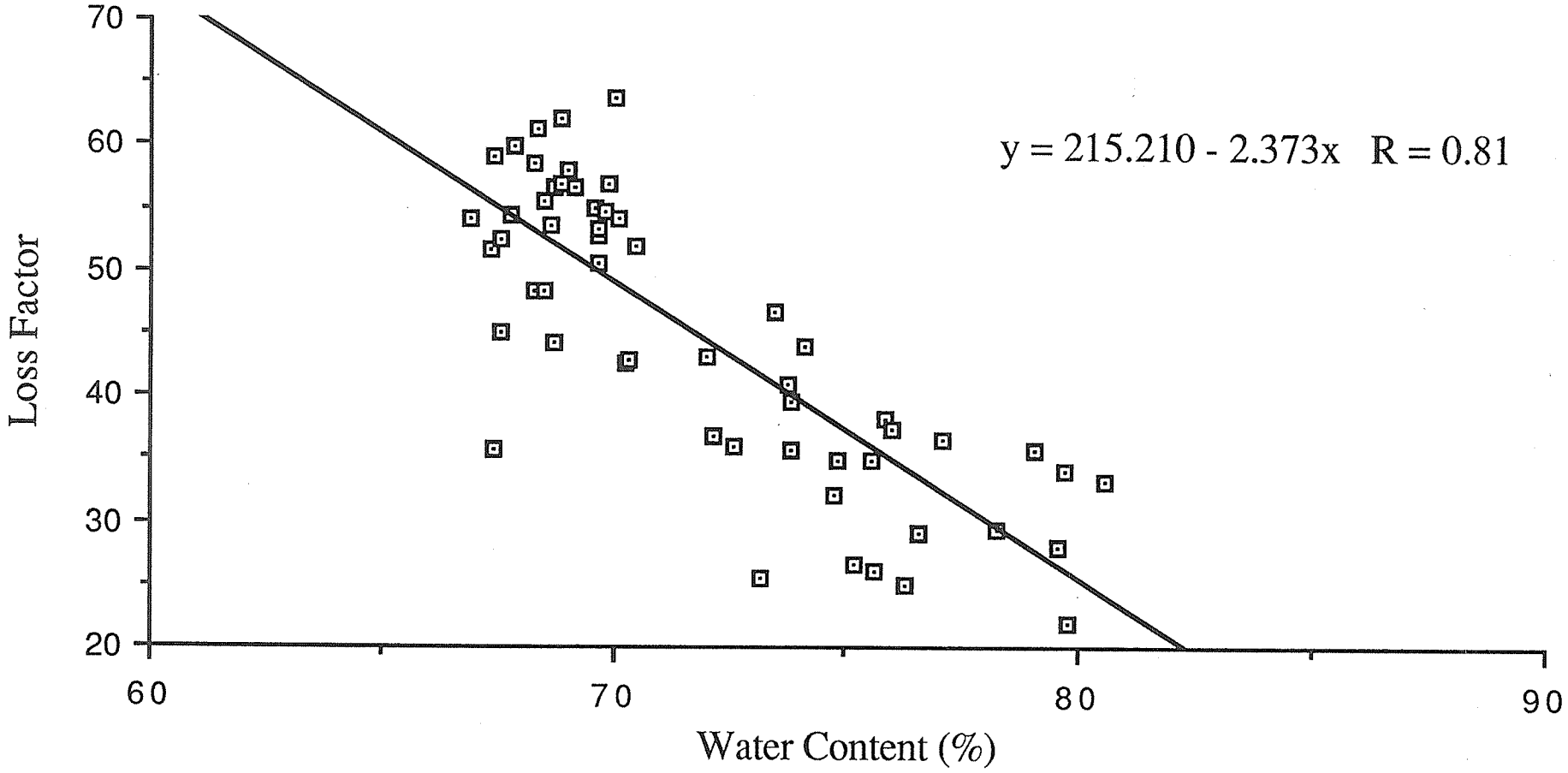

Loss Factor vs. Water Content

Frequency = 250 MHz

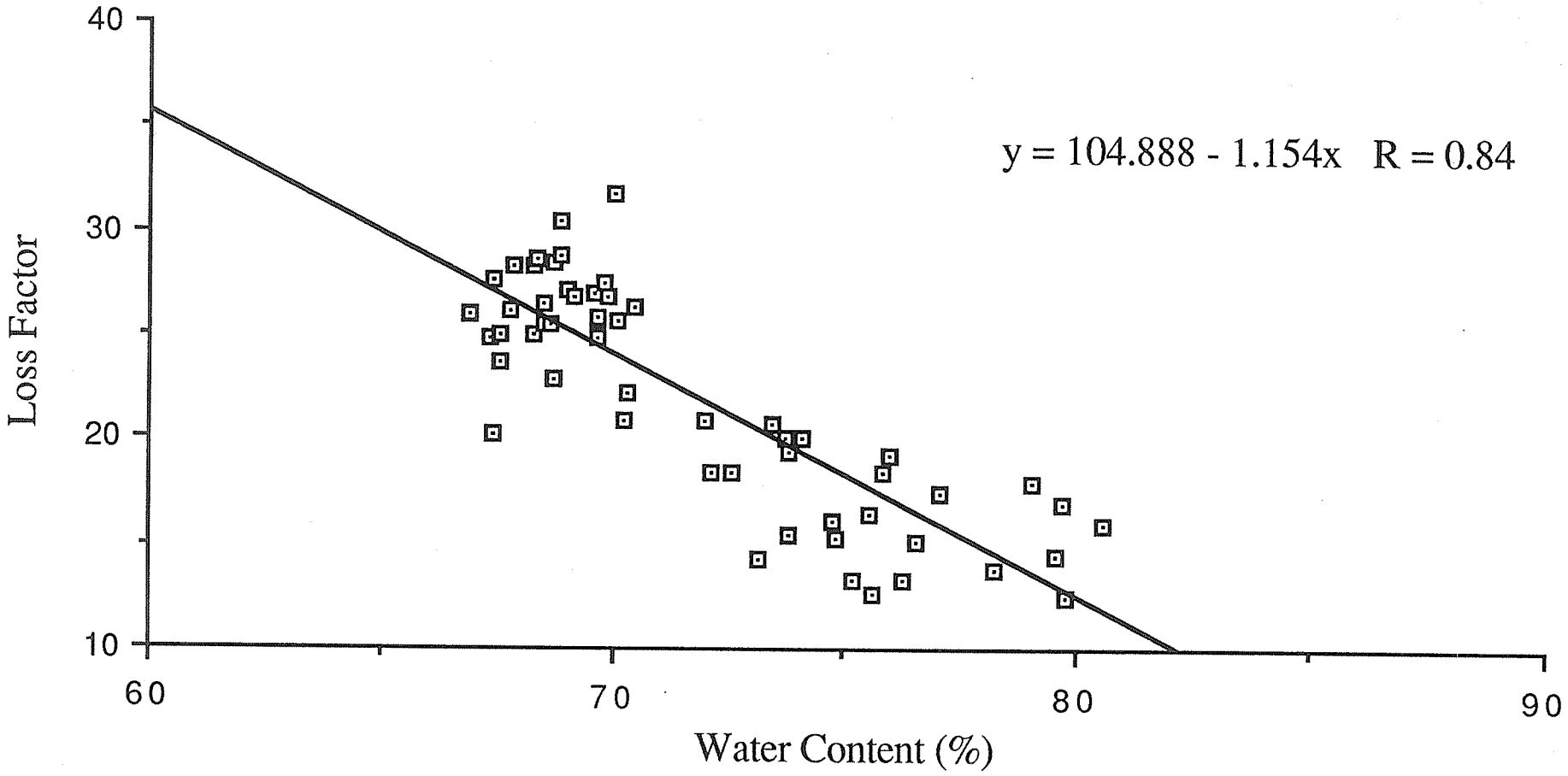

Loss Factor vs. Water Content

Frequency = 500 MHz

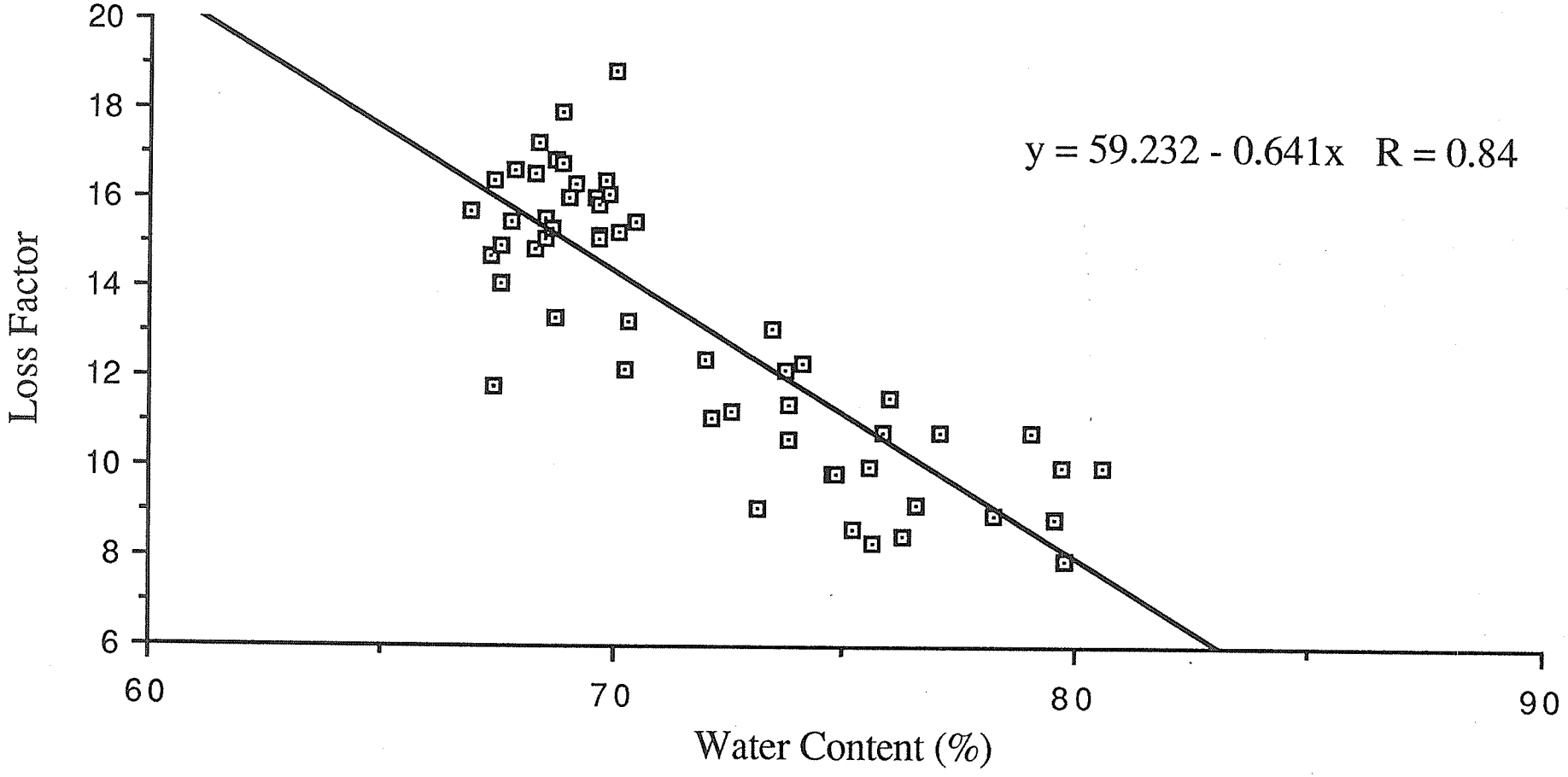

Loss Factor vs. Water Content

Frequency = 750 MHz

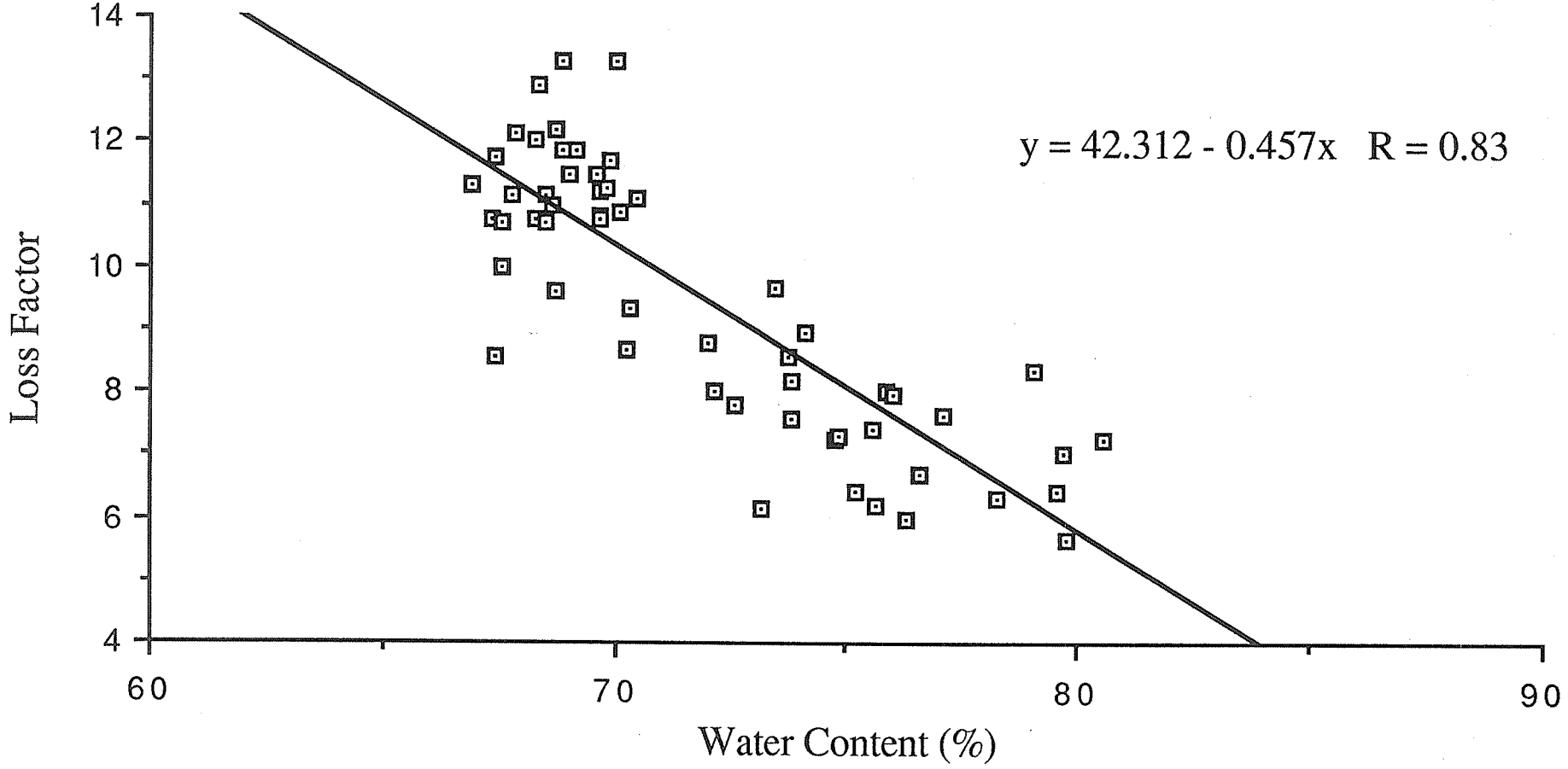

Loss Factor vs. Water Content

Frequency = 1000 MHz

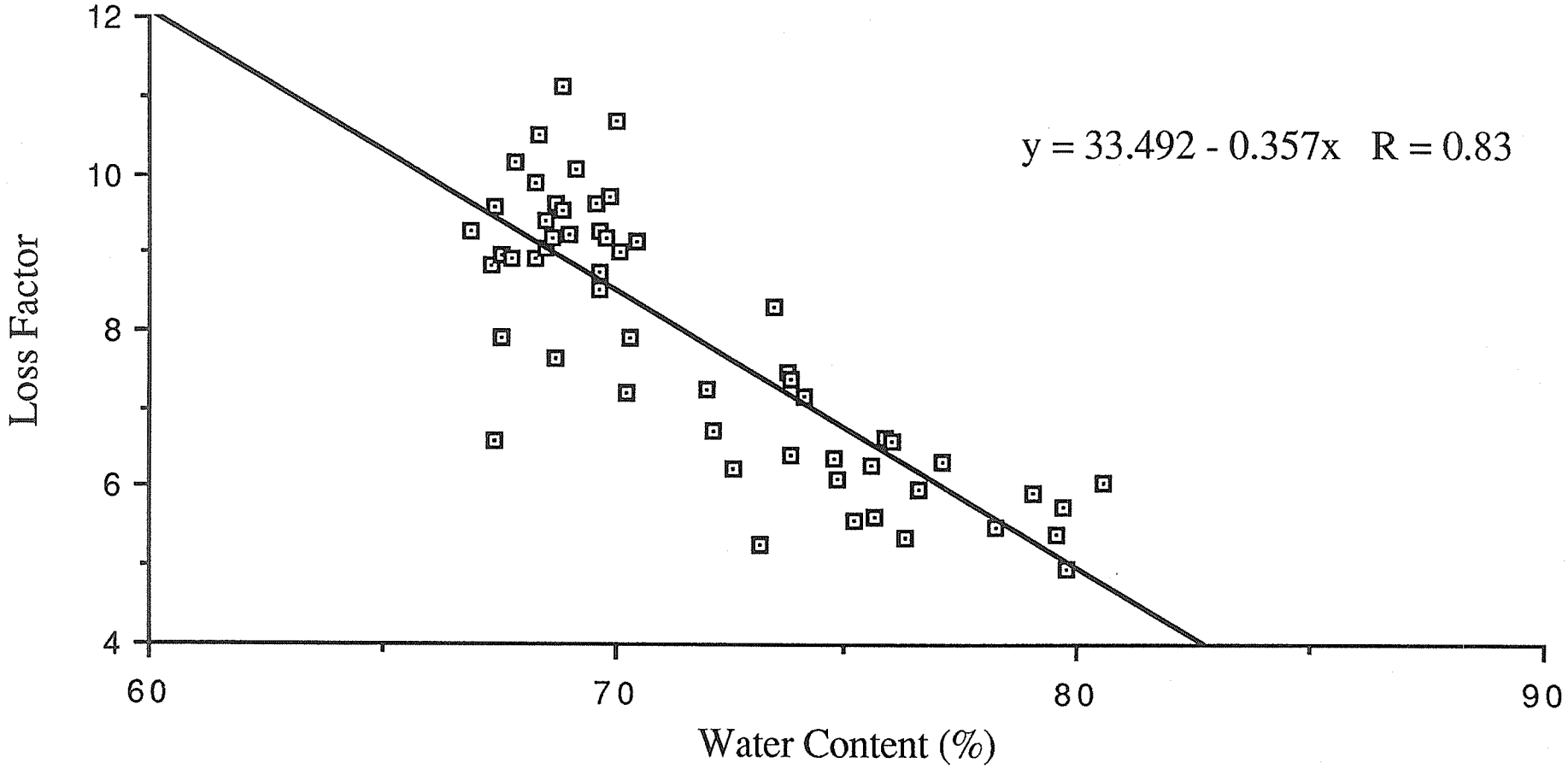

Appendix E

Real Dielectric Constant and Loss Factor

vs.

Water Content

for In-Vivo Production of Osmotic Edema

Dielectric Constant vs. Water Content

Frequency = 100 MHz

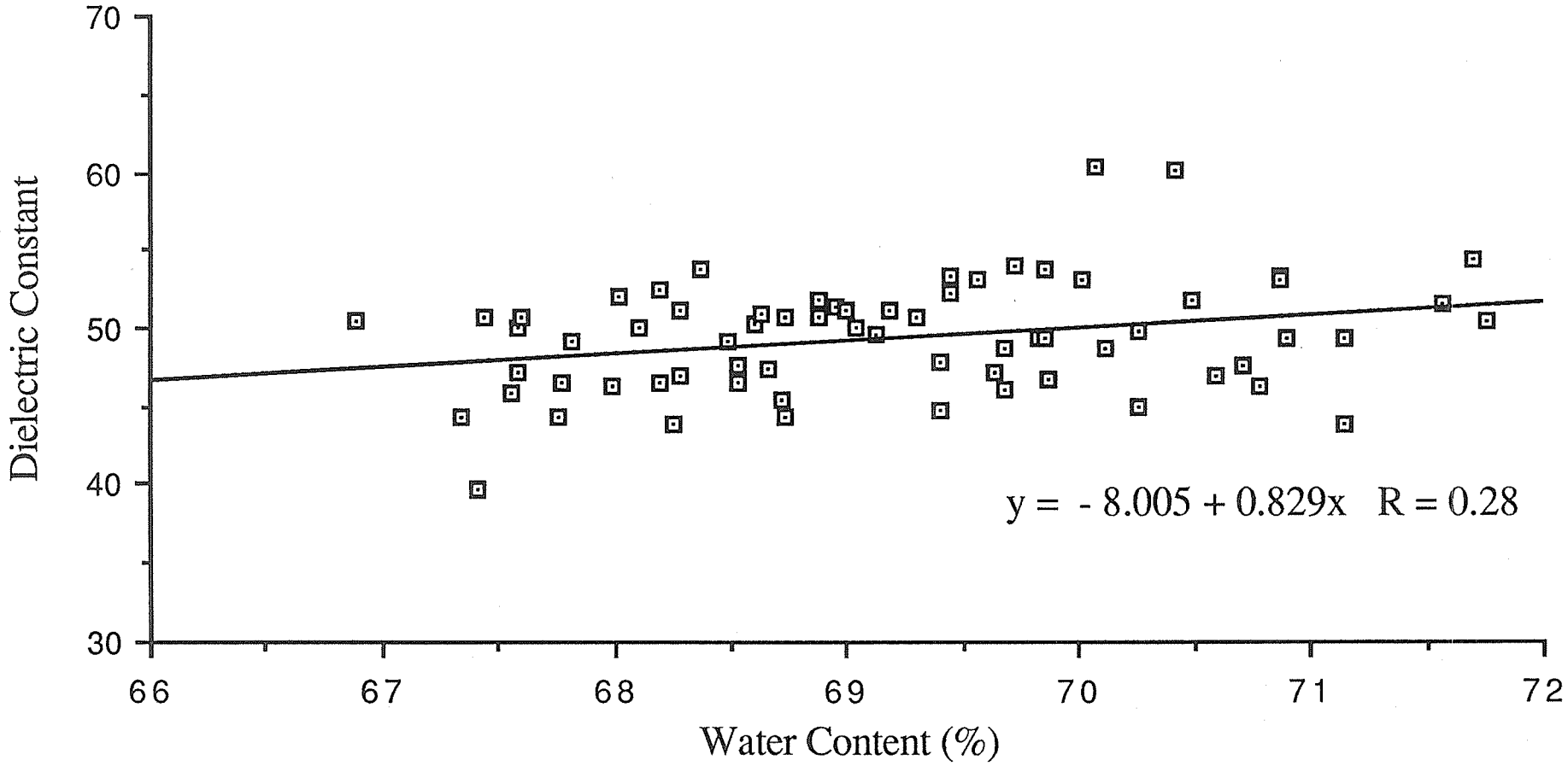

Dielectric Constant vs. Water Content

Frequency = 250 MHz

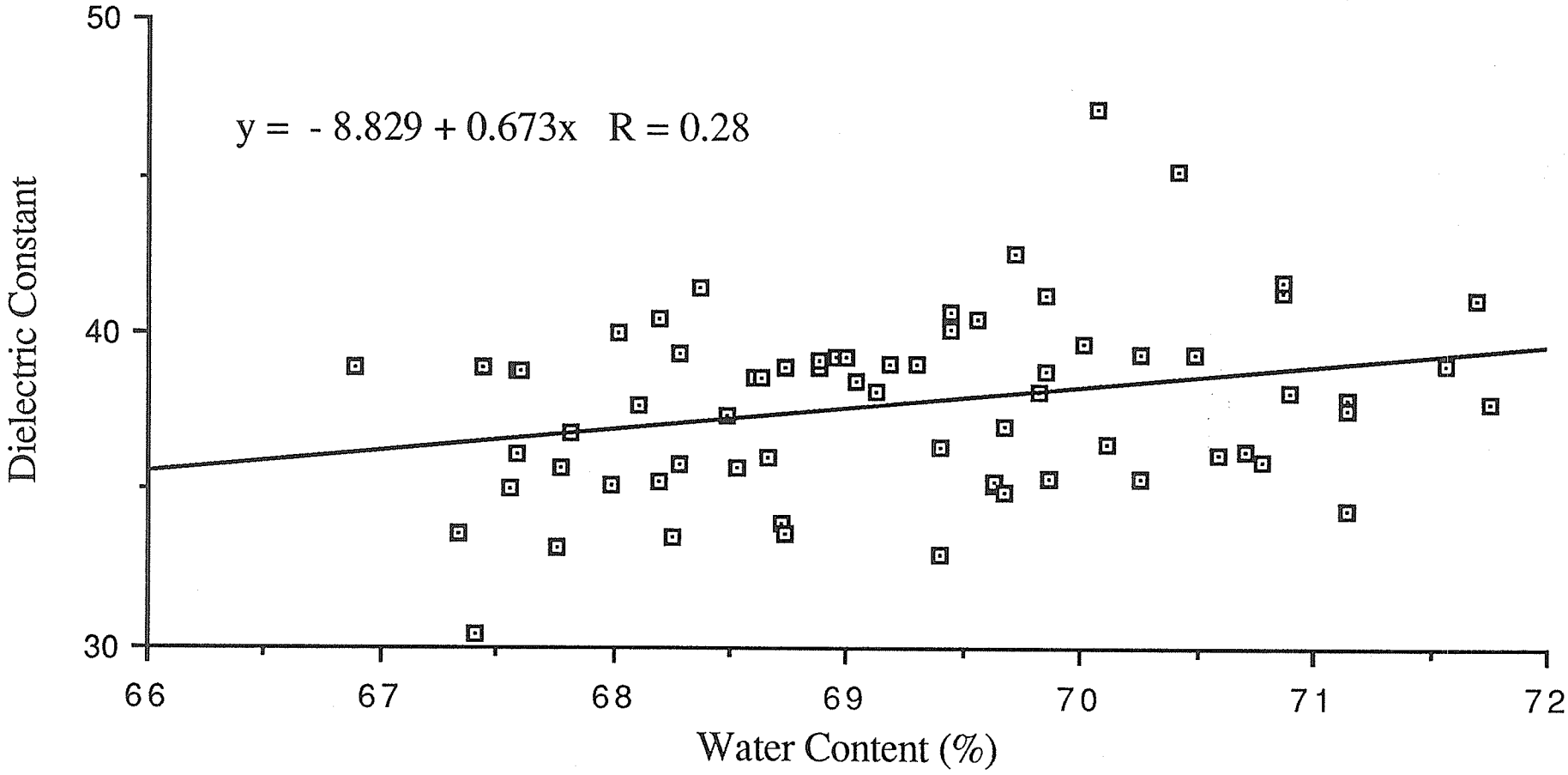

Dielectric Constant vs. Water Content

Frequency = 500 MHz

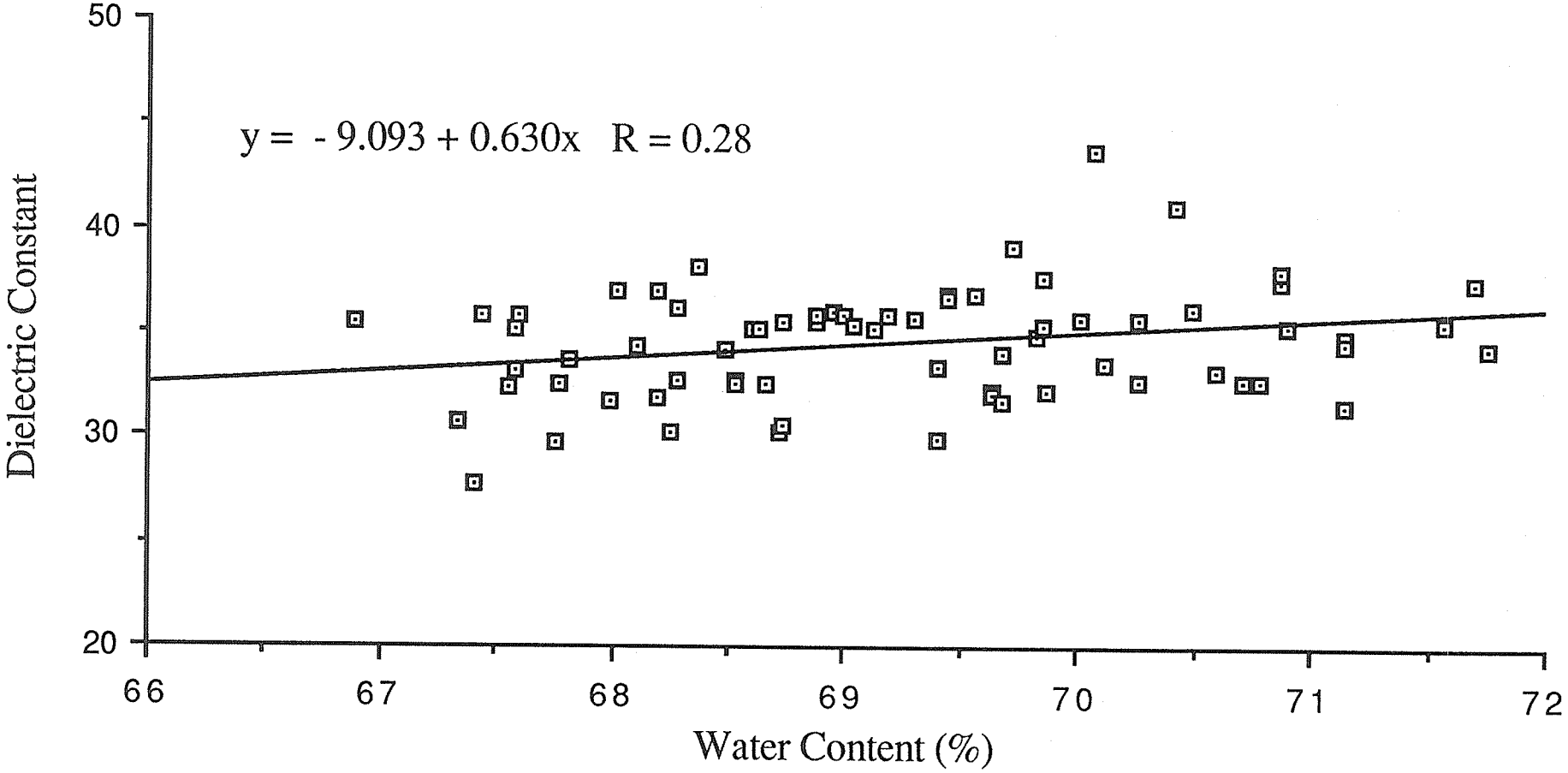

Dielectric Constant vs. Water Content

Frequency = 750 MHz

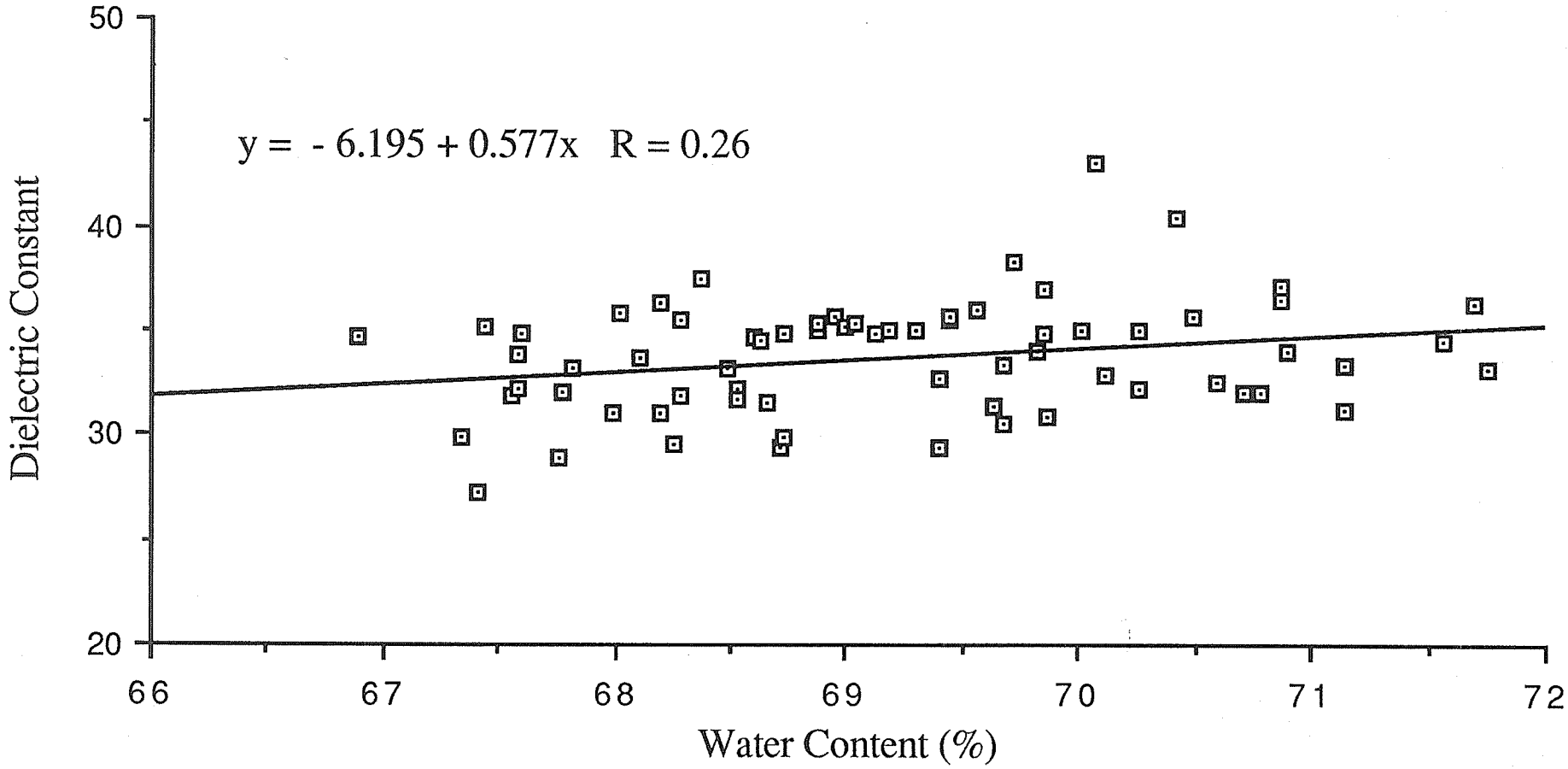

Dielectric Constant vs. Water Content

Frequency = 1000 MHz

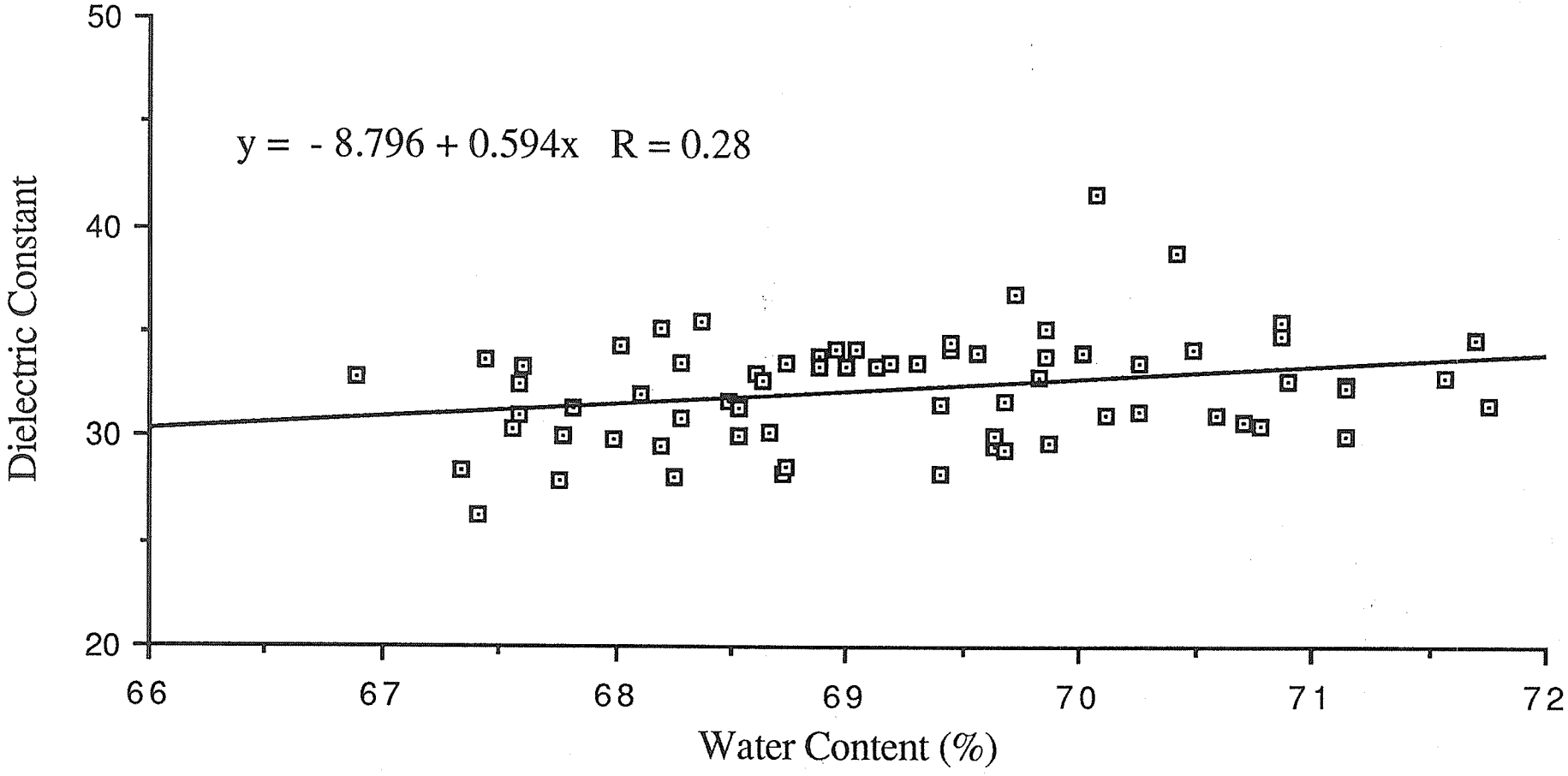

Loss Factor vs. Water Content

Frequency = 100 MHz

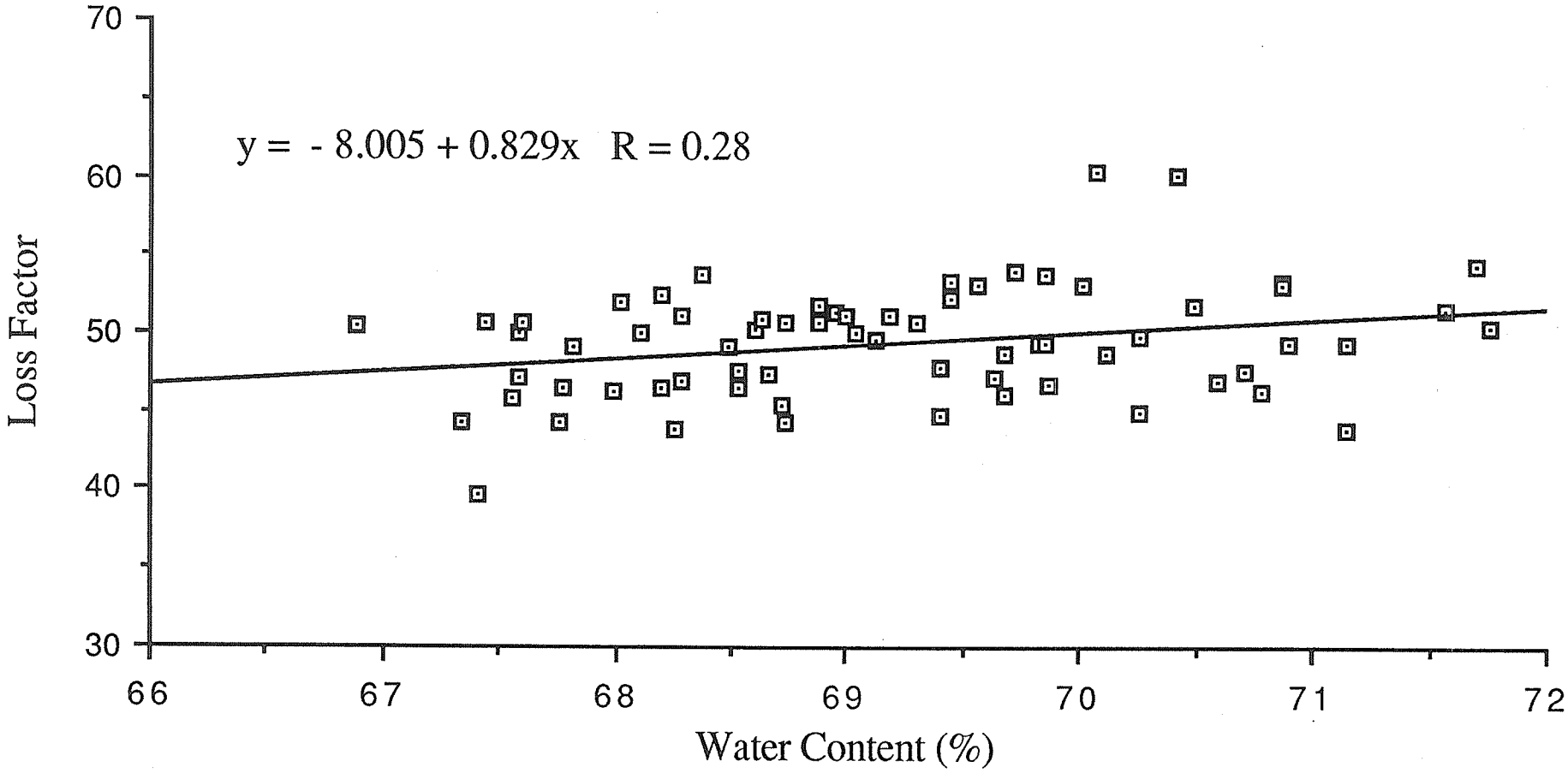

Loss Factor vs. Water Content

Frequency = 250 MHz

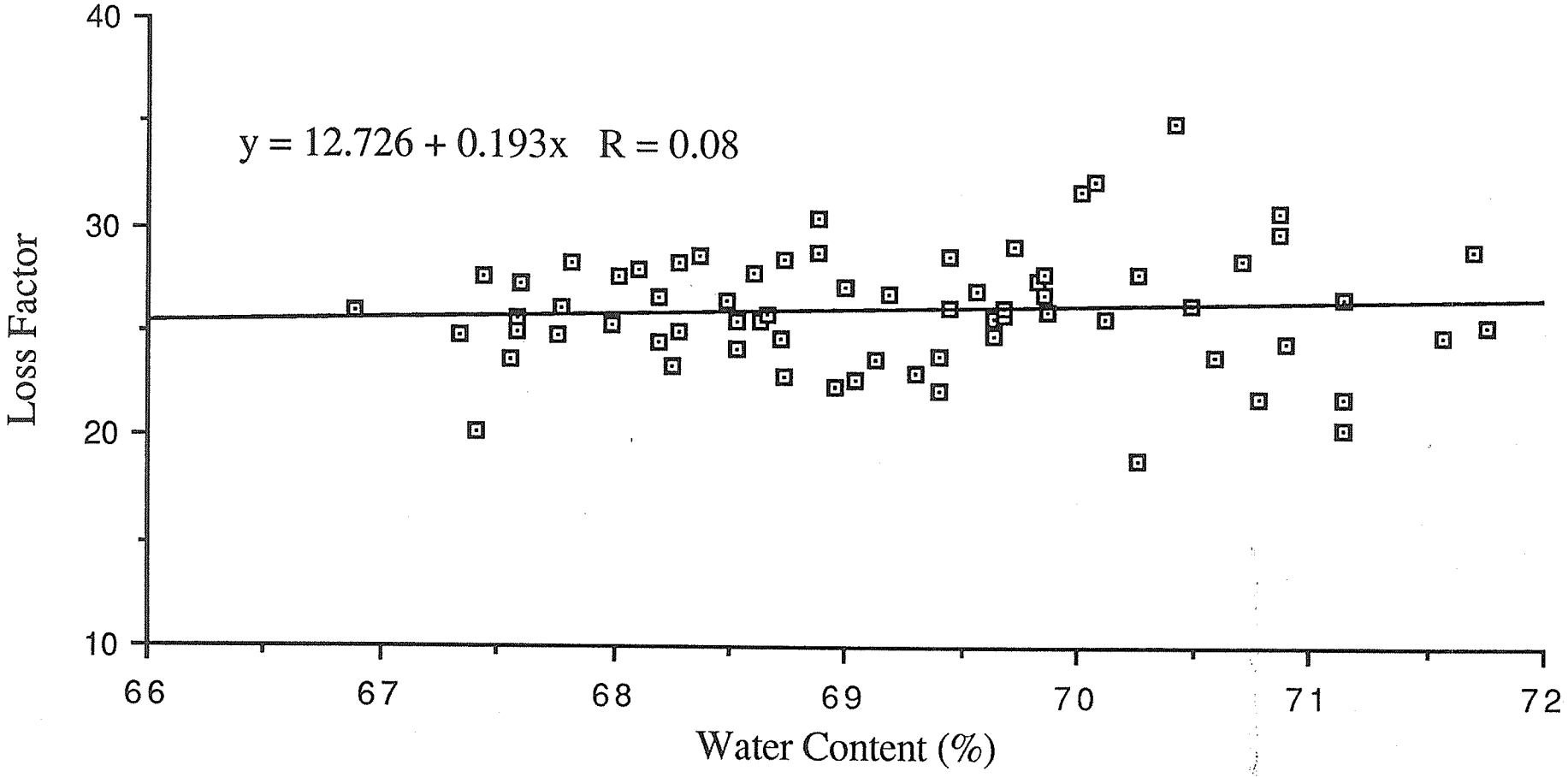

Loss Factor vs. Water Content

Frequency = 500 MHz

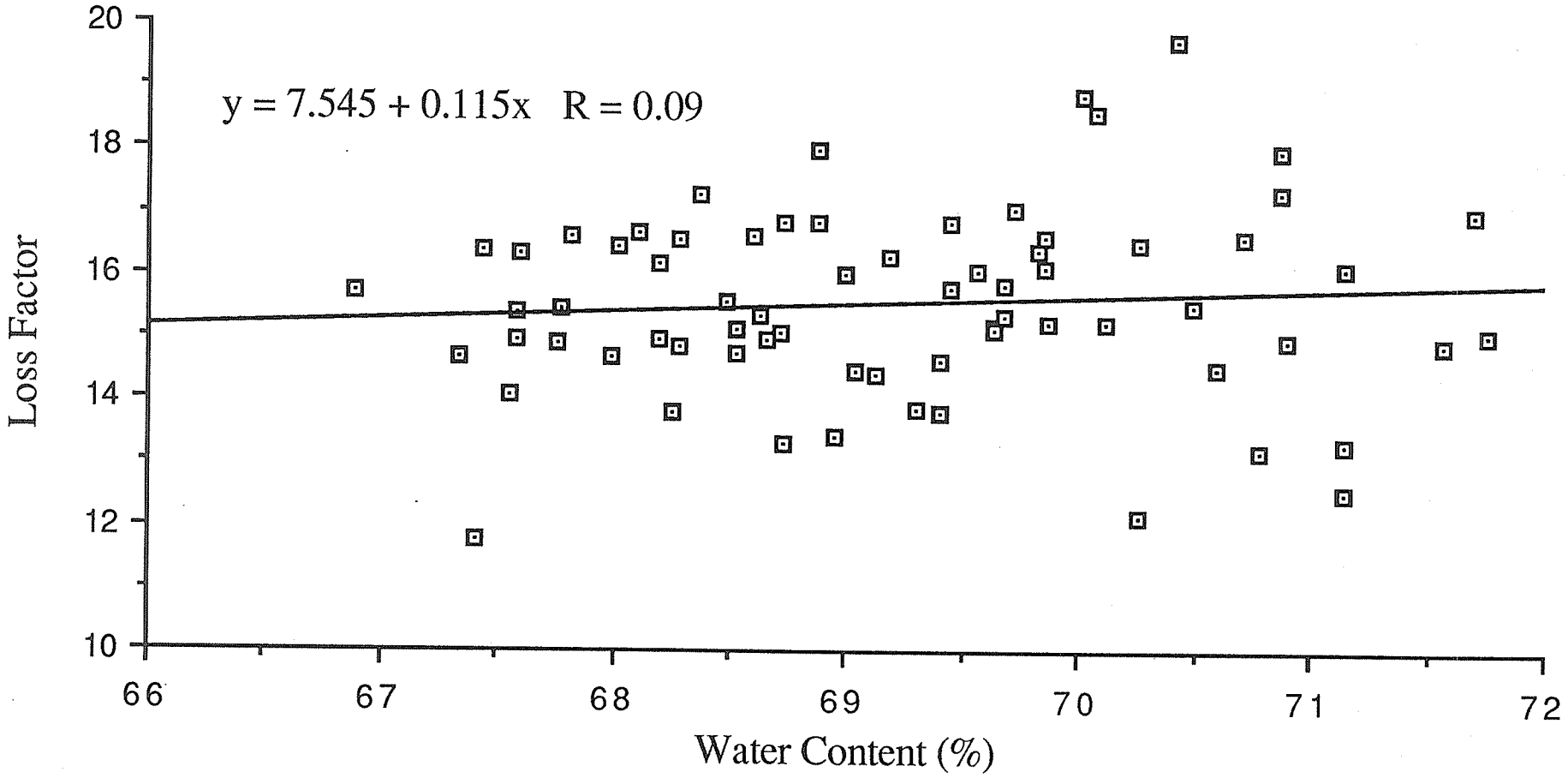

Loss Factor vs. Water Content

Frequency = 750 MHz

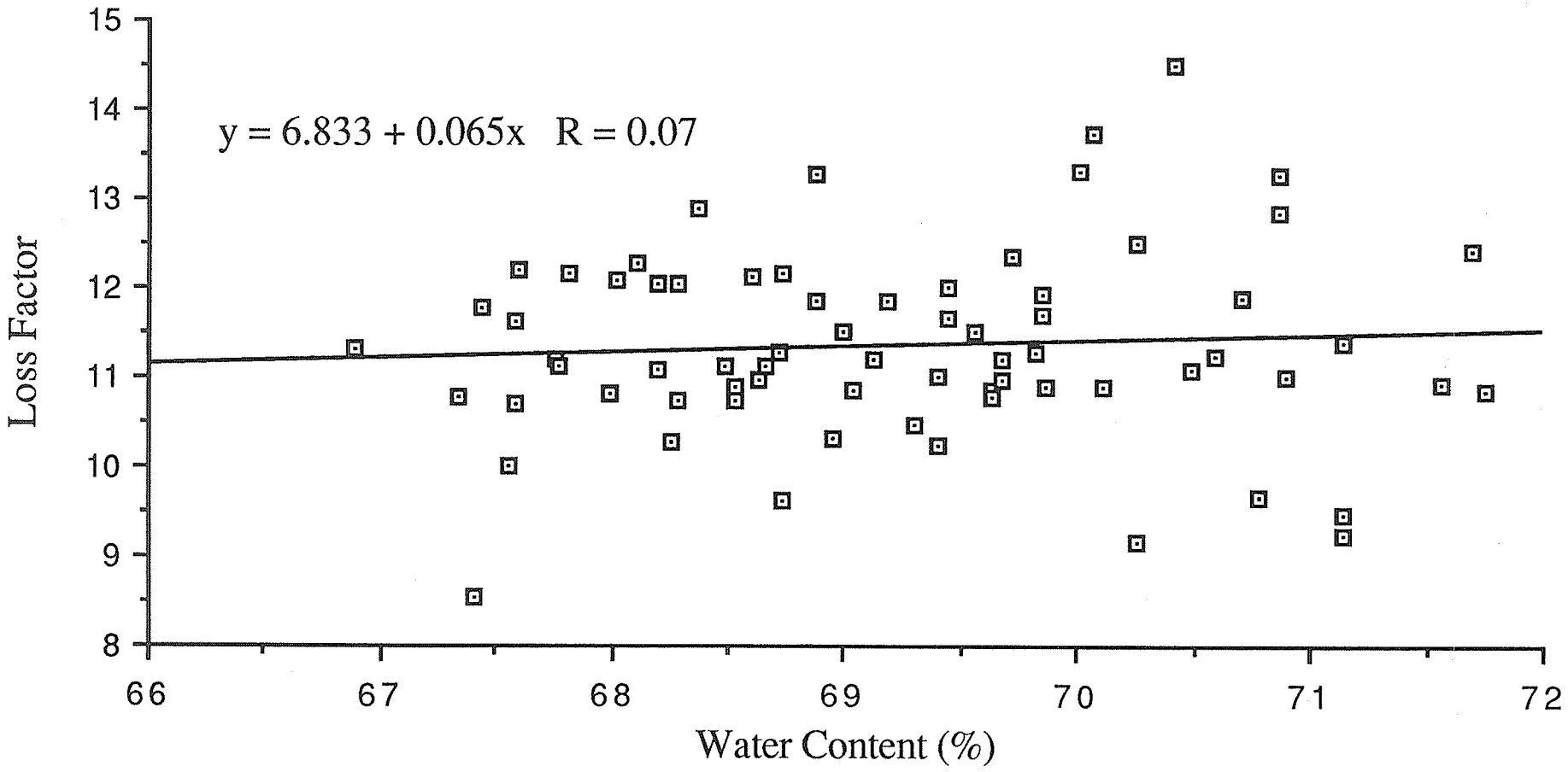

Loss Factor vs. Water Content

Frequency = 1000 MHz

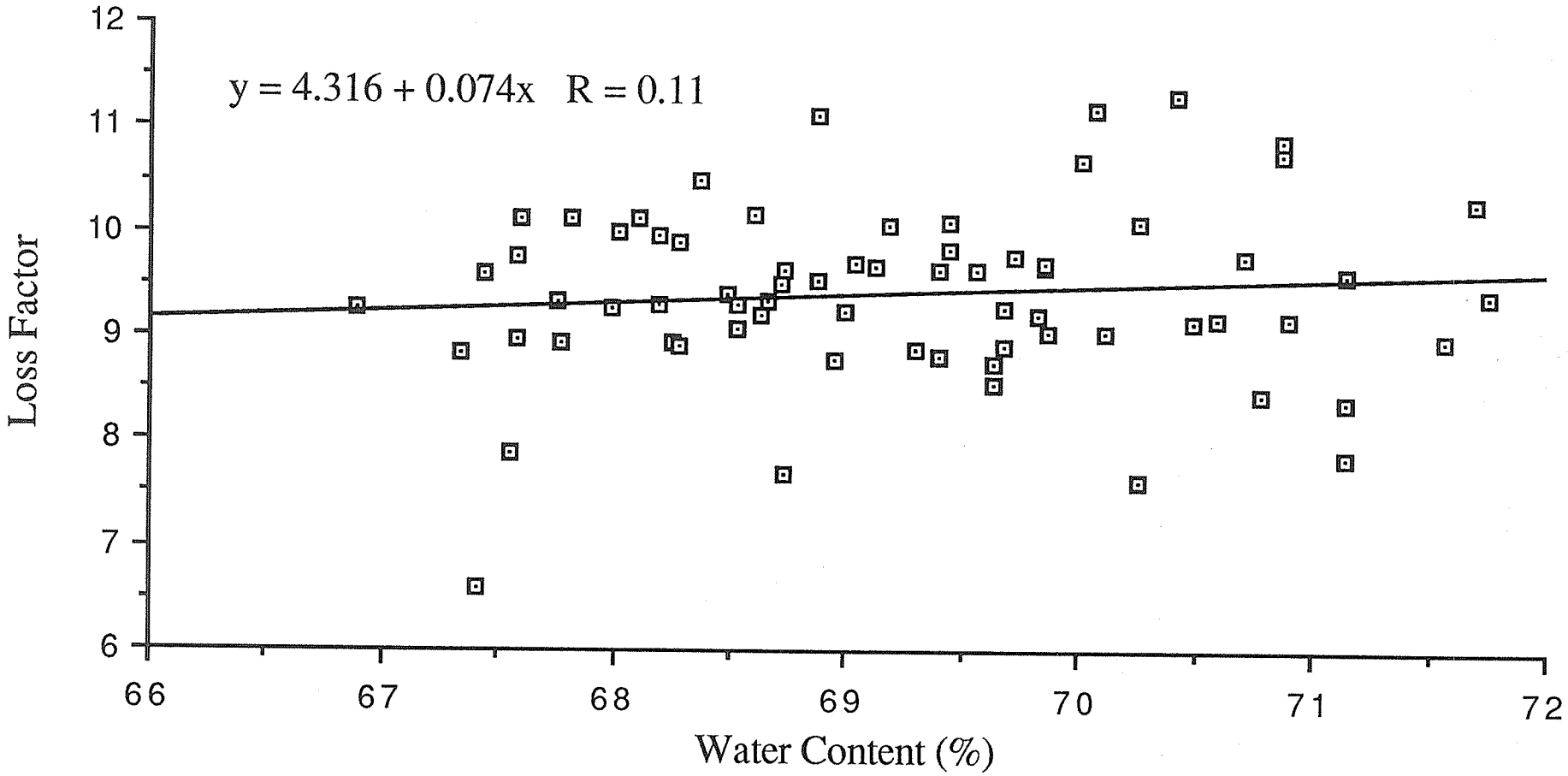

Appendix F

Real Dielectric Constant and Loss Factor

vs.

Time

for Vasogenic Edema Progression

Dielectric Constant vs. Time

Frequency = 100 MHz

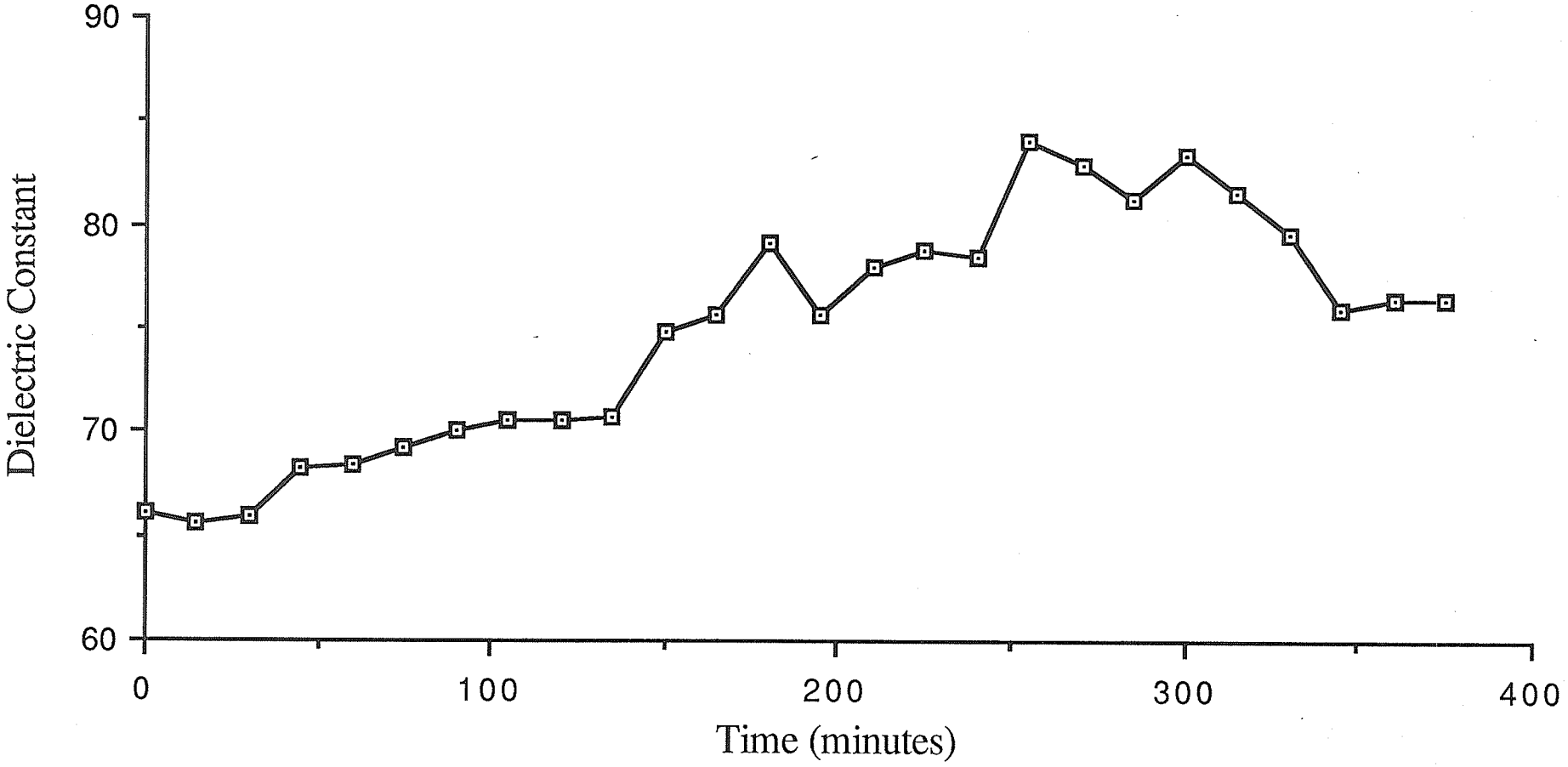

Dielectric Constant vs. Time

Frequency = 250 MHz

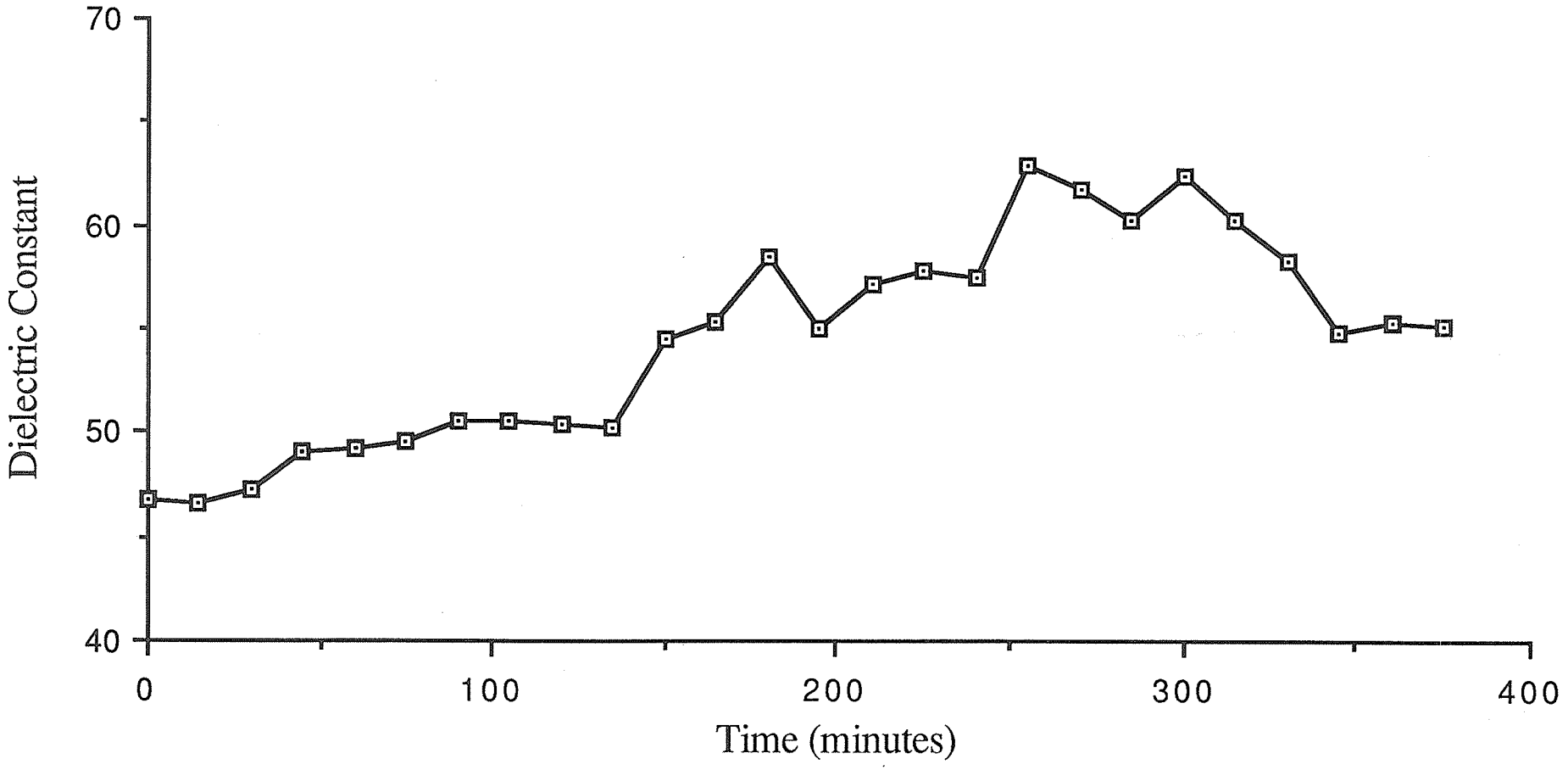

Dielectric Constant vs. Time

Frequency = 500 MHz

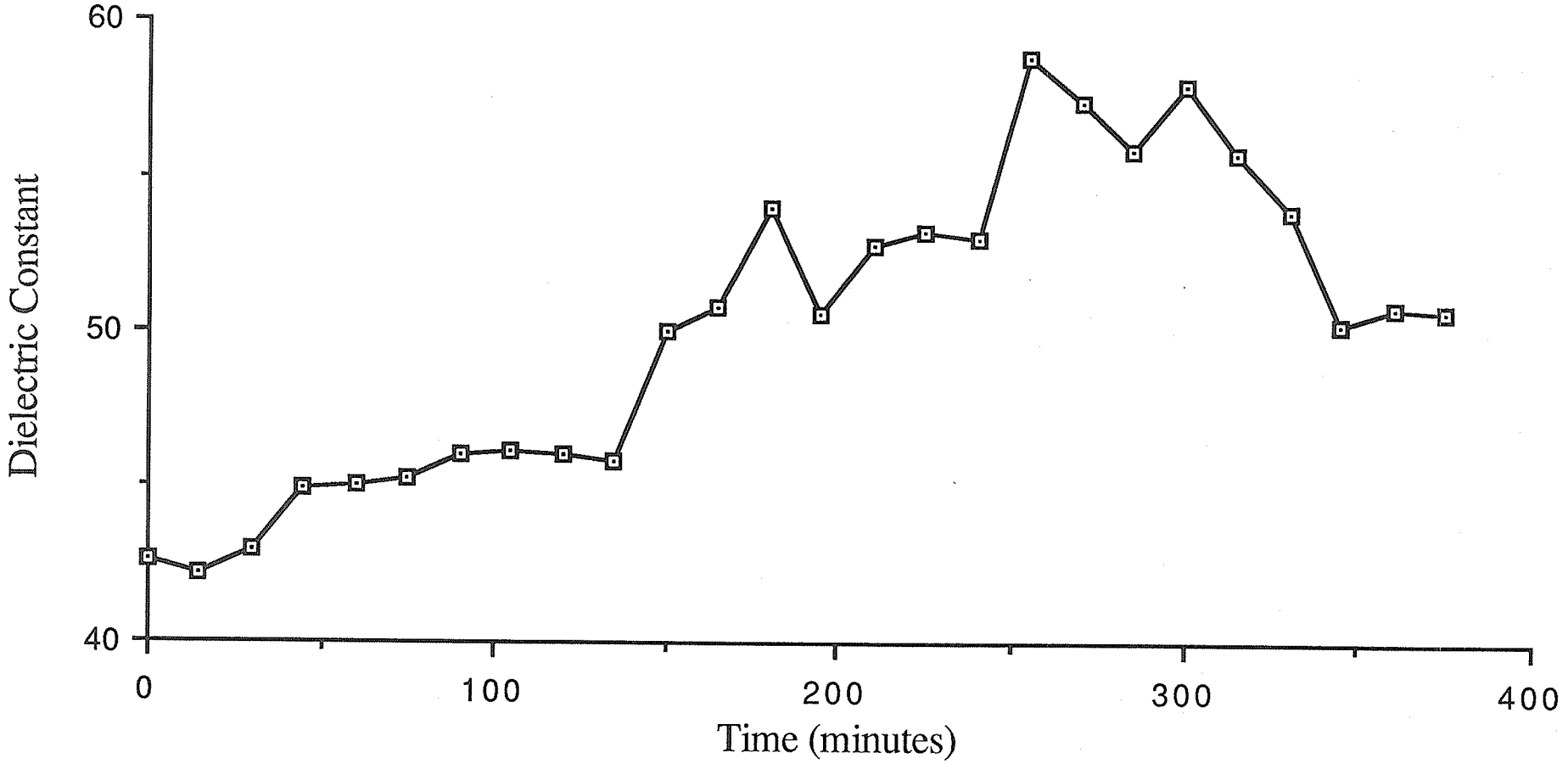

Dielectric Constant vs. Time

Frequency = 750 MHz

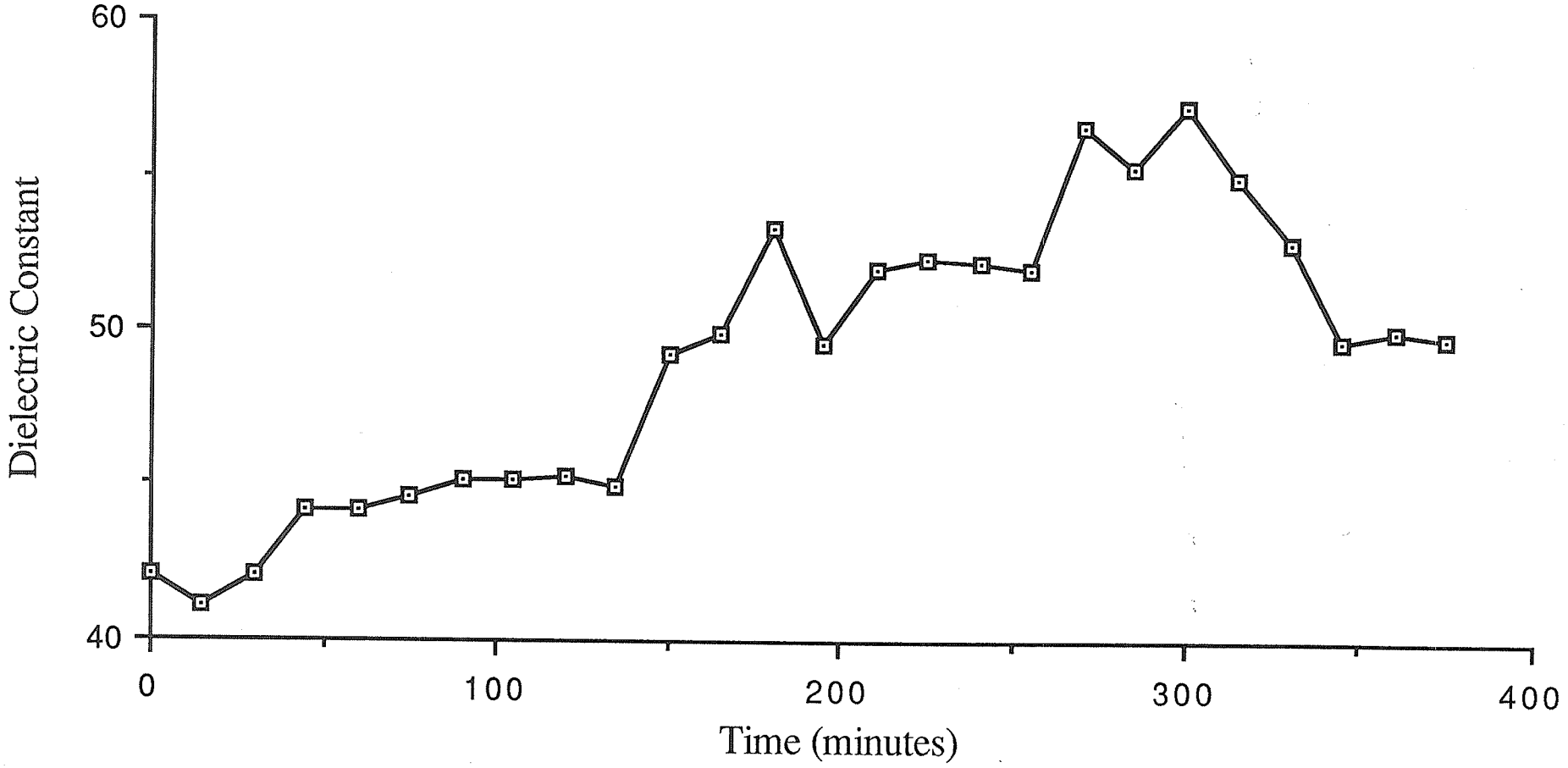

Dielectric Constant vs. Time

Frequency = 1000 MHz

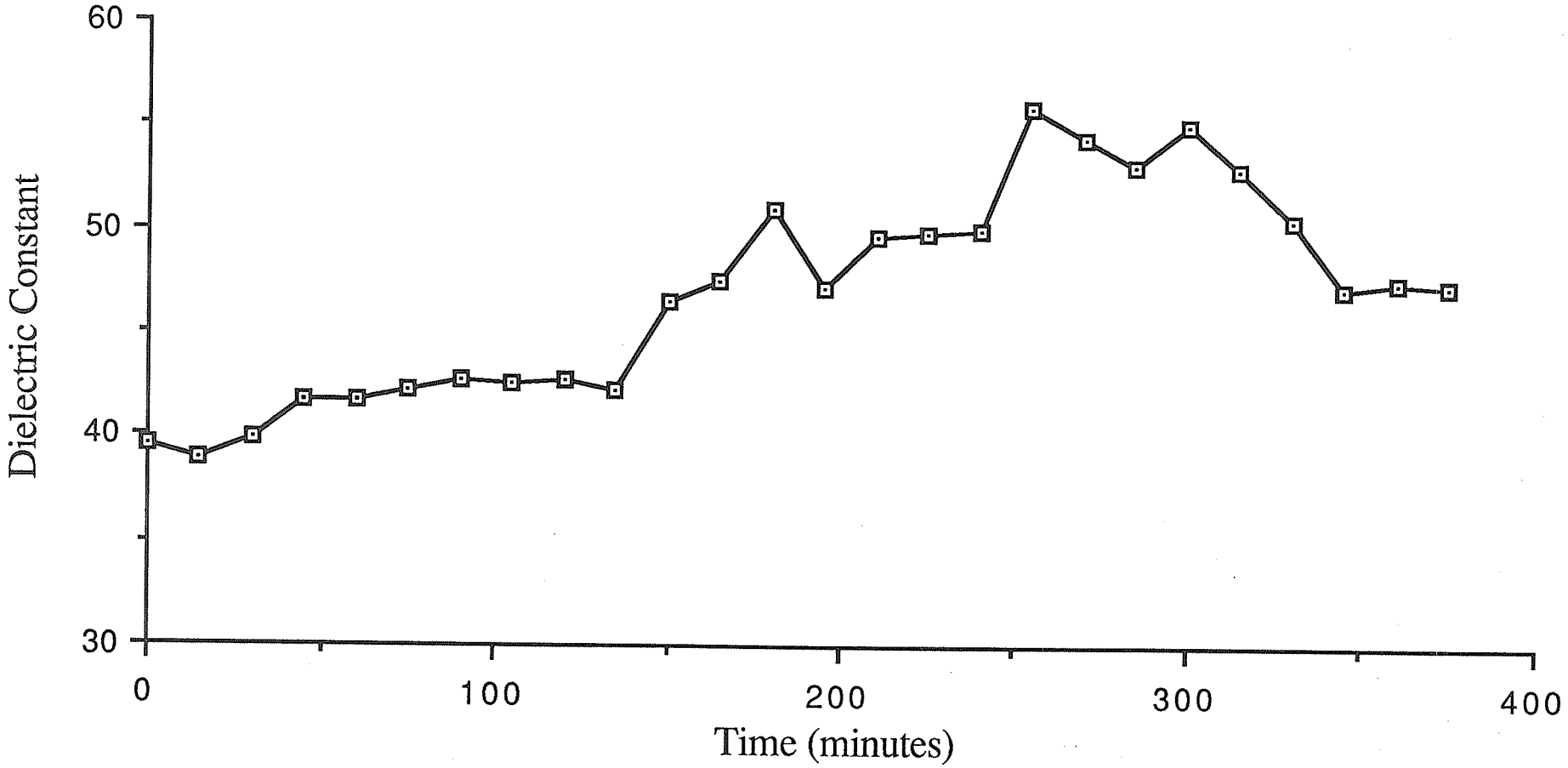

Loss Factor vs. Time

Frequency = 100 MHz

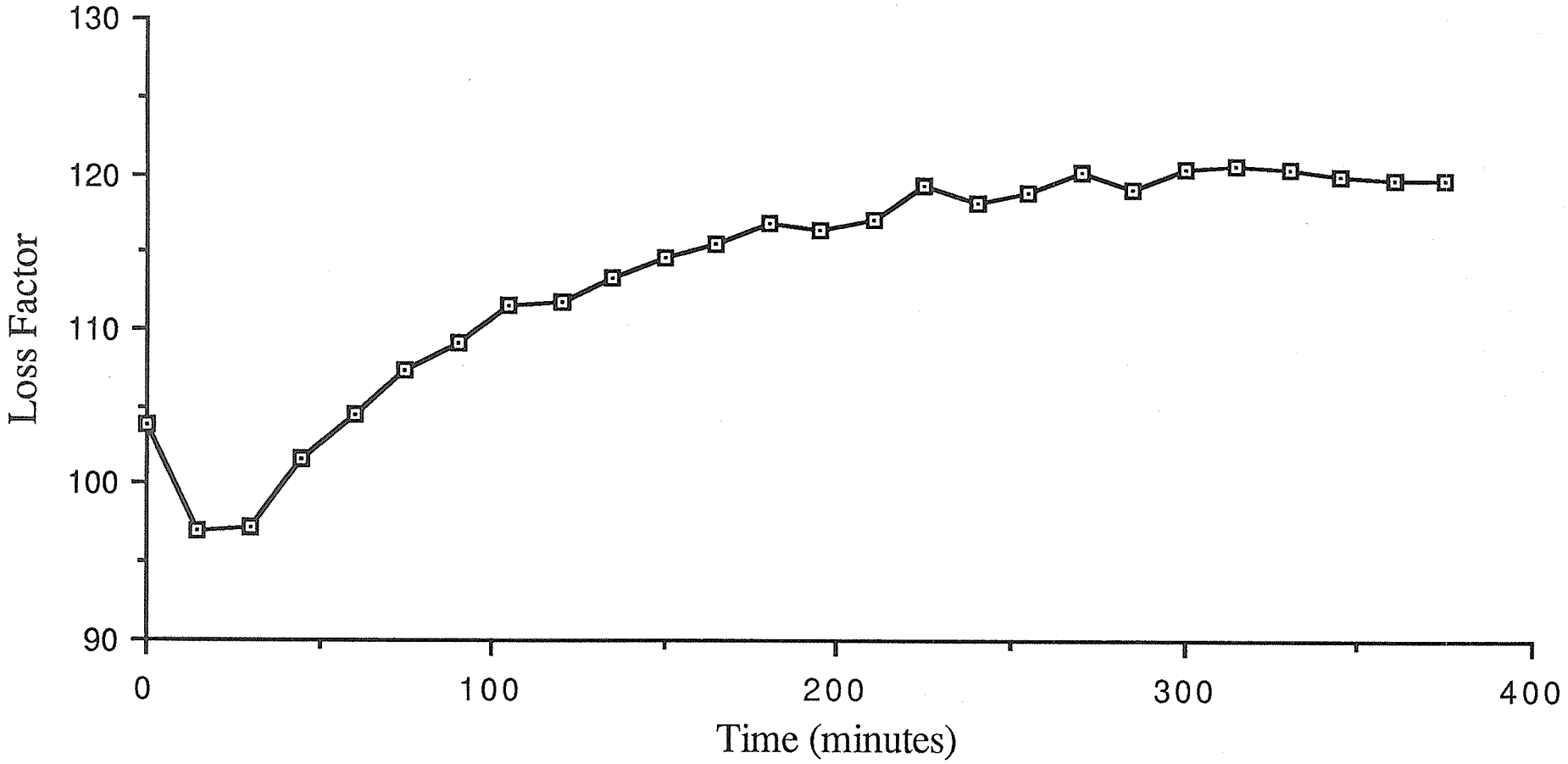

Loss Factor vs. Time

Frequency = 250 MHz

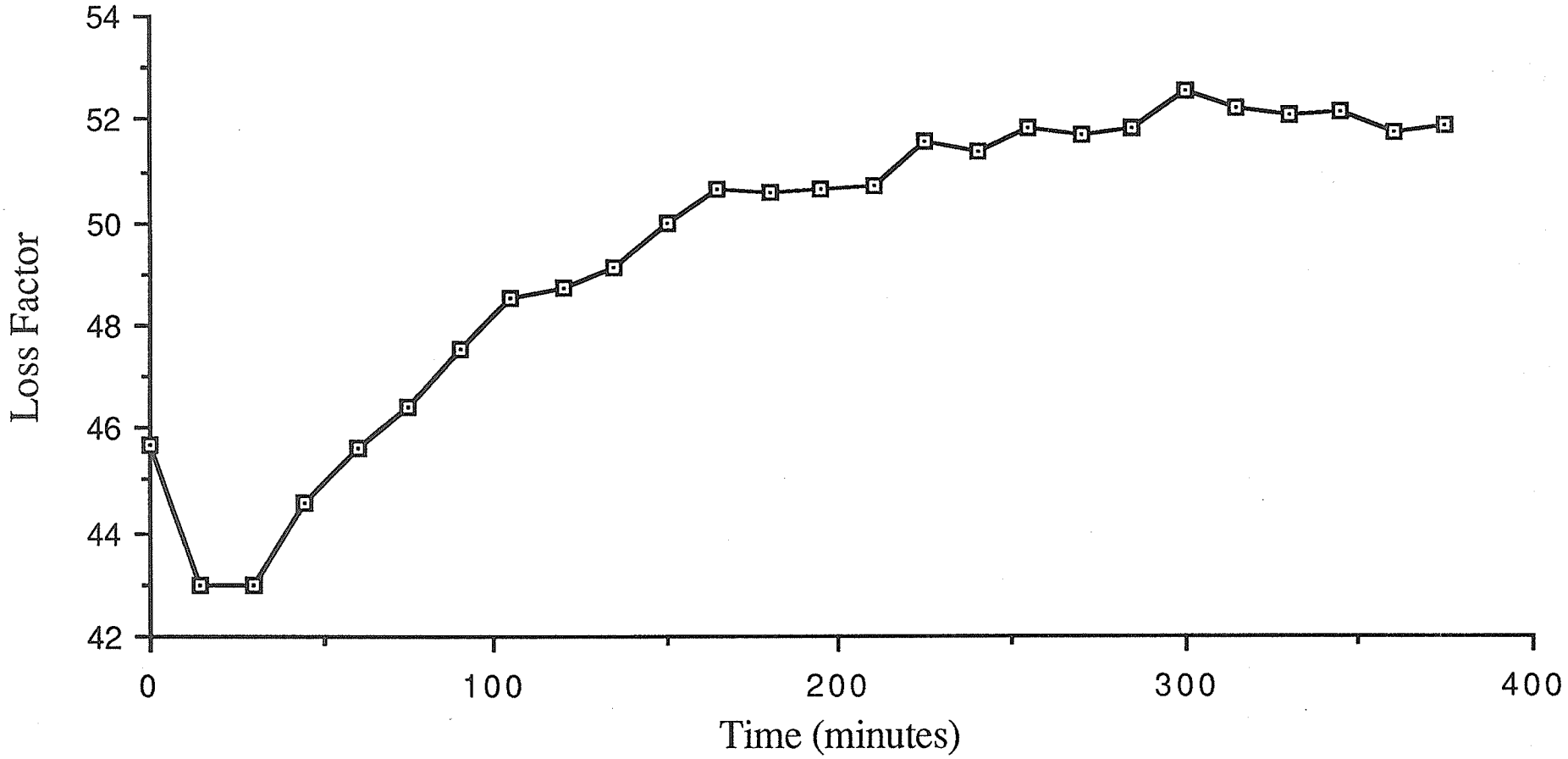

Loss Factor vs. Time

Frequency = 500 MHz

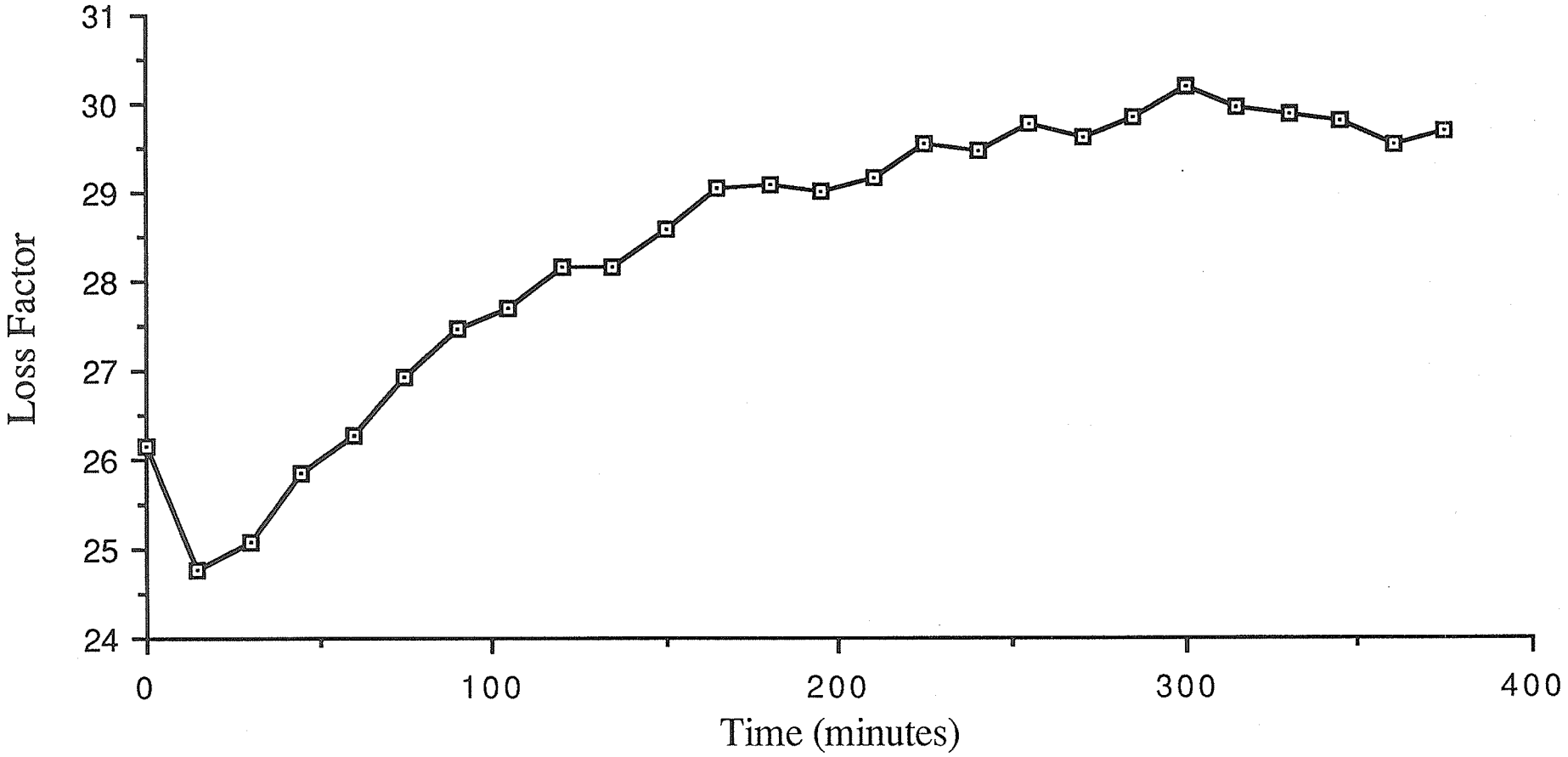

Loss Factor vs. Time

Frequency = 750 MHz

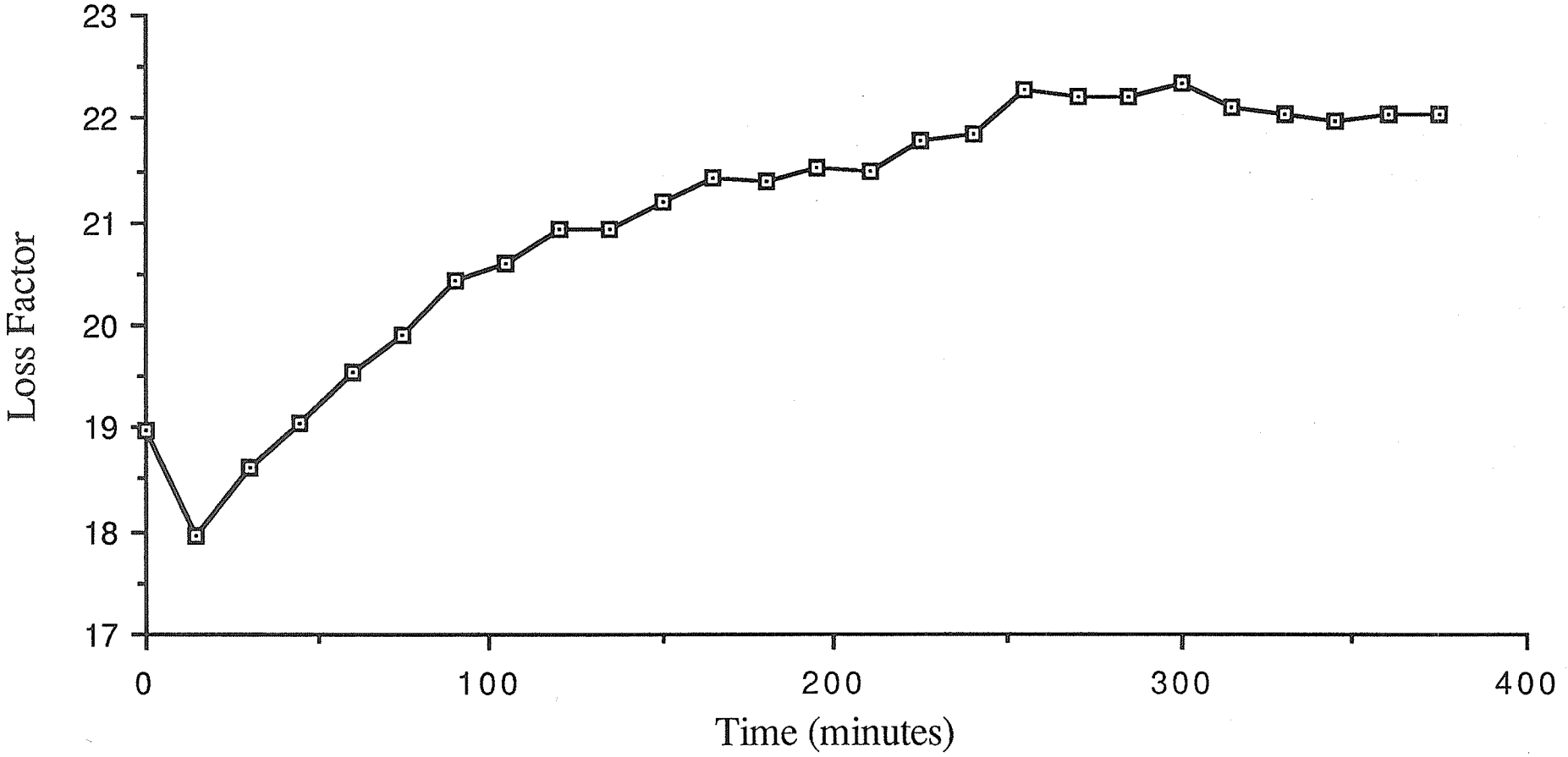

Loss Factor vs. Time

Frequency = 1000 MHz